DOKUZ EYLÜL UNIVERSITY
GRADUATE SCHOOL OF NATURAL AND APPLIED SCIENCES

FABRICATION AND CHARACTERIZATION OF NANOCOMPOSITE THIN FILMS FOR DIELECTRIC APPLICATIONS

by
Serdar GÜLTEKİN

October, 2016
İZMİR

FABRICATION AND CHARACTERIZATION OF NANOCOMPOSITE THIN FILMS FOR DIELECTRIC APPLICATIONS

A Thesis Submitted to the
Graduate School of Natural and Applied Sciences of Dokuz Eylül University
In Partial Fulfillment of the Requirements for the Degree of Master of Science in Nanoscience and Nanoengineering

by
Serdar GÜLTEKİN

October, 2016
İZMİR

M.SC THESIS EXAMINATION RESULT FORM

We have read the thesis entitled **"FABRICATION AND CHARACTERIZATION OF NANOCOMPOSITE THIN FILMS FOR DIELECTRIC APPLICATIONS"** completed by **SERDAR GÜLTEKİN** under supervision of **PROF. DR. ERDAL ÇELİK** and we certify that in our opinion it is fully adequate, in scope and in quality, as a thesis for the degree of Master of Science.

Prof. Dr. ERDAL ÇELİK

Supervisor

Asist. Prof. Dr. IŞIL BİRLİK

(Jury Member)

Assoc. Prof. Dr. Serafettin Demiz

(Jury Member)

Prof. Dr. E. Ilknur Çöcen

Director

Graduate School of Natural and Applied Sciences

ACKNOWLEDGMENTS

This thesis could not have been submitted without the help and contribution of several individuals who provided their valuable supports.

Firstly, I would like to state my special thanks to my supervisor Prof. Dr. Erdal ÇELİK, for his priceless advices, invaluable experiences, his constructive ideas and scientific guidance throughout the course of this thesis. It was my pleasure to work with him.

I would also like to present my sincere thanks to Assoc. Prof. Dr. Ömer Mermer for sincere assistance and support at all times. I am especially indebted to Dr. Tuncay DİKİCİ, Metin YURDDAŞKAL for all of their assistance that they provided me in the times of need. A special thank goes my project partners Selim DEMİRCİ, Çağlar ÖZER, Serdar YILDIRIM, for their helps and supports in various steps of the thesis. Also I need to thank my dear friend Ozan YLMAZ for his help and support.

I owe great gratitude to Sıdıka YILDIRIM for her constant encouragement and priceless helps. The successful completion of this study would not have been possible without her invaluable support, encouragement and presence in my life

Last but not least, I cannot thank enough to my dear parents, Kasım GÜLTEKİN, Şükriye GÜLTEKİN and my siblings Kibar GÜLTEKİN KURT and Cihangir GÜLTEKİN whose encouragement, support and presence illuminate my way and provide all the success that I have.

This work was supported by TUBITAK (The Scientific and Technological Research Council of Turkey) under project number of SBAG-113S069.

Serdar GÜLTEKİN

FABRICATION AND CHARACTERIZATION OF NANOCOMPOSITE THIN FILMS FOR DIELECTRIC APPLICATIONS

ABSTRACT

PVA/ TiO2, PMMA/TiO2 nanocomposite thin films were manufactured by simple and cost effective spin coating method on silicon substrates for dielectric application. PVA and PMMA granules dissolved in appropriate solvent. TiO2 nano powders were manufactured by sol-gel technique. Silicon substrates were manufactures via ingot production, wafer slicing, lapping, polishing and cleaning process respectively. In order to evaluate solution characteristics; turbidity, pH values, contact angle were measured by different devices. In order to determine optimum process parameter Differential Thermal Analysis-Thermogravimetry (DTA-TG) and Fourier Transform Infrared (FTIR) devices were used for both thin film and nano powder production. To determine best spinning parameter spin coater device was employed. Phase identification of the films was performed using X-Ray Diffraction (XRD) and surface morphology was investigated using Scanning Electron Microscopy (SEM). Surface topography, roughness and film thickness was investigated by Atomic Force Microscopy (AFM) and profilometer respectively. Optical properties of the films were analyzed by UV-VIS spectrophotometer. Dielectric measurements were carried out using high resolution dielectric analyzer. The effect of TiO2 nanoparticles on the crystallinity, micro-structure was investigated. It was found that TiO2 nanoparticle increases the crystallinity of nanocomposites. The dielectric parameters such relative permittivity and dielectric loss were significantly affected by TiO2 nanoparticle content. It was found that alternating current (A.C.) conductivity increased with increasing frequency and increasing TiO2 filler. The results show that PVA/TiO2 nanocomposite thin film were produced by spin coating method and can be used different dielectric application. PMMA / TiO2 nanocomposites also can be partially used in practice after the optimizing production parameters.

Keywords: PVA/TiO2, PMMA/TiO2, nanocomposite, thin film, dielectric and optic properties spin coater, sol-gel.

DİELELTRİK UYGULAMALAR İÇİN NANOKOMPOZİT İNCE FİLMLERİN ÜRETİMİ VE KARAKTERİZASTYONU

ÖZ

PVA/TiO2 ve PMMA/TiO2 nanokompozit ince filmler silikon altlıklar üzerine, dielektrik uygulamalarda kullanım potansiyelini incelemek üzere basit ve maliyet etkin döndürme kaplama yöntemiyle üretilmiştir. PVA ve PMMA granülleri uygun çözücülerde çözülmüş ve TiO2 nano tozlar sol-gel yöntemiyle üretilmiştir. Silikon altlıklar, ingot üretimi wafer dilimleme, perdahlama ve parlatma işlemlerinden geçirilerek hazırlanmıştır. Solüsyon karakteristiklerini belirlemek maksadıyla, solüsyonların turbititeleri, pH değerleri, temas açıları uygun cihazlarla ölçülmüş, optimum üretim parametrelerini amacıyla DTA ve FTIR cihazları hem TiO2 tozlar hem de oluşturulan filmler üzerinde kullanılmıştır. Kaplama işlemi sırasında en iyi döndürme basamakları döndürme kaplama cihazı kullanılarak oluşturulmuştur. Elde edilen fazların kristal yapıları ve oluşturulan filmlerin yüzey morfolojisi XRD ve SEM cihazları kullanılarak belirlenmiştir. Hazırlanan ince filmlerin yüzey morfolojisi, yüzey pürüzlülüğü ve kalınlıkları AFM profilometre ile incelenmiştir. UV-VIS spektrofotometre ile filmlerin optik özellikleri belirlenmiş, dielektrik özelliklerin karakterize edilmesi için yüksek çözünürlüklü dielektrik ölçüm cihazı kullanılmıştır. Polimerik yapı içerisine eklenen TiO2 nano partiküllerin kompozit yapının dielektrik, optik, mikroyapısal özelliklere etkisi incelenmiştir. Kompozit yapı bünyesindeki TiO2 içeriğinin artmasıyla kristalinitenin arttığı, dielektrik katsayısının ve dielektrik kaybın azımsanmayacak düzeyde etkilendiği görülmüştür. Bununla beraber alternatif akım iletkenlik değerinin de artan TiO2 içeriğiyle arttığı tespit edilmiştir. Elde edilen sonuçlar göstermiştir ki PVA/TiO2 nanokompozit ince filmler döndürme kaplama yöntemiyle üretilebilir ve farklı dielektrik uygulamalarda kullanılabilir. PMMA/TiO2 nanokompozit yapısının ise üretim parametrelerinin optimize edilerek kısmen dilelektrik uygulamalarda kullanılabileceği görülmüştür.

Anahtar kelimeler: PVA/TiO2, PMMA/TiO2, nanokompozit, ince film, dielektrik ve optik özellikler, döndürme kaplama, sol-gel.

CONTENTS

Page

LIST OF FIGURES

Page

LIST OF TABLES

Page

CHAPTER ONE
INTRODUCTION

1.1 General

Over past decades lots of research works on nanocomposite structures because of their potential of applicability in many different fields, fuels cells, photonic application, EM detectors, thin film transistors (Chandar Shekar, Sathish & Sathyamoorthy, 2011; El-Toony, 2011; Saikia, Saikia, Gogoi & Saikia, 2011; Tintu et al., 2010; Yahya, Akhtar, Masun & Kashif, 2011). Nanocomposites often exhibit unusual properties when compared with their virgin counterparts depending upon their sizes, shapes and stabilizing agents. The main idea behind nanocomposites is to mix organic and inorganic materials into nanocomposites with control at molecular level over interfaces, structures, and morphologies etc. (Mane, Navale, Mane, Naushad & Patil, 2015). Many researchers try to combine advantages of organic materials (i.e. light weight and flexibility) and inorganic materials (i.e. mechanical strength, thermal stability and chemical resistance) to produce new type material (Lamastra et al., 2008).

In spite of the fact that the greater numbers of polymers are unable to conduct electricity, their insulating properties are made used in the electronic industry. For instance they gained importance in the construction of sensor devices (Adhikari & Majumdar, 2004). Many scientists aimed to develop new and different type of radiation sensor which is able to measure low or high doses of ionizing radiation (Augustyniak et al., 2015). Recently some polymeric materials have being introduced as sensing material in dosimeter devices. Polyvinyl butyral (PVB) based radiation sensor was developed for different application field such as industrial radiation processing or food irradiation applications (Abdel-Fattah & El-Kelany, 1998; Al Zahrany, Rabaeh & Basfar, 2011). Polymer gel dosimeters based on N-(Hydroxymethyl) acrylamide and hydroxypropyl cellulose gel were considered for radiation therapy planning (Basfar, Moftah, Rabaeh & Almousa, 2015; Hiroki, Yamashita, Kimura, Nagasawa & Taguchi, 2015). The among the polymers,

poly(vinyl) alcohol (PVA), which is eco-friendly, water soluble and easily film forming nature at room temperature attracted the researchers because of its unique electronic, mechanical and optical properties in engineering technology. PVA and its composite structures are used as sensing materials in different type of sensors such as humidity, dew, carbon, gas, strain, piezoresistive, optical and radiation (Abargues, Rodriguez-Canto, Albert, Suarez & Martínez-Pastor, 2014; Amin, Karmakar & Winther-Jensen, 2013; Bhat, Nate, Bhat & Bhatt, 2007; Devallance & Nan, 2014; Dupare, Shirsat & Aswar, 2009; Irimia-Vladu & Fergus, 2006; Jiang, Fei, Jiang, Wang & Zhang, 2014). It also is one of the fascinating polymeric material which is applicable for composite applications due to the its good hosting behavior (Bouropoulos, Psarras, Moustakas, Chrissanthopoulos & Baskoutas, 2008; Fu et al., 2007; Lee, Bhattacharyya, Easteal & Metson, 2008). In addition for commercial applications, PVA could be appropriate option because it shows good price/performance ratio. Another polymer which had good attention from researchers is poly(methyl methacrylate) PMMA. It is a linear thermoplastic polymer like PVA. PMMA has good mechanical properties such as high Young's modules and mechanical strength, low elongation at break. It also one of the hardest thermoplastic polymers owing this future it shows highly starch resistive characteristic. On the contrary of the PVA, PMMA is not too sensitive to humidity. So that it exhibits low water absorbing capacity which made it has good dimensional stability. To further enhance the properties of these polymers, the addition of an inorganic material is advantageous for forming a composite (Sugumaran & Bellan, 2014). One of these additives is titanium dioxide (TiO_2) which is a high band-gap semiconductor and has high dielectric constant (Majewski, Schroeder & Grell, 2005; Wang et al., 2004). Both PVA and TiO_2 have been employed as gate dielectrics in electronic devices (Chakraborty, Bera, Bhattacharya & Maiti, 2005; Kim, Yoon, Am Kim & Suh, 2005). For TiO_2 it is not easy to form as film on a substrate because of its physical properties, such as brittleness and also film forming process of TiO_2 requires high temperature that is relatively expensive (Ramos et al., 2014). In addition PMMA and PVA can be processed at lower temperatures, compared to TiO_2 thin films but its dielectric constant is not as high as TiO_2 films (Ortiz, Facchetti & Marks, 2009). There are several methods to produce TiO_2 such as sol-gel (Celik, Keskin,

Kayatekin, Ak Azem & Özkan, 2007), anodization (Jaroenworaluck, Regonini, Bowen, Stevens & Allsopp, 2007), magnetron sputtering (Wang, Li, Ba, Huang & Yu, 2015), flame spray pyrolysis (Erol, Sancakoglu, Yurddaskal, Yildirim & Çelik, 2013) etc. Among them, flame spray pyrolysis is one of the easiest, well controlled, novel and short production term methods presented in the literature (Erol et al., 2013).

In our study, TiO_2 nanoparticles are produced by flame spray pyrolysis method. PMMA/TiO_2 and PVA/TiO_2 nanocomposite thin films with various weight percentages of TiO_2 are manufactured by cost effective spin coating method. In this work, the morphological, structural, optical and dielectric properties of PMMA,PVA, and PMMA/TiO_2, PVA/TiO_2 nanocomposite samples were investigated and obtained results were analyzed in detail.

1.2 Organization of the Thesis

The aim of this thesis is to develop new and different materials to use in dielectric applications as dielectric film. With this respect we focused on polymer based nanocomposite materials and decided to choice PVA and PMMA as matrix material which held remarkable interest due to their attractive mechanical, optic and electronic properties. As a filler material TiO_2 which is a transparent, high band-gap semiconductor and has high dielectric constant was employed Combining advantages of organic materials such as PMMA, PVA (i.e. light weight and flexibility) and inorganic materials which is TiO_2 (i.e. mechanical strength, thermal stability and chemical resistance) could be a good way to obtain new materials. Two different types of nanocomposite materials which are PVA/TiO_2 and PMMA/TiO_2 including various amount of TiO_2 were produced. Optical dielectrical, morphological properties of this nanocomposite film were analyzed.

With this context Chapter one provide theoretical information about the area of research and the research objectives of this thesis. In Chapter two, theoretical information about dielectric phenomena and dielectric materials, nanocomposites and

polymeric nanocomposites, sol-gel process, spin coating and wafer cleaning process were explained. Chapter three provides experimental studies including the materials used to produce component of nanocomposite, production and characterization technique. In Chapter four, observations during the optimization and production process and characteristics of the products and effect of TiO_2 on dielectric properties of PMMA and PVA were given. Finally the conclusion and future plans are summarized in Chapter Five.

CHAPTER TWO
THEORITICAL BACKGROUND

2.1 Dielectric Phenomena

The difference in the energy band gap of semiconductors and dielectrics (or insulator) is basic distinction between these two types of materials. At the room temperatures and normal pressures, the dominant charge carriers in a semiconductor are generated mainly by thermal excitation in the bulk because the semiconductor has a small energy band gap; hence, a small amount of energy is sufficient to excite electrons from full valence band to an upper empty conduction band. However in a dielectric material, the energy band gap is relatively large and charge carriers are mainly injected from the electrical contacts or other external sources. This is why band-to-band transitions need higher amount of energy for dielectric materials. A material is formed mainly from atoms or molecules, these atom and molecules is consist of electron and nuclei. The electrons farthest from the nuclei of the atoms have various bound to other the atoms or molecules coupled with the free charges. These charges are affected by external forces, such as electric fields, magnetic fields, electromagnetic waves, mechanical stress, or temperature, resulting in the occurrence of all dielectric phenomena. Once dielectric material is exposed to electric field the dielectric phenomena occurs. This phenomena comprise mainly electric polarization, resonance, relaxation, energy storage, energy dissipation; thermal, mechanical, and optical effects and their interrelations; and electrical aging and destructive breakdown for nonmagnetic dielectric materials (Kao, 2004b).

2.1.1 Dielectric Constant

The explanation of dielectric constant relate to the permittivity of the material (symbol use here ε). The permittivity means the ability of a material to polarize in response to an applied field. It is the ratio of the permittivity of the dielectric to the permittivity of a vacuum (Equation 2.1). Physically it means the greater the

polarization developed by a material in an applied field of given strength, the greater the dielectric constant will be (Ahmad, 2012).

In SI units, permittivity ε is measured in farads per meter (F/m or $F \cdot m^{-1}$).

$$\varepsilon_r = \frac{\varepsilon}{\varepsilon_o} \rightarrow \varepsilon_r = \frac{C.d}{\varepsilon_o.A} \tag{2.1}$$

where ε_r is the relative permittivity of the material, ε_0 is permittivity of vacuum which is $8.8541878176 \times 10^{-12}$ F/m, *C* is measured capacitance, d is the thickness of the material, A is the surface area of the material.

Generally dielectric materials are made out of inorganic substances eg. Silicon dioxide, aluminum oxide. Recently polymeric materials attracted the researchers because of its unique electronic, mechanical and optical properties in engineering technology. This is due to the easier processing, flexibility, able to tailor made for specific uses and better resistance to chemical attack They are also applicable for composite applications due to the its good hosting behavior. Hence polymeric materials are gaining wider use as dielectric materials. (Bouropoulos et al., 2008; Kumar, Jat, Khanna, Vijayan & Banerjee, 2012).

2.1.2 Relaxation, Dielectric Loss and Complex Permittivity

Dielectric constant can be mentioned in complex form as in Equation 2.2 below

$$\varepsilon^* = \varepsilon' - j\varepsilon'' \tag{2.2}$$

ε^* is the complex permittivity, ε' real part of permittivity which is dielectric constant, ε'', imaginary part which is the dielectric loss. The ratio between the dielectric loss with the dielectric constant is quantified as in Equation 2.3 (Singh, Agarwal, Sanghi & Khasa, 2012).

$$tan\ \delta = \frac{\varepsilon''}{\varepsilon'} \tag{2.3}$$

The first model of relaxation phenomena in dielectrics is derived from Debye relaxation model. In this model, real and imaginary part of permittivity can be depicted as in Figure 2.1 (Debye, 1929).

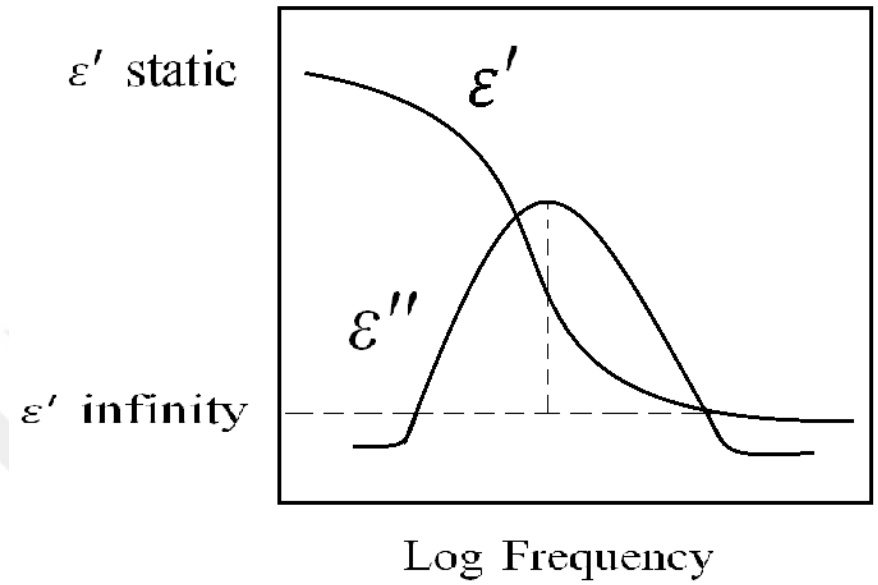

Figure 2.1 Debye dielectric dispersion curve (Debye, 1929).

In an AC circuit, the dielectric loss can be expressed as function of phase angle between the current and voltage. The loss is usually addressed in terms of tan δ. For a dielectric materials tan δ is assumed as 0. However in practice application, it is tried to reached to 0 as possible (Ebeoğlugil, 2011).

The cause of dielectric loss occurs is lack of polarization process in molecules to follow the rate of change of the oscillating applied electric field. Dipol in dielectric materials needs time to return to its original random orientation which is expressed relaxation time. This phenomenon does not occur instantaneously but the polarization diminished exponentially. Once the AC current frequency well faster than the relaxation time, the polarization cannot follow the oscillating frequency resulting in the energy absorption and dissipated as heat resulting the dielectric loss (Ahmad, 2012).

2.1.3 Conducting and Dielectric Materials

Conducting materials or conductors have many o free charge carries. For instance, metals contain free electrons. These charge carrier electrons can move freely. Thanks to these electrons metallic materials can easily conduct electric or heat. When a piece of metal is inserted to two plates which are charged without touching, the charge on the plate makes the electrons on the metal move toward the surface. But the electrons on the metal could not leave the surface which cause non-uniform charge distribution resulting a positive charge on the surface and negative space charge on the other one. This phenomenon is similar to polarization of the neutral atoms. With this respect, It can be said that charge Q on plate A induces a negative charge equal in magnitude but opposite in polarity on one surface of the metal close to plate A. Same thing goes for other metal surface as opposite charge and other plate B (Figure 2.3). So, in the vacuum space between plates and the metal surfaces, we have Equation 2.4;

$$\sigma_{so} = D_o = \varepsilon_o F_o \quad \longrightarrow \quad \varepsilon_o = \frac{\sigma_{so}}{F_o} \tag{2.4}$$

The electric field F_o and the associated electric flux density D_o produced by the free surface charges of density σ_{so} on the plates in vacuum space (free space). However, inside the metal there is no electric flux based on Gauss's law, as shown in Figure 2.2, and hence, $F = 0$. We have Equation 2.5 (Kao, 2004a)

$$\varepsilon_s = \frac{\sigma_s}{F} \rightarrow \infty \tag{2.5}$$

The permittivity of metals is ∞ under static fields only. Under a time-varying field or an alternating field, the charges induced on the metal surfaces may not follow instantaneously the time-varying field. In this case, the permittivity is not infinite, but a finite value. We shall discuss this phenomenon further in later sections (Kao, 2004a).

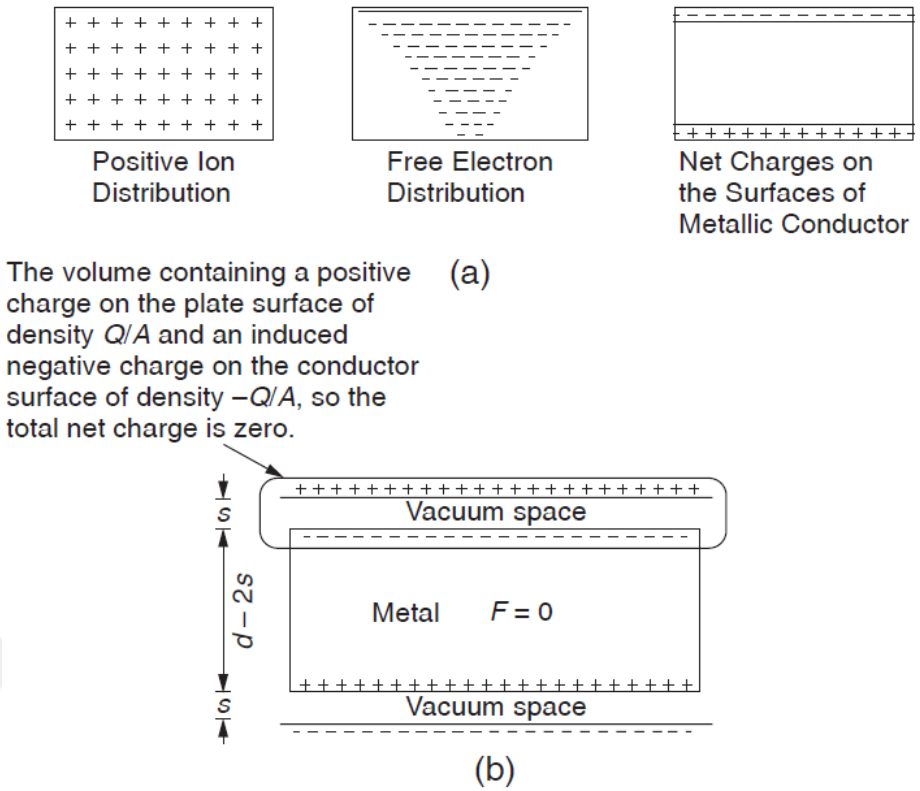

Figure 2.2 (a) Induced net charges on the surfaces of a metallic conductor in the presence of a static electric field, and (b) the charge on the plate with the surface charge density σs inducing a charge equal in magnitude but opposite in polarity on the surf (Kao, 2004a).

On the other hand permittivity (or relative permittivity, which is generally referred to as the dielectric constant) is one of the important future for dielectric. In general the permittivity is independent of the electric field strength for fields below a certain critical field, at or above which carrier injection into the material becomes important. However the frequency of the alternating electric field strongly affects the permittivity value. It also depends on such chemical component of the material as well ass and physical parameter of the environment such as temperature and pressure, etc (Kao, 2004a).

A dielectric material is made up of atoms or molecules that possess one or more of five basic types of electric polarization.

1. Electronic polarization
2. Atomic or ionic polarization

3. Dipolar polarization
4. Interface or space charge polarization

Each type of polarization requires time to perform; this is main reason why the degree of the overall polarization depends on the time variation of the electric field. In the first place, we take into account a perfect dielectric material. This kind of materials does not include mobile charge carriers (electrons or ions). If a piece of such a dielectric material is put near the system shown in Figure 2.3, the system always intent to decrease the potential energy in between the plates, so it try to attract materiel near to system into the space between the plates (Kao, 2004a).

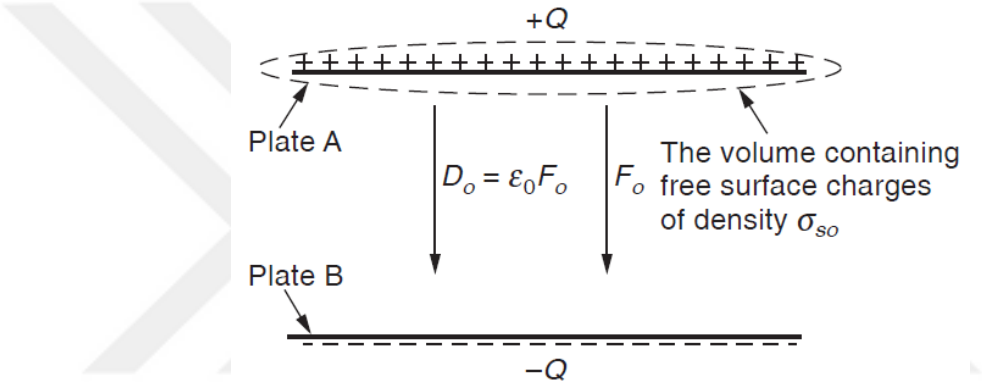

Figure 2.3 The electric field Fo and the associated electric flux density Do produced by the free surface charges of density σ_so on the plates in vacuum space (free space) (Kao, 2004a).

When the piece of the material put inside the space between the metal plates with the original surface of density σ_s unaltered, as shown in Figure 2.4, the potential between the plates produced by the original charge Q on the plates decrease to a smaller value. As a matter of fact, with Q on the plates remaining constant, the ratio of the electric field in free space F_o to that filled with the dielectric material F is the so-called dielectric constant or relative static permittivity, $\varepsilon_{sr} = \varepsilon_s/\varepsilon_o$ (Kao, 2004a).

With the dielectric material, one portion of σ_s is used to compensate the polarization charges on the surfaces of the material in contact with the metal plates. This portion of σ_b is bound at the locations with its charge opposite in polarity and equal in magnitude to the polarization charges of the material, as shown in Figure 2.4.

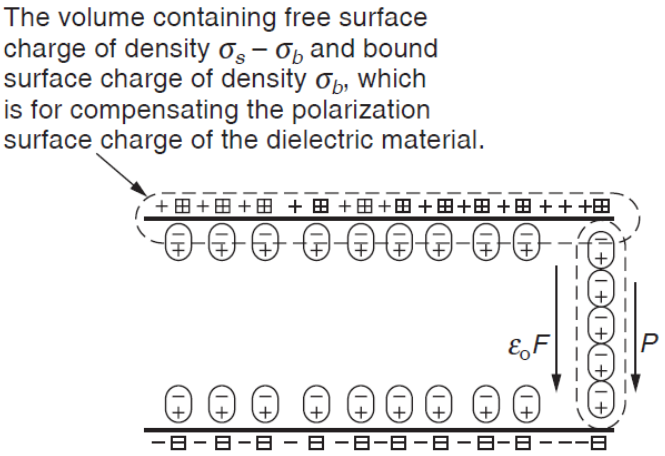

Figure 2.4 The surface charge of density σ_s consisting of two portions: the bound charge σ_b and the free charge σ_s - σ_b. The free charge portion produces the electric Field F and the electric flux density of ε_o F, while the bound charge portion produces pol polarization *P*. + and - denote the free positive and negative charges, respectively, and + and - denote the bound positive and negative charges, respectively (Kao, 2004a).

As we mentioned previously a dielectric material is made up of atoms or molecules that possess at least one electric polarization. When an electric field is applied to an ideal dielectric material there is no long range transport of charge but only a limited rearrangement such that the dielectric acquires a dipole moment and is said to be polarized. Different kind of polarization could be occurred during the process. Ebeoğlugil says that "Electronic polarization (P_{el}), in which the applied field displaces the electronic charge relative to the atom nucleus to give a dipole. Atomic polarization (P_{ion}), which occurs in all materials, is a small displacement of the electrons in an atom relative to the nucleus; in ionic materials there is, in addition, ionic polarization involving the relative displacement of cation and anion sub lattices. Dipolar materials, such as water, can become polarized (P_{dip}) because the applied electric field orients the molecules. Finally, space charge polarization (P_{sc}) involves a limited transport of charge carriers until they are stopped at a potential barrier, possibly a grain boundary or phase boundary." The total polarization under an applied electric field is given by Equation 2.6 and this arithmetically sums the contribution: The various polarization processes are illustrated in Figure 2.5 (Moulson & Herbert, 2003).

$$P_{tot} = P_{el} + P_{ion} + P_{dip} + P_{sc} \quad (2.6)$$

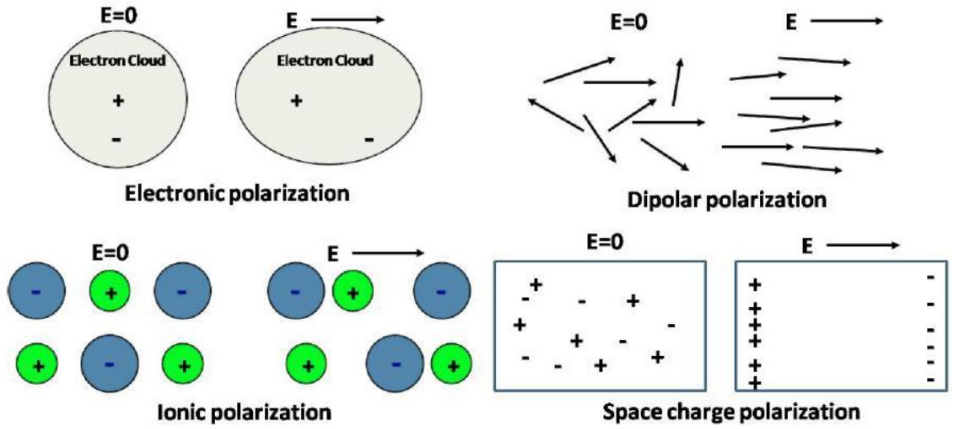

Figure 2.5 Schematic representations of various polarization mechanisms (Ebeoğlugil, 2011)

Electronic polarization: It occurs in neutral atoms which has same quantity of negative and positive charge. Under the electric field, nucleus take position with respect to the electric field resulting electronic polarization (Sagadevan & Sundaramb, 2014).

Atomic/ionic polarization: This type of polarization occurs when a molecule share it's electrons asymmetrically with another, and cause the electron cloud to be shifted towards the stronger binding atom, when electric field applied, the atoms acquire charges of opposite polarity and an external field acting on these net charges will tend to change the equilibrium positions of then atoms themselves, leading to the atomic polarization (Sagadevan & Sundaramb, 2014).

Dipolar/orientational polarization: When two molecules transfer some of valance electrons to form ionic bound between other molecules, a permanent dipole moment will originate in them. This permanent dipole moment has same value with the product of charges of transferred electrons. Once electric field E exist, the molecules carrying a permanent dipole moment will take a position through to direction of E. This process could be possible only in dipolar materials having permanent dipole moments (Sagadevan & Sundaramb, 2014).

Space charge polarization: If the materials comprise charge carriers this type of polarization could be presented. Charge carriers in the dielectric materials are able to migrate by diffusion, fast ionic conduction, or hopping, etc cloud be caused a macroscopic field distortion. Such a distortion appears to an outside observer as an increase in the capacitance of the sample and may be indistinguishable from the real rise of the dielectric permittivity. This type of polarization is unique among the electronic polarization types. Because it could be accompanied by macroscopic charge transport. In addition, the space charge polarization can be divided in class which is hopping polarization and interfacial polarization. In dielectric materials, a phenomena which is called hoping polarization could be formed by hoping of ions and vacancies, or electrons and holes from one site to another site. Similarly the separation of the mobile positive and negative charges under an electric field can produce an interfacial polarization (Sagadevan & Sundaramb, 2014).

2.1.4 Classification of Dielectric Materials

Dielectric materials can be classified into two major categories: Non ferroelectric (normal dielectric or linear dielectric or para electric) materials and ferroelectric (nonlinear dielectric) materials. The linear dielectric materials can be again subdivided into two classes based on the mechanism of electric polarization as nonpolar and dipolar materials (Smyth, 1966).

2.1.4.1 Non ferroelectric Materials

The dielectric materials which are exhibiting a linear relationship between the polarization and applied electric field are known as linear dielectrics. This class of materials gets polarized with the application of the field and gets depolarized on the removal of field. Based on the nature of the polarization mechanism, the linear dielectrics can be grouped as follows

Non polar materials: This type of materials comprise a single type of atom, such as silicon (Si), diamonds (C), inert elements in gas, liquid, or solid phase. An electric

field can cause only elastic displacement of the electron cloud (mainly the valence electron cloud) in materials of this class. Hence non polar materials have only electronic polarization (Kao, 2004a).

Polar materials: In materials of this class both elastic displacement of electron clouds and the relative positions of ions occur because of that these materials show electronic polarization as well as ionic polarization. It is possible that there are molecules in these kinds of materials and these molecules consist of more than one kind of atom without any permanent dipole moment. Such as ionic crystals; in this case the total polarizability is the sum of the ionic and electronic polarizabilities as described in Equation 2.7 (Kao, 2004a).

$$\alpha = \alpha_e + \alpha_i \tag{2.7}$$

Dipolar materials: The materials of this class have: electronic, ionic and orientation. Thus the total polarizability of these materials can be expressed like in Equation 2.8

$$\alpha = \alpha_e + \alpha_i + \alpha_0 \tag{2.8}$$

Materials in this class permanent dipoles show spatial orientation under the electric field resulting in orientational polarization. In liquids and gases, this process occurs predominantly in liquids and gases. In addition, this process occurs some solids, such as solid hydrochloric and sulfuric acids within a certain range of temperatures. Below the critical temperature all dipoles are frozen. Hence they lose their capability to contribute orientational polarizability. But for most materials, the dipoles are frozen in below the melting point of the material. It should be remembered that dielectric materials, not only have single crystal but also they may contain either amorphous or polycrystalline. These structures have a large quantity of various traps. Moreover they are conductive and always involve charge carriers (electrons, holes, or both) injected from electrical contacts. With this respect, the

total polarizability in this class should be addressed as describe in Equation 2.9 which include the space charge polarizability;

$$\alpha = \alpha_e + \alpha_i + \alpha_0 + \alpha_d \quad (2.9)$$

where α_d in the space charge polarizability includes $\alpha_h + \alpha_c$ (Kao, 2004a).

Different type of dielectric materials has been used for different purpose because of their different dielectric properties. Inorganic materials for example metal oxides show higher permittivity characteristic when compared to polymeric materials. In fact inorganic materials owe to ions and polar groups for their high dielectric constant. In Table 2.1, dielectric constant of some inorganic and organic materials was given air having a dielectric constant of 1.02 is taken as reference dielectric.

Among the materials in Table 2.1, PVA and PMMA as polymeric materials attract the attention of scientist because of their attractive properties. For PVA, good film forming results, good processibility, biocompatibility and good chemical resistance are several unique characteristic. On the other hand PMMA is a high-strength; amorphous polymer showing good dimensional stability, thermal stability and outdoor wearing properties. Owing to these characteristics, PMMA is among the most heavily studied polymers. Both these two polymers have potential for nano/micro composites and dib lock copolymers/blends (Sugumaran & Bellan, 2014).

PVA: Polyvinyl alcohol is an artificial polymer, and is called as various name such as PVOH; Poly(Ethenol), Ethenol, homopolymer; PVA; Polyviol; Vinol; Alvyl; Alcotex which is essentially made from polyvinyl acetate through hydrolysis The formula of PVA is $(C_2H_4O)_x$. This polymer is biodegradable and soluble in water. The melting point of PVA 230 °C and 180–190 °C (356-374 degrees Fahrenheit) for the fully hydrolyzed and partially hydrolyzed grades, respectively and above the 200 °C it decomposes rapidly. Partially hydrolyzed and fully hydrolyzed PVA molecules is depicted in Figure 2.6.

Table 2.1 Dielectric constant of several polymers and inorganic materials (Barber et al., 2009).

Material	Dielectric constant	Material	Dielectric constant
TiO_2	80	PQV	2.8
SiO_2	3.9	PEN	2.2
Al_2O_3	9	PEEK	3.5
$BaTiO_3$	1700	PVDF-HFP	12
ZrO_2	25	PS	2.6
SrTiO3	2000	PTFE	1.9
Y_2O_3	15	PMMA	2-4
Ta_2O_5	22	PVA	2-4

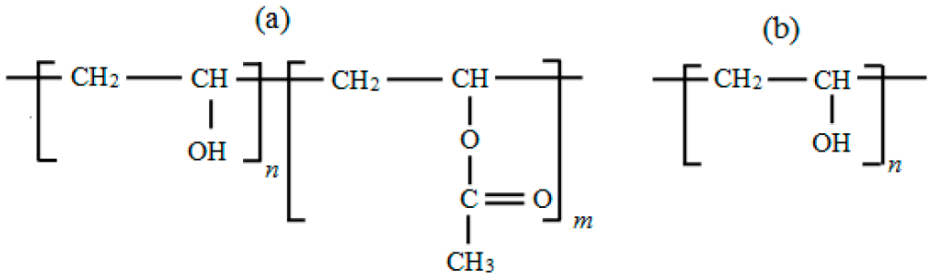

Figure 2.6 Structural formula of PVA (a) partially hydrolyzed, (b) fully hydrolyzed

PVA molecule chain can be various lengths depending on initial length of vinyl acetate polymer. With this respect molecular weight of PVA may be any value between 20,000-400,000 Figure 2.7 depicts a typical vinyl alcohol and polyvinyl PVA molecules.

PVA shows excellent film forming performance, emulsifying and adhesive properties. It can also be used resistant to oil, grease and solvents. It has high tensile strength and flexibility, as well as high oxygen and aroma barrier properties. However PVA is affected dramatically by humidity it can absorb the water. With this respect its physical properties are strongly depends on humidity of environment where it is employed. The water, which acts as a plasticizer, will then reduce its tensile strength, but increase its elongation and tear strength (Fromageau, Brusseau, Vray, Gimenez & Delachartre, 2003). PVA has been employed for different purpose in many different sectors including food, pocketing, medical, toys etc. (Gaaz et al., 2015). It also has good electrical properties owing this, PVA have big potential to

use electronic applications. Many researchers focused on this polymer to investigate how PVA or PVA based composites could be used as new material on the electronic application. There many work about PVA for different field. For example Bhargav and his friends studied about electronic properties of PVA:NaF polymer electrodes for electrochemical applications (Bhargav, Mohan, Sharma & Rao, 2009). Miaudet and his colleagues investigated the thermo-electrical properties of PVA-nanotube composites. Bin and hic coworker studied on Morphology and mechanical and electrical properties of oriented PVA–VGCF and PVA–MWNT composites (Bin, Mine, Koganemaru, Jiang & Matsuo, 2006) and there are many other studies. Various properties of PVA was given in Table 2.2

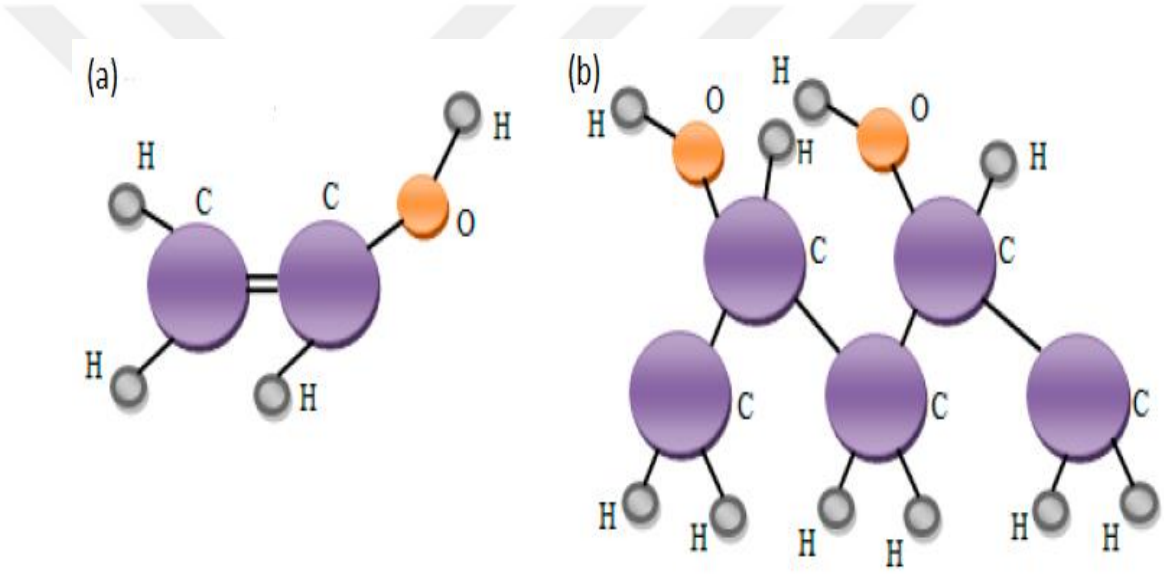

Figure 2.7 (a) structure of vinyl alcohol; (b) structure of poly vinyl alcohol (Baker, Walsh, Schwartz & Boyan, 2012)

PMMA; poly(methyl methacrylate) is one of the most common used polymer among the Poly (methacrylates). Poly(methyl methacrylate) or poly (methyl 2-methylpropenoate) is the polymer of methyl methacrylate, The chemical formula of PMMA is $(C_5H_8O_2)_x$. Other name of this polymer is methyl methacrylate resin. PMMA can be obtained free-radical polymerization of methyl methacrylate in mass (when it is in sheet form) or suspension polymerization as shown in Figure 2.8.

Table 2.2 Various properties of PVA

Property	Value
Electrical Resistivity	10^{15} - 10^{16} Ω.cm
Density	1.19-1.31 g/cm3
Dielectric Constant	2 - 4
Loss factor, 20°C, 1000 Hz, 60% humidity	0.05
Glass Transition Temperature	85 °C
Melting Point	200 °C
Transmission	85 - 93 %
Refractive Index	1.52-1.55

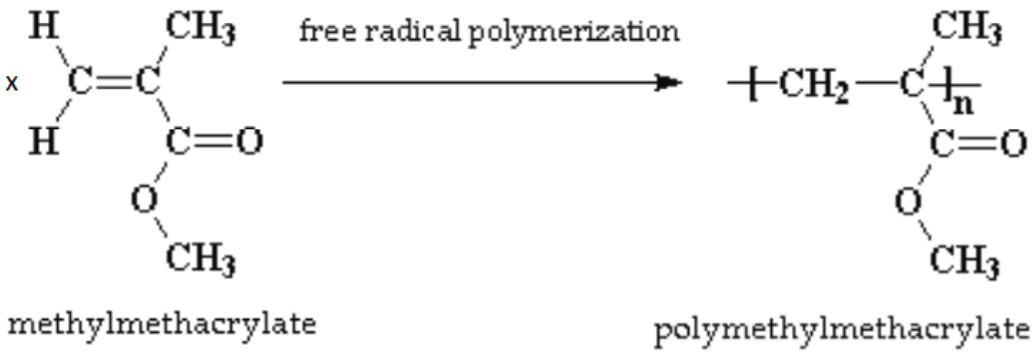

Figure 2.8 Polymerization of methyl methacrylate

PMMA is a linear thermoplastic polymer. PMA has a lack of methyl groups on the backbone carbon chain. PMMA has good mechanical properties such as high Young's modules and mechanical strength, low elongation at break. It also one of the hardest thermoplastic polymers owing this future it shows highly starch resistive characteristic. On the contrary of the PVA, PMMA is not too sensitive to humidity. So that it exhibits low water absorbing capacity which made it has good dimensional stability. Various physical properties of PMMA is listed in Table 2.3 (Ali, Karim & Buang, 2015).

PMMA cost effective and general purpose material. It have been used many different areas such as optic, vehicles, electrical engineering, medicine (Goseki &

Ishizone, 2015). PMMA take attention because of these unique properties. Particularly electronic properties of this polymer attracted scientist. Many researches have been done about PMMA its composite structures. For instance Zhen and his friends focused on conductivity and dielectric properties of PMMA (Zheng & Wong, 2003). Chen and his coworker studied about conductive properties of PMMA/graphite nanocomposite (Chen, Weng, Wu & Wu, 2003). Bohnke and his colleagues galled PMMA into lithium electrodes and investigate electrical properties of this structure (Bohnke, Frand, Rezrazi, Rousselot & Truche, 1993).

Table 2.3 Various properties of PMMA (Ali et al., 2015)

Property	**Value**
Electrical Resistivity	10^{14} - 10^{15} Ω.cm
Density	1.188 g/cm^3
Dielectric Constant	2.8 - 4
Loss factor, 20°C, 1000 Hz, 60% humidity	0.04
Glass Transition Temperature	110 to 120 °C
Melting Point	220-240°C
Transmission	80 - 93 %
Refractive Index	1.490 - 1.498

2.2 Nanocomposites

The field of composite involves the study of multiphase material including more than one phase. However nanocomposite means that where at least one of the constituent phases has one dimension less than 100 nm. This definition includes porous media, colloids, gels and copolymers. Size limits for these effects have been proposed, <5 nm for catalytic activity, <20 nm for making a hard magnetic material soft, <50 nm for refractive index changes, and <100 nm for achieving superparamagnetism, mechanical strengthening or restricting matrix dislocation movement (Sinirlioğlu, 2010)

The promise of nanocomposites lies in their multifunctionality, the possibility of realizing unique combinations of the mechanical, electrical, thermal, optical, electrochemical, catalytic properties which is unachievable with one of the individual component. The multifunctional behavior for any specific property of the material is often more than the sum of the individual components. Both simple and complex approaches to creating nanocomposite structures exist. Yet there are tremendous challenges in reaching this promise. They include control over the distribution in size and dispersion of the nano size components, tailoring and understanding the role of interfaces between structurally or chemically dissimilar phases on bulk properties (Ajayan, Schadler & Braun, 2006).

In nanoscale materials length scale is very important because it is possible to control the fundamental properties of materials such as their melting temperature, magnetic properties, charge capacity and even their color, without changing the materials chemical compositions. The main reason behind why nanoscale materials exhibit different properties from bulk ones is exceptionally high surface area to volume ratio of the reinforcing phase and its exceptionally high aspect ratio. The reinforcing material can be made up of particles (e.g. minerals), sheets (e.g. exfoliated clay stacks) or fibers (e.g. carbon nanotubes or electrospun fibers). In Figure 2.9, two type of nanocomposite structure are represented respectively nanoparticle and nanofiber. The area of the interface between the matrix and reinforcement phase(s) is typically an order of magnitude greater than for conventional composite materials. The matrix material properties are significantly affected in the vicinity of the reinforcement Additive of the nanomaterials into a matrix may result in enhanced optical properties, dielectric properties, heat resistance or mechanical properties such as stiffness, strength and resistance to wear and damage (Sinirlioğlu, 2010).

This large amount of reinforcement surface area means that a relatively small amount of nanoscale reinforcement can have an observable effect on the macroscale properties of the composite. For example, adding carbon nanotubes improves the electrical and thermal conductivity. Other kinds of nanoparticulates may result in

enhanced optical properties, dielectric properties, heat resistance or mechanical properties such as stiffness, strength and resistance to wear and damage. In general, the nano reinforcement is dispersed into the matrix during processing. The percentage by weight (called mass fraction) of the nanoparticulates introduced can remain very low (on the order of 0.5% to 5%) due to the low filler percolation threshold, especially for the most commonly used nonspherical, high aspect ratio fillers (e.g. nanometer-thin platelets, such as clays, or nanometer-diameter cylinders, such as carbon nanotubes). Nanomaterial additives can provide in comparison to both their conventional filler counterparts and base material. Properties which have been shown to undergo substantial improvements include:

a) Mechanical properties e.g. strength, stiffness, modulus and dimensional stability (Tjong, 2006).

b) Thermal stability (Petersson, Kvien & Oksman, 2007).

c) Flame retardancy and reduced smoke emissions.

d) Chemical resistance (Croce et al., 1999).

e) Electrical conductivity (Chen et al., 2011).

f) Optical properties (Sanchez, Lebeau, Chaput & Boilot, 2003).

g) Permittivity (Singha & Thomas, 2008).

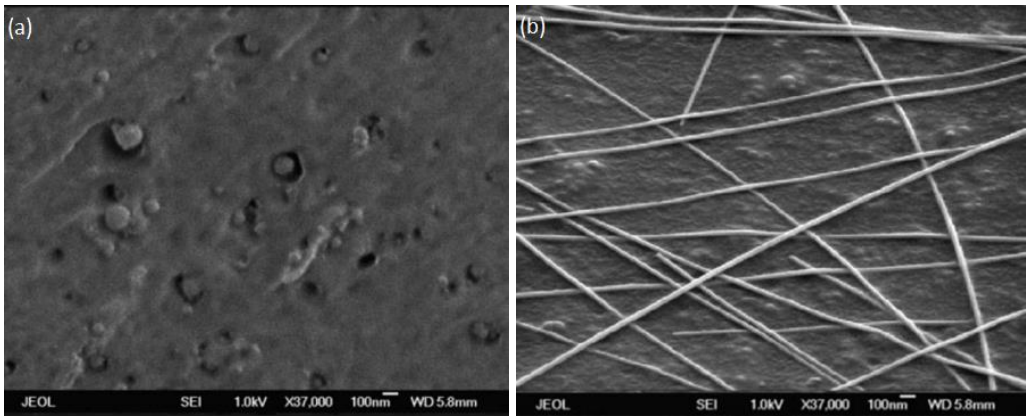

Figure 2.9 Field-emission electron micrograph showing cavitation surrounding weakly bound (a) nanoscale alumina particles (b) silver nanowire in PMMA (Ajayan et al., 2006).

2.2.1 Polymeric Nanocomposites

Recently lots of research works on polymeric nanocomposites are going on around the globe because of their application potential in many different areas due to

their ability to combine the properties of both polymers and dopants. To further enhance the properties of the polymer, the addition of an inorganic material is advantageous for forming a composite (Tintu et al., 2010).

Polymeric nanocomposites are a polymer or copolymer having dispersed in its nanoparticle. Main feature of polymeric nanocomposite, in contrast to conventional composites, is that the reinforcement is on the order of nanometer deeply affected final macroscopic properties. To reinforce polymers, it is common to physically disperse in the polymeric host inorganic fillers chosen from a variety of different shapes, such as fibers(Olson, Piris, Collins, Shaheen & Ginley, 2006), particle (Wang, Xia & Zhang, 2001), platelets or spheres (Kalaitzidou, Fukushima & Drzal, 2007). This approach attempts to combine acceptable processibility typical of thermoplastic polymers with desired characteristics from the inorganic filler, such as high modulus, high oxidation resistance, or high use temperature. Ideally, the resultant properties represent not only the volumetric averaging of contributions from individual components, but also the synergic effects of the components included. In such cases, the improvement of physical properties can often be found at relatively lower filler inclusion.

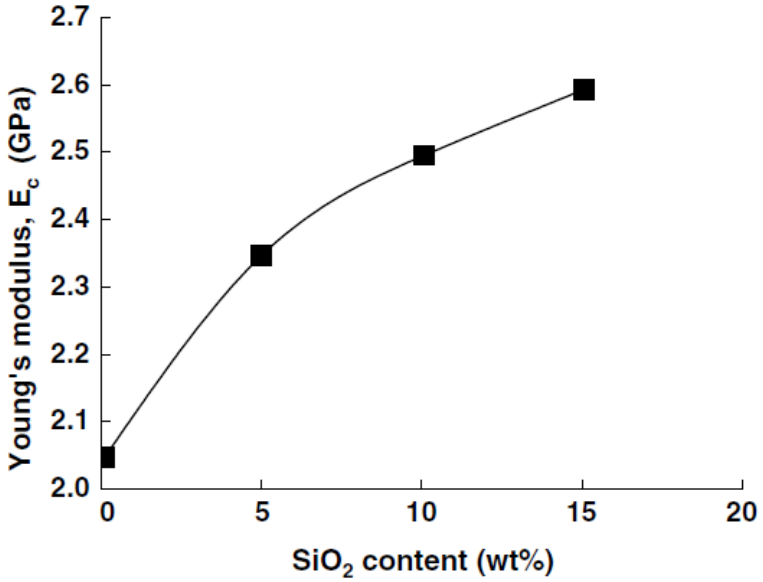

Figure 2.10 Tensile modulus of nylon 6 nanocomposites as a function of SiO_2 particle content (Fu, Feng, Lauke & Mai, 2008)

As the filler is decreased to smaller than 100 nm, the resulting composites, termed nanocomposites, may achieve dramatic improvements in such physical properties as gas barrier, thermal stability, elastic modulus, and ultimate mechanical properties (Andrady, Merkel & Toy, 2004; Vollenberg & Heikens, 1989). In Yun-Fu work, it was observed that mechanical properties of nylon 6 could be enhanced by adding SiO_2 particle. Figure 2.10 depicts Young's modulus of nylon 6/SiO_2 composite structure depending on SiO_2 content. Such substantial enhancement can be attributed mainly to the filler particle surface properties and interfacial interactions that become increasingly important with decreasing particle size. Nanofillers exist in various shapes, such as spherical metallic particles and semi-conductive particles (Balazs, Emrick & Russell, 2006; Shenhar, Norsten & Rotello, 2005; Vaia & Maguire, 2007), layered and fibrous nanofibers (Barnes, Sell, Boland, Simpson & Bowlin, 2007) and carbon nanotubes (Barnes et al., 2007; Thostenson, Ren & Chou, 2001).

The physical properties exhibited by polymeric nanocomposites are determined by the quality and the nature of dispersion of the nanofillers in the polymer matrix. However, it is known that the surface energy substantially increases with the decrease of particle size. Consequently, nanoparticles tend to aggregate in order to reduce the total surface energy, creating a pervasive manufacturing challenge. To ameliorate this problem, nanoparticles are often grafted or otherwise modified with organic groups (commonly alkyl ammonium surfactants) similar or compatible with the polymer matrix, followed by melt-mixing or in-situ polymerization(Drazkowski, Lee & Haddad, 2007). The resulting materials feature microstructure and properties that are quite sensitive to processing conditions. The complexities mentioned concerning "top-down" nanocomposites processed by dispersion, coupled with the fact that the size scale of fillers approaches the molecular scale, present the need for a synthetic approach utilizing nanoscale monomers that would naturally disperse and feature covalent incorporation. Polymer-inorganic nanocomposites that combine the advantages of inorganic and organic materials often exhibit unexpectedly improved properties. The properties of polymer composites depend on the type of incorporated nanoparticles, their size and shape, their concentration and interactions with the polymer matrix. During the last decade, many nano sized clusters involving clay

layered silicates, carbon nanotubes have been developed to prepare polymer-inorganic hybrids.

2.3 Sol-Gel Process

The sol-gel process is a wet chemical technique that uses either a chemical solution or colloidal particle to produce integrated network which called gel. Sols are dispersions of colloidal particles in a liquid. Colloids are solid particles with diameters of 1-100 nm. A gel is an interconnected, rigid network with pores of submicrometer dimensions and polymeric chains whose average length is greater than a micrometer (Hench & West, 1990).

Metal alkoxides and metal chlorides are typical precursor for sol-gel process. In general sol-gel process consists of three steps, hydrolysis and polycondensation of alkoxide or nitrate precursors, followed by gelation, drying and sintering. Sol-gel precursors undergo chemical reaction with solvents and the other species present in the solution. One of the most efficient models used to predict those reactions is the Partial Charge Model. Various atomic or molecular groups called ligands can bind to a complex C or cation M either directly or by substituting another ligand. The mechanism of the transformation depends on the partial charge of the different atoms in the species. Those with a negative partial charge are nucleophilic, and those with a positive charge are electrophilic. Similarly, in a substitution reaction, the new ligands with the highest partial charge is the nucleophile while the group in the metal complex with the highest positive charge is the leaving group (Pierre, 2013).

2.3.1 Hydrolysis and Condensation Reaction

Hydrolysis can be expressed by deprotonation of a solvated M cation and it consists in the loss of a proton by one or more of the water molecules that surrounds the M in the first solvation shell during hydrolysis process. As a consequence, the aqua ligand molecule, H_2O that is bonded to the metal is either transformed into an

hydroxo ligand, OH^-, if only one proton leaves, or into an oxo ligand O^{-2}, if two protons detaches.

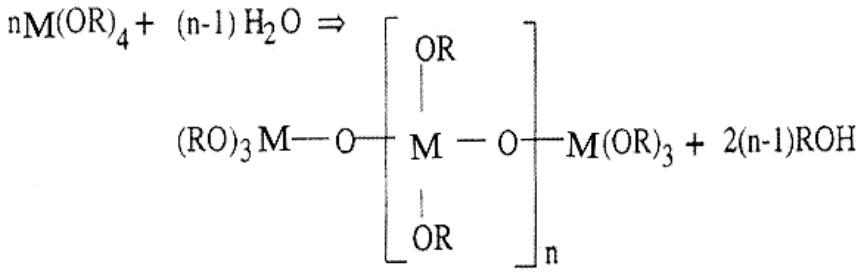

(Hydrolysis) (2.9)

After hydrolysis, condensation reaction occurs to form a polynuclear complex consisting of two metal atoms. Condensation, in aqueous solutions, is the result of either an olation or an oxolation reaction. In either case, one must be quite careful as the oxygen present sometimes speeds the reaction to a point where it becomes necessary to work in the neutral atmosphere of argon in order to control it (Pierre, 2013). In the first case, transfer of the H to an OR ligand according to the reaction below (olation process);

$$2M(OR)_{x-1}(OH) \longrightarrow M_2O(OR)_{2X-3}OH + ROH \quad (2.10)$$

In the second case, transfer of the H to an OH group according to Reaction (2.11), condensation is called oxolation.

$$2M(OR)_{x-1}(OH) \longrightarrow M_2O(OR)_{2X-3}+H_2O \quad \text{(Condensation)} \quad (2.11)$$

Hydrolysis and condensation both keep on going thus gradually building up a tridimensional network that, at the end, often forms a solid phase. This process is accelerated by heat as the rate of the both reactions increases together with the temperature. Since the kinetics of hydrolysis and condensation, and hence the overall reaction and the type of polymers formed, depends on the pH, a great variety of materials with different structures can be obtained. These include linear polymers as

well as dense colloidal particles and smaller ones with more or less weakly bonded cross-linked clusters of polymers (Pierre, 2013).

2.3.2 Gelation

Gelation is a process according to which a sol or solution, transforms to a gel. It consists of establishing links between the sol particles or the solution molecules so as to form 3-dimensional solid network. Gelation occurs when the extent of polymerization reactions ξ reaches a critical value ξc. This precise critical stage, when for the first time a polymer of infinite size is formed by comparison with the molecular scale, defines the gel point. In a practical manner, at this point the product resulting from polymeric condensations transforms suddenly from a viscous liquid to a material with elastic properties (Pierre, 2013).

Gelation can be described in a more abstract fashion within the frame work of critical phenomena in thermodynamics in particular by the percolation theories. The most simple of the percolation models is isotropic such as the bond percolation and the site percolation (Figure 2.11). In these models, either a bond is established or a site is occupied with probability p, in a completely random fashion throughout a geometrical network (Pierre, 2013).

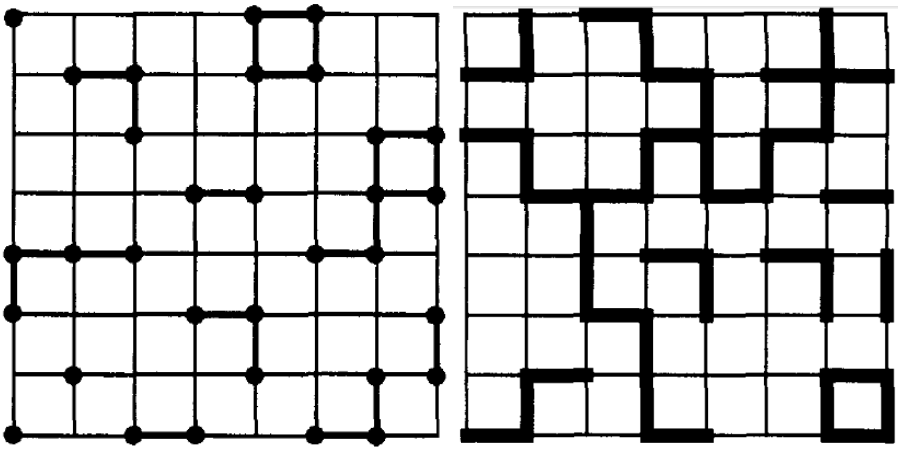

Figure 2.11 (a) Site percolation and (b) bond percolation on a square bi-dimensional network (Hench & West, 1990).

2.3.3 Drying and Sintering

Drying is irreversible transformation of the gel which is composed of a solid network and liquid matrix. The capillary mechanism explains well the reproducible adsorption hysteresis curves of water in silica gels. This mechanism can be summarized as follows:

- Evaporation creates a liquid vapor meniscus at the exit of pores in the gel.
- This induces a hydrostatic tension in the liquid, which is balanced by an axial compression on the solid.
- The latter compression makes the gel shrink.
- As a result of shrinkage, more liquid is fed to the menisci at the exit of the gel pores, where it is evaporated and so on (Pierre, 2013).

The specific surface area of the porosity is an evolution named sintering. Sol-gel ceramics just after drying and even after heat treatments at intermediate temperatures often have a very high specific surface area and an extremely small grain size. Since states with a lower Gibbs free energy are more stable at a given temperature and pressure, the specific surface area should tend to decrease, an evaluation which can proceed according to two types of pore evaluation: (a) by changing the shape of pores but not their volume and (b) by eliminating the pores. Hence, the dense materials can be obtained after the sintering process (Pierre, 2013).

2.4 Spin Coating

Homogeneity and uniformness of thin film is significant parameter for many different applications such as MEMS and IC circuit. Spin-coating technique is one pf the easiest process to do this. In this process, solution is first deposited on the desired substrate, and then the substrate is accelerated rapidly to the one rotation rate. Liquid flows radially, owing to the action of centrifugal force, and the excess is ejected off the edge of the substrate. The film continues to thin slowly until disjoining pressure

effects cause the film to reach an equilibrium thickness or until it hardens due to a dramatic rise in viscosity from solvent evaporation. The final thinning of the film is then solely due to solvent evaporation (Lock, Walton & Fernsler, 2008).

The dynamics of spin coating process very complex because corporation of fluid rheology and solvent evaporation resulting make mathematically modeling of it extremely challenging A simple model first proposed by Meyerhofer has been found to capture much of the essential characteristics of the spin coating process even though it decouples evaporation and flow. The film thinning process is treated as occurring through two distinct stages. In the first stage, film thinning is only due to radial outflow. The second stage in which all thinning is due to solvent evaporation is entered (Meyerhofer, 1978).

However there are many experimental study about the film thickness of polymeric films. Two of them is depicted Figures 2.12 and 2.13. In this figure the film thickness of polystyrene and poly methyl methacrylate film with different concentration are shown (Hall, Underhill & Torkelson, 1998).

As it can be seen that in Figures 2.12 and 2.13 the film thickness decrease with increasing rotation speed. For instance when 1 wt % PS solution is rotated on desired substrate at 500 rpm, the film thickness of it is 90 nm. On the other hand the same solution rotated at 3000 rpm, the film thickness decreased to 10 nm. In addition the concentration of the polymer solution effects the thickness. When more concentrated solution is used the film will be thicker. As it evident in Figure 2.12,the PS film coated at using 1 wt % and 10 w t% is approximately 8 nm and 2000 nm respectively. This is because of the viscosity of the solution. Increasing viscosity cause increasing force between the polymer molecules in solution and make it stronger against the centrifugal force. The same phenomenon is valid for PMMA film. In Figure 2.13 film thickness of PMMA prepared with different concentration versus spin speed was depicted (Hall et al., 1998).

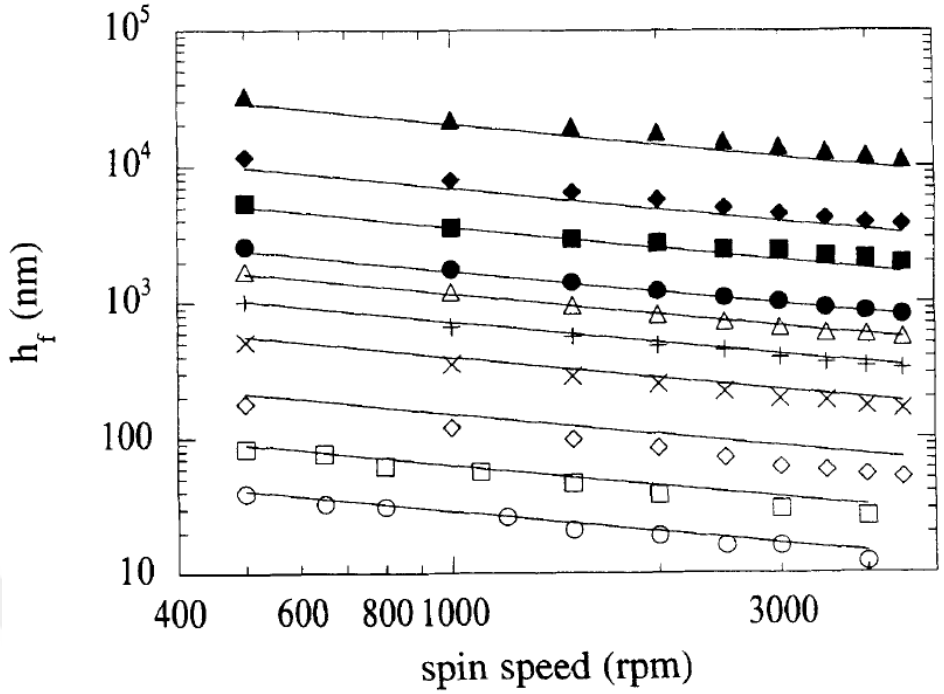

Figure 2.12 Film thickness, h_f as a function of spin speed and initial polymer solution concentration for PS in toluene: (O) 0. 5 wt%. (□)1 wt%. (◊) 2 wt% (X) 4 wt%, (+) 6 wt%, (Δ) 8 wt%, (●) 10 wt%, (■) 15 wt%, ( ) 20 wt%, and (▲) 30 wt% (Hall et al., 1998).

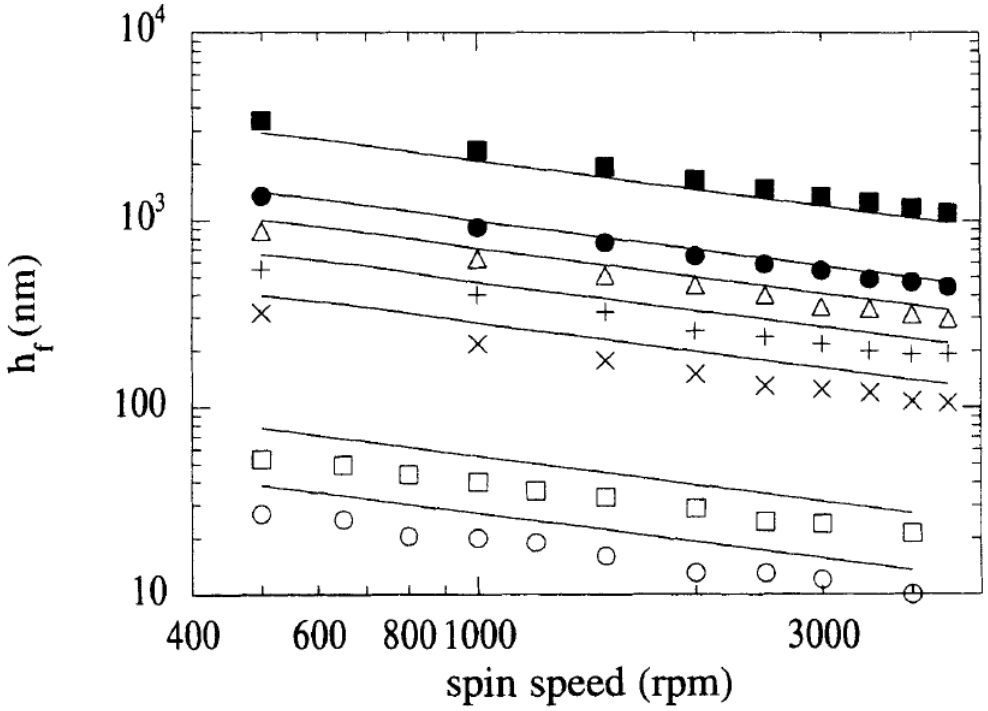

Figure 2.13 Film thickness, h_f as a function of spin speed and initial polymer solution concentration for PMMA in toluene: (O) 0. 5 wt%. (□)1 wt%. (◊) 2 wt% (X) 4 wt%, (+) 6 wt%, (Δ) 8 wt%, (●) 10 wt%, (■) 15 wt% (Hall et al., 1998).

Repeatability is an important factor for spin coating process. Subtle parameters can cause dramatic differences in coated films. Figure 2.14 show the process of a typical spin coating. Typical spin coating process consists of two steps which are high speed spin.to get thinner solution region after the dispensing of the fluid on the substrate and drying step to eliminate excess solvents from the resulting film. There are two common approach to dispense the fluid; static dispense and dynamic dispense. In static dispense, a small puddle of the fluid which may be 1-10 cc is deposited on substrate surface and start the rotate. However dynamic dispense is the process of depositing of the fluid whilst the substrate is rotating at approximately 500 rpm (Ebeoğlugil, 2011).

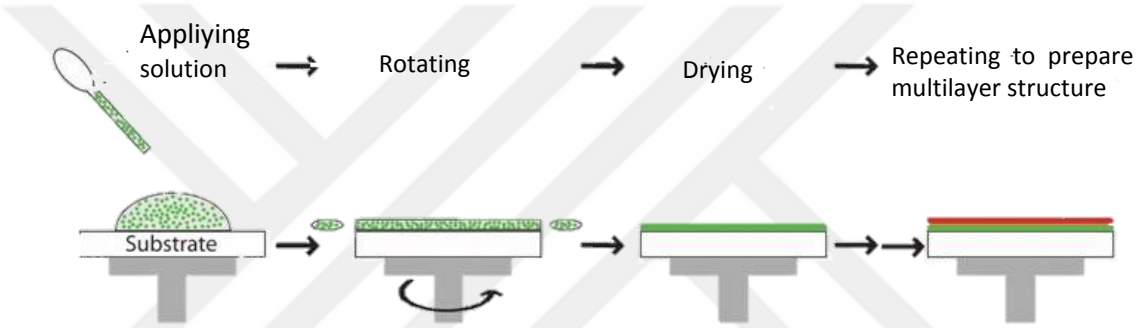

Figure 2.14 Schematic illustration of typical spin coating process

2.5 Wafer Cleaning

Since 1950s the scientist has noticed how important substrate surface should be clean. With the increasing requirement of high performance and reliable devices, VLSI and ULSI silicon circuit technologies became more important. Deeply the way used to avoid contamination has become significantly important. Especially sodium ions metals and particles which is known as trace impurities is detrimental if exist in semiconductor during fabrication process. Impurities must also cleaned from the wafer surfaces before the low temperature process such as dopant implanting, chemical vapor deposition, plasma reactions. After low temperature process remained impurities could be very critical at high temperature processes which is thermal oxidation, diffusion, epitaxial growth) because they may spread and diffuse into the semiconductor interior (Kern, 1990).

Many wafer cleaning techniques have been tested and several are being used. The generally most successful approach for silicon wafers without metallization uses wet chemical treatments based on hydrogen peroxide chemistry. This process has remained essentially unchanged during the past 25 years, but important advances have been made in its technical implementation. During the early stages of silicon wafer processing until about 1970, one used organic solvent extraction, boiling nitric acid, aqua region, concentrated hydrofluoric acid, and hot acid mixtures as cleaning chemicals. Mixtures of sulfuric acid-chromic acid led to chromium contamination and caused ecological problems of disposal. Mixtures of sulfuric acid and hydrogen peroxide caused sulfur contamination. Aqueous solutions containing hydrogen peroxide had long been used for cleaning electron tube components but not for semiconductors. In general, impurity levels and particles in process chemicals were high and in themselves tended to lead to surface contamination. Particulate impurities were removed by ultrasonic treatment in detergent solutions or by brush scrubbing. The first caused frequent wafer breakage and the second often deposited more debris from the bristles than it removed from the wafer surfaces (Kern, 1990).

The first systematically developed cleaning process for bare or oxidized silicon wafers was based on a two-step oxidizing and complexing treatment with hydrogen peroxide solutions: (i) an alkaline mixture at high pH followed by (ii) an acidic mixture at low pH. The choice of chemicals was based on reaction chemistry, oxidation potentials, reagent purity, reagent volatility, safety, and economy. The process was developed at RCA, introduced to device production in 1965, and published in 1970 (Kern, 1970). In the first treatment step the wafers are exposed to a hot mixture of water-diluted hydrogen peroxide and ammonium hydroxide. This procedure was designed to remove organic surface films by oxidative breakdown and dissolution to expose the silicon or oxide surface for concurrent or subsequent decontamination reactions. Group IB and IIB metals and several other metals, including gold, silver, copper, nickel, cadmium, zinc, cobalt, and chromium, are dissolved and removed by the complexing effectiveness of ammonium hydroxide; copper, for example, forms the $Cu(NH3)_4^{+2}$ amino-complex. The second treatment step exposes the rinsed wafer to a hot mixture of water-diluted hydrogen peroxide

and hydrochloric acid. This procedure was designed to remove alkali ions, and cations such as $A1^{+3}$ Fe^{+3} and Mg^{+2} that form NH_4OH- insoluble hydroxides in basic solutions. This second step also eliminates metallic contaminants that were not entirely removed by the first treatment, such as gold. Electrochemical displacement replating of heavy metals from the solution is prevented by formation of soluble complexes with the dissolved metal ions (Kern, 1990).

The method above is known "RCA Standard Clean". This is still the primary method used in the industry. RCA method is also can be used for relatively small application such as experimental process in a laboratory.

CHAPTER THREE
EXPERIMENTAL STUDIES

3.1 The Aim of Thesis

Over past decades lots of research works on nanocomposite structures because of their potential of applicability in many different fields, fuels cells, photonic application, EM detectors, thin film transistors. In this thesis we tried to produce new type of composite materials which have unique properties and easy to apply different dielectric application. We manufactured different type ceramic nanoparticles that are TiO_2 by sol-gel method to add into different type polymer matrix which are PVA and PMMA. Then these composite structures were formed as thin film. With this respect TiO_2 ceramic nanoparticles were separately added into prepared different polymer solutions with different weight ratio. The aim of this thesis is to clarify preparation, characterization, development and application of polymeric nanocomposite film using as a combination of colloidal suspension using spin coating system. The new approach is to explore both the science and technology of how nanoparticles affect polymer structure and connect the results to materials properties, and show the engineering concepts that can be used to produce or improve an electronic device by design.

To obtain optimum parameters for produce nanocomposite thin film, sol-gel derived nanoparticles were added into polymer matrix with different ratio. Before the spin coating process Si wafer substrate were cleaned using solvent clean + RCA01 + HF dip method (details of cleaning procedure were discussed in later part of thesis.) In order to use suitable process regime and to define chemical structure and reaction type of intermediate temperature products, DTA-TG and FTIR analyses were performed in the powder production using xerogels produced at different temperatures. XRD device was employed to determine phase structure of ceramic nanoparticles and composite structure. Colloidal suspensions including TiO_2 nanoparticles were produced and nanocomposite thin films were formed on the silicon substrate by cost effective spin coating technique. Surface morphologies of

the films were investigated using SEM and AFM. Thickness measurements of the films were investigated through profilometer. Dielectric properties of the nanocomposite films were determined using Dielectric Analyzer.

3.2 Materials

3.2.1 Substrate Preparation

To get Si wafer substrate, firstly Si ingot was manufactured by Czochralski technique. PVA Tepla Czochralski device in Dokuz Eylül University Center for Fabrication and Application of Electronic Materials was employed for this mission. In this technique High-purity, semiconductor-grade silicon (only a few parts per million of impurities) is melted in a crucible at 1425 degree Celsius, usually made of quartz. Dopant impurity atoms such as boron or phosphorus can be added to the molten silicon in precise amounts to dope the silicon, thus changing it into p-type or n-type silicon, with different electronic properties. A precisely oriented rod-mounted seed crystal is dipped into the molten silicon. The seed crystal's rod is slowly pulled upwards and rotated simultaneously. By precisely controlling the temperature gradients, rate of pulling and speed of rotation, it is possible to extract a large, single-crystal, cylindrical ingot from the melt. Occurrence of unwanted instabilities in the melt can be avoided by investigating and visualizing the temperature and velocity fields during the crystal growth process (Aleksic, Zielke & Szymczyk, 2002). This process is normally performed in an inert atmosphere, such as argon, in an inert chamber, such as quartz.

After Silicon ingot manufactured ingot, the ingot should be sliced by diamond wire saw by using STX-1202 system. During this process speed of diamond wire affects the wafer surface. There are two speed of the system that should be take account in to get optimum result one of these speed is rotation speed, other is feed speed. With this respect optimization studies should be done. After slicing wafer should be lapped and polished to be coated. For this step of substrate preparation two consumables were used which are 9 micron Al_2O_3 particles for lapping process and

Ce_2O_3, colloidal silica for polishing. Optimum parameter for Wafer slicing, laping and polishing process in our study is showed Table 3.1.

Table 3.1 Optimum parameter to prepare Si substrate

Operation	Drum Rotation speed	Feed rate	Plate rotation rate	Consumables
Slicing	5 m/s	1mm/min	-	Diamond Wire
Lapping	-	-	40 rpm	9 micron Al_2O_3
Polishing	-	-	70 rpm	3 micron Ce_2O_3, Colloidal silica

3.2.1.1 Substrate Cleaning

First of all surface of the substrate must be cleaned. It is necessary to avoid any impurity on the substrate. There also should not be any chemical interaction at the interface between coating and substrate due to the fact that it influences device performance. Prepared Silicon wafer were cleaned by solvent clean, deionized water rinse, RCA clean, deionized water rinse, HF dip and deionized water rinse and lastly blow dry respectively.

The materials that is needed for silicon wafer cleaning process is listed below

- Acetone
- Methanol
- Ammonium hydroxide
- Hydrogen peroxide
- Dilute (2%) hydrofluoric acid
- Distilled water

Solvent clean

In this step of wafer cleaning acetone was used as a solvent. Acetone can clean oils and organic residuals on the wafer surface but acetone is also leave its own

residual on the wafer. This is why a two-solvent method is used. Acetone and methanol was poured different container separately. Container with acetone was warmed up 55 ^{o}C degree and silicon wafer put into acetone bath. The silicon wafers was placed in acetone 10 min. Then wafer was removed and placed in methanol 2-5 min. Lastly they were rinsed with distilled water.

RCA-1 clean

RCA clean is used to remove organic residues from silicon wafers. During this proces, a thin oxide film forms on the wafer surface. The general recipe is for RCA-1 cleanser is:

325 ml DI water
65 ml NH_4OH (27%)
65ml H_2O_2 (30%)

First 325 ml distilled water and 65 ml NH_4OH (27%) mixed and heated up 70 ^{o}C degree and then 65ml H_2O_2 (30%) was added to this solution. Bobbling of the solution indicate that it is ready to use. Wafer was soaked the solution for 15 min. then removed from solution and rinsed distilled water from a tap.

HF dip

Hydrofluoric which is one of the strongest acids was used to remove native silicon dioxide from wafers. Because this acid very strong it should be used with diluted (2%). Wafers were soaked the solution for 2 min and removed and rinsed with distilled water.

3.2.2 Precursor Materials

In our study we synthesized ceramic filler which is TiO_2. As Matrix material PVA and PMMA was employed. Precursor materials were chosen from alkoxide-based chemical materials which can be easily dissolved in solvents for ceramic nanoparticle production. These precursors were diluted by different solvents which are generally alcohol-based liquids such as methyl alcohol, ethyl alcohol. Titanium (IV)

isopropoxide ($C_{12}H_{20}O_4Ti$, 97 %, Aldrich Chemistry) for production of TiO_2. As chelating agent Acetic acid, glacial $C_2H_4O_2$ was chosen to dissolve powder precursors. To prepare polymeric solution we used two different polymer respectively PVA ($[-CH_2CHOH-]_n$ Aldrich) PMMA ($[CH_2C(CH_3)(CO_2CH_3)]_n$ Aldrich). Solvent for polymers shows difference distilled water and Chloroform ($CHCl_3$ Aldrich) for PVA and PMMA respectively. In addition Non-ionic surfactant Triton X-100 *(Aldrich)* was used to get lower surface tension. Chemical materials which were employed for production of ceramic nanoparticle and polymeric solution are listed in Table 3.2, indicating chemical types, names, formulas and purity percentages.

Table 3.2 All chemicals used for production of TiO_2 powders and polymeric solutions

Material	Chemical Type	Chemical	Formula	Purity
Nano filler	Precursor	Titanium (IV) isopropoxide	$C_{12}H_{20}O_4Ti$,	97 %
	Solvent	Ethanol	C_2H_5OH	100 %
	Chelating Agent	Acetic acid, glacial	$C_2H_4O_2$	99.90 %
Polymeric solution	Granule	Poly (vinyl alcohol)	$[CH_2CHOH]n$	99 %
		Poly (metyl methacrylate)	$[CH_2C(CH_3)(CO_2CH_3)]n$	99 %
	Solvent	Chloroform	$CHCl_3$	99 %
		Distilled Water	H_2O	100 %
Suspension	Surfactant	Triton X-100	$C_{14}H_{22}O(C_2H_4O)_n$	100 %

3.3 Production Techniques

3.3.1 Powder Preparation

All solvent and chemicals were of analytical grade and were used without further purification. Precursors were weighed in appropriate amounts in the defined molar ratio to prepare Ti based solutions. Firstly, 3.052 ml of titanium (IV) isopropoxide was hydrolyzed in the 10 ml of absolute ethanol under magnetic stirring in order to get TiO_2 solution at room temperature. After stirring of the solution for 30 min, 1 ml glacial acetic acid was added into the solution.

Gelation, which is a process according to which a sol, or a solution, transforms to a gel, occurred within 1 day (24 hours) in these experiments. As solvent evaporate gel start to form. Gels were initially dried at room temperature, and followed by drying at 70 ^{o}C for 5 hours in air. TiO_2 based xerogels were produced after drying process.

3.3.2 Polymeric Solution Preparation

In this part there are two main solutions, these are PVA and PMMA based solutions. There different solution were prepared for each polymer which have different concentration which are 4 % wt, 2 % wt and 1 % wt for PVA and PMMA solution separately. Hydrolyzed PVA granules were dissolved in deionized water by heating 85 ^{o}C. 1 wt.% of Non-ionic surfactant Triton X-100 was than mixed with PVA solution to get lower the surface tension. The hot solution was stirred until the polymer was completely dissolved and a clear viscous solution is obtained. PMMA granules were dissolved in 100 ml chloroform. The polymer solution was stirred at 50 ^{o}C until the polymer was completely dissolved and a clear viscous solution is obtained. Table 3.3 shows materials which used to prepare the polymeric solution. Flow chart of the whole nanocomposite thin film process production was illustrated in Figure 3.1

Table 3.3 Materials which used to prepare the polymeric solution.

Solution Type	Solvent	Polymer Concentration	TiO_2 Nanofiller Ratio	Dispersant	Surfactant
PVA	Distilled Water	4 % wt	20 % wt of PVA	Methanol	Triton X-100
			10 % wt of PVA		
			5 % wt of PVA		
		2 % wt	20 % wt of PVA		
			10 % wt of PVA		
			5 % wt of PVA		
		1 % wt	20 % wt of PVA		
			10 % wt of PVA		
			5 % wt of PVA		
PMMA	Chloroform	4 % wt	20 % wt of PMMA	Methanol	----
			10 % wt of PMMA		
			5 % wt of PMMA		
		2 % wt	20 % wt of PMMA		
			10 % wt of PMMA		
			5 % wt of PMMA		
		1 % wt	20 % wt of PMMA		
			10 % wt of PMMA		
			5 % wt of PMMA		

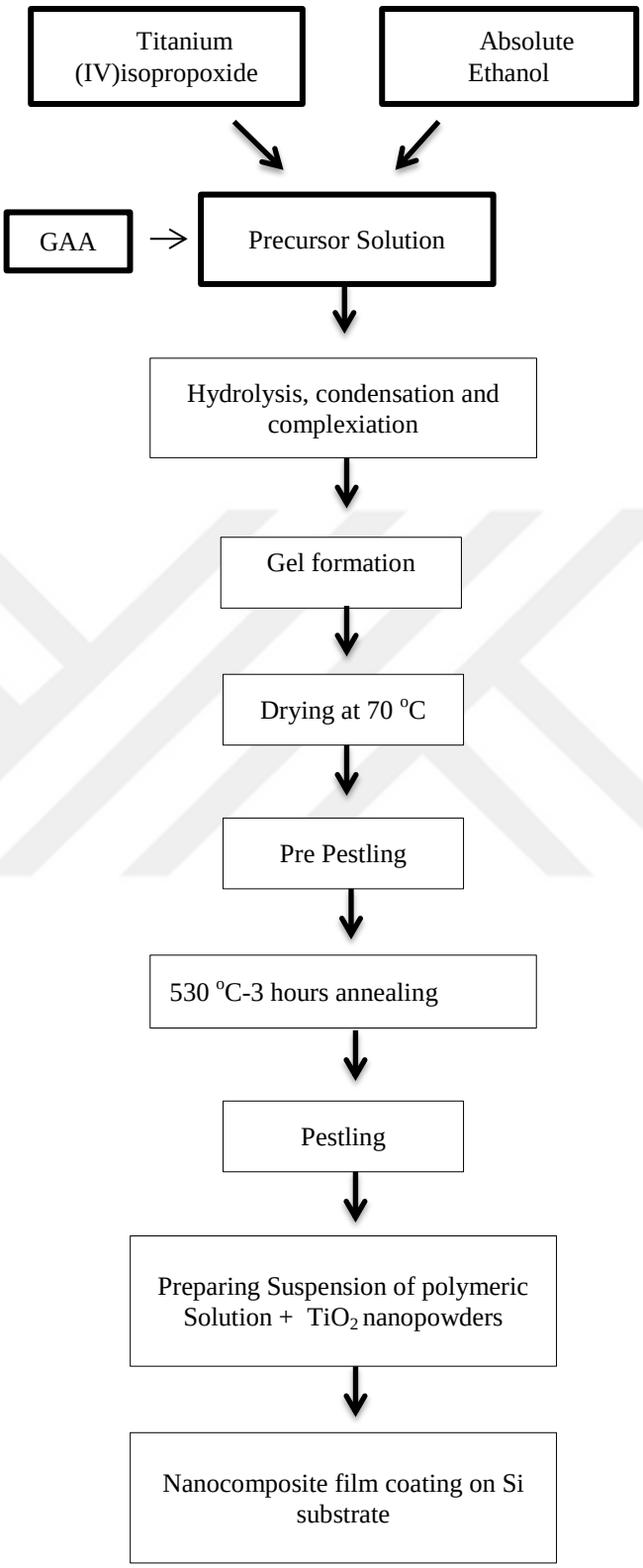

Figure 3.1 Flow chart preparation of Polymer/TiO_2 nanocomposite thin film

3.3.3 Milling

Sol-gel derived TiO_2 powders were milled in mortar for 30 minutes after drying process. This helps TiO_2 particle to sustain their size respectively smaller. Same process was carried out after heat treatment. Because after heat treatment it is possible that the particles aggregate to each other and form respectively larger particle which is submicron size. Pestling allows the particle to be nanometer size, otherwise the particle may precipitate in polymeric solution. Figure 3.2 depicts Pestling equipment with TiO_2 particle.

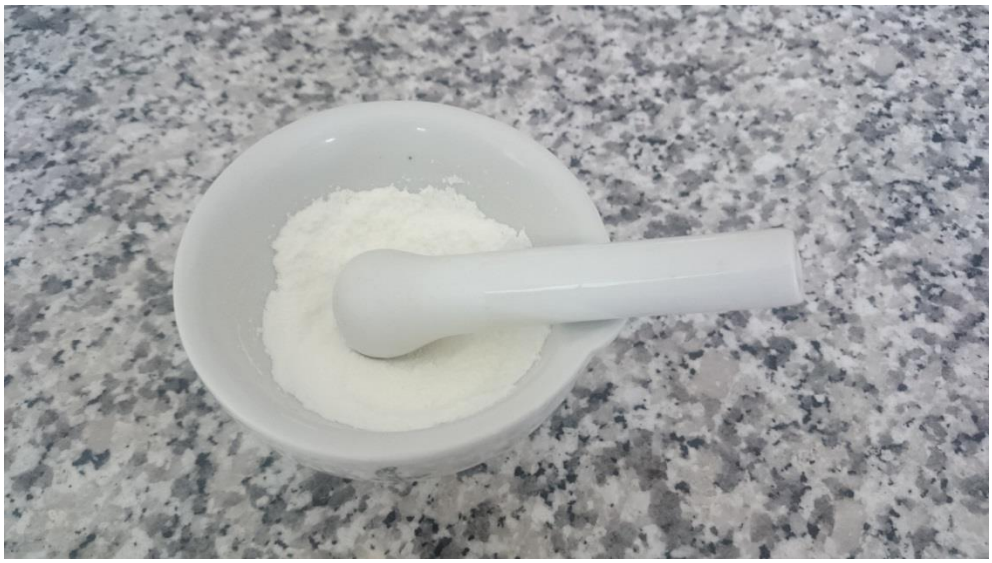

Figure 3.2 Milling equipment

3.3.4 Heat Treatment

A Lab Companion drying oven was used dry sol gel derived TiO_2 and evaporate the solvent of nanocomposite coating on Si substrate. Protherm box furnace in was effectively used for the calcining and annealing processes of TiO_2 powders. For the heat treatment regime of the samples, the temperature of the furnace was raised to 450 ^{o}C which is temperature of forming of anatase phase with heating rate of 10 ^{o}C/min and then kept at this temperature for 2 hours in air. End of this procedure, a cooling

process was performed to take out the powder samples from the tube furnace. The heating regime for the powders is illustrated in Figure 3.3.

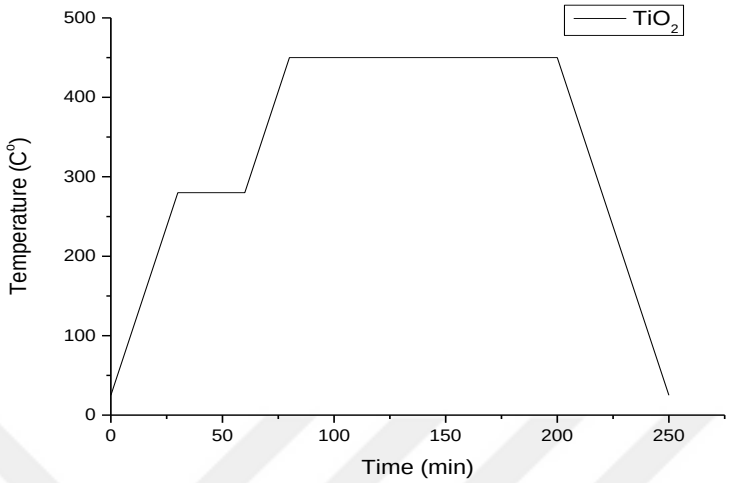

Figure 3.3 Heat treatment regime for TiO_2

3.3.5 Colloidal Suspension Preparation

To get colloidal suspension, firstly polymeric solution should be prepared. It was explained how polymeric solution prepared in previous sections. Before dispersing TiO_2 nanoparticles in PVA solution, they were suspended in methanol to avoid agglomeration in viscous PVA solution. Then 5 wt.%, 10 wt.% and 20 wt.% of TiO_2 nanoparticles suspended in methanol were mixed with PVA solutions. Final mixture was then sonicated 1 hour at room temperature. To disperse homogeneously TiO_2 in aqueous PVA solution ultrasonic probe was employed.

3.3.6 Spin Coating

The Polymer nanocomposite films were coated on Si substrate by using spin coater (Polos Spin150i) to get homogen film. Different spinning parameters such as spinning rate, acceleration time were used to control the film thickness in this system. Three different spinning rate including 2500 rpm, 5000 rpm and 7500 rpm was applied for dispersion whose polymer concentration is 4 % wt, 2 % wt and 1 %

wt which has 10 % wt TiO_2 nanofiller to determine optimum coating parameters. Table 3.4 shows spinning parameter for different polymer/TiO_2 dispersion.

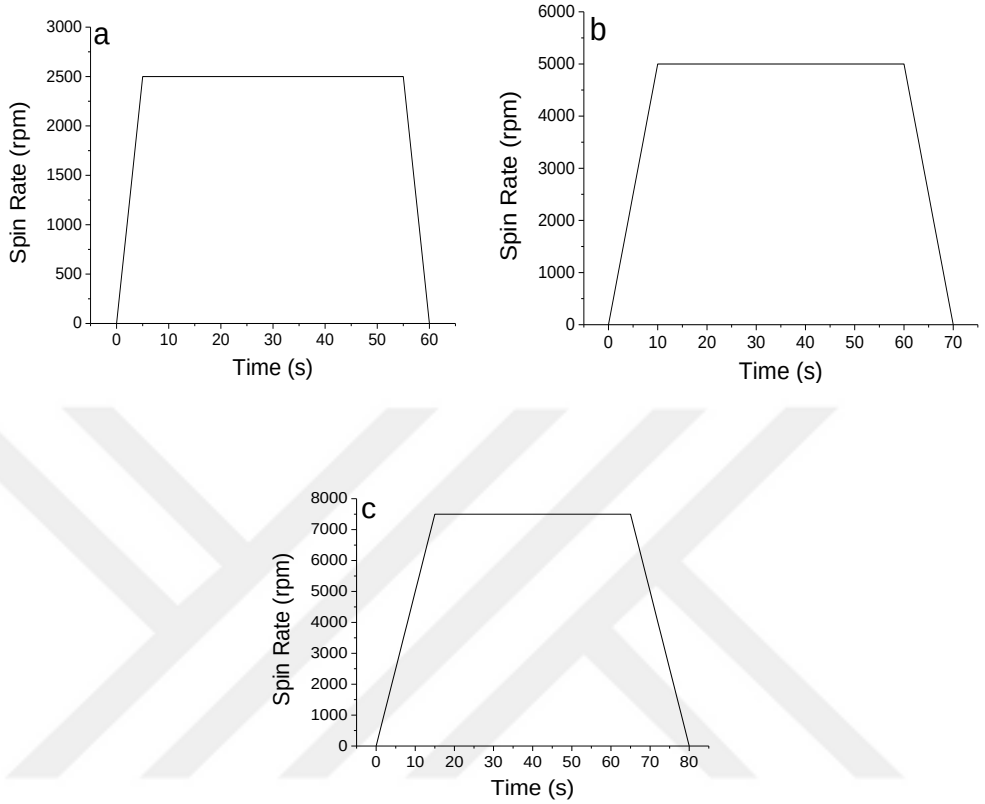

Figure 3.4 Spinning parameter (a) 2500 rpm, (b) 5000 rpm, (c) 7500 rpm max speed

There exists a unique relationship among deposition quality and solution parameters such as film thickness, wettability, viscosity, pressure etc. Each parameter is expected to improve surface quality depending on solution characteristics. As shown in Figure 3.4 (a), (b) and (c) the acceleration rate is 500 rpm/sec^2. 3 Different final spin rate such as 2500 rpm 5000 rpm and 7500 rpm was used to get optimum surface properties. The acceleration rate is kept same for 3 different spin rate. The total spinning time was 60, 70 and 80 second respectively. This means the device is spinned 50 second at 2500 rpm, 60 second at 5000 rpm, 70 second at 7500 rpm.

In spin coating process during acceleration period the dispersion was spread the surface of Si substrate. Further stage of spinning solution evaporated and color of

coating change because solution in the dispersion evaporated. Third step is the deceleration step which has same rate with acceleration.

Table 3.4 Spinning parameter for different polymer/TiO_2 dispersion.

Solution Type	TiO_2 Nanofiller Ratio	Polymer Concentration	Spin Rate	Total Spinning Time	Nomenclature
PVA in Distilled Water	10 % wt of PVA	1 % wt	2500 rpm	60 second	1PVA25
			5000 rpm	70 second	1PVA25
			7500 rpm	80 second	1PVA25
		2 % wt	2500 rpm	60 second	2PVA50
			5000 rpm	70 second	2PVA50
			7500 rpm	80 second	2PVA50
		4 % wt	2500 rpm	60 second	4PVA75
			5000 rpm	70 second	4PVA75
			7500 rpm	80 second	4PVA75
PMMA in Chloroform	10 % wt of PMMA	1 % wt	2500 rpm	60 second	1PMMA25
			5000 rpm	70 second	1PMMA50
			7500 rpm	80 second	1PMMA75
		2 % wt	2500 rpm	60 second	2PMMA25
			5000 rpm	70 second	2PMMA50
			7500 rpm	80 second	2PMMA25
		4 % wt	2500 rpm	60 second	4PMMA25
			5000 rpm	70 second	4PMMA50
			7500 rpm	80 second	4PMMA50

3.4 Characterization

3.4.1 Solution Characterization

In sol-gel process, different solution characteristic should be determined to obtain optimum final particle properties different characteristic of solutions should be determined. With this respect various characterization studies were done.

3.4.1.1 The Ph Measurement

The pH measurement refers to determination of the activity of hydrogen ions in an aqueous solution. Many important properties of a solution can be determined from an

accurate measurement of pH, including the acidity of a solution and the extent of a reaction in the solution.

Many chemical processes and properties, such as the speed of a reaction and the solubility of a compound, can also depend greatly on the pH of a solution. In this study HANNA HI83141 ph meter was used to determine pH values.

3.4.1.2 Turbidity Measurement

Turbidity (or the relative cloudiness of a liquid) measurement gives information about how clean solution we prepares using optical laws. Light is passed through the sample and is scattered in all directions because of the particles in liquid. The light that is scattered at a 90° angle to the incident light is then detected by a photo diode and is converted into a signal linearized by the analyzer and displayed as an NTU (Nephelometric Turbidity Units) value. The more suspended particles there are in a liquid, the more light will be scattered, resulting in a higher NTU value. In the experiment, turbidity measurements of the prepared precursor solutions were performed by using TB1 Turbidimeter.

3.4.1.3 Fourier Transform Infrared Spectroscopy (FT-IR)

Fourier Transform Infrared (FTIR or IR) spectroscopy is an analytical technique which is used to measure the absorption of various infrared light wavelengths of organic or inorganic materials of interest. The infrared absorption bands identify the specific molecular components or structures. The infrared light vibrates the chemical bound in the materials. The vibrational motions of the chemical bond show frequencies in the infrared regime. The IR spectrum can be generally divided into three frequency (or wavenumber/wavelength) regions: the far IR (10~400 cm^{-1}), the middle IR (400~4,000 cm^{-1}) and the near IR (4,000~14,000 cm^{-1}), with the middle IR region being employed in most IR spectroscopic investigations. In our study Perkin Elmer Spectrum BX instrument equipped with ATR apparatus in the spectra range between 4000 and 650 cm-1 with a resolution of 4 cm^{-1}. (400~4,000 cm^{-1}) range was

used to get IR spectrum of PVA, PMMA, and TiO_2 nanocomposite of these two polymer.

3.4.2 Material Characterization

3.4.2.1 Differential Thermal Analysis- Thermal Gravimetric Analysis (DTA-TGA)

Thermal analysis of PVA, PMMA and TiO_2 nanocomposite of these two polymers was carried out using PerkinElmer STA 6000 Model Differential Thermal Analysis-Thermal Gravimetry. With this equipment thermal characteristic of pure polymers and their composite form which contain TiO_2 nanoparticle. Analysis range was determined as 25-600 ^oC heating rate was 10 ^oC/min.

During the thermal analysis temperature change in the samples give information about the chemical (phase transition, reduction, oxidation and decomposition) and physical (boiling, melting and sublimation) changes of a sample and these can be endothermic or exothermic. DTA is able to be used to study any process in which heat is absorbed or evolved. The number, shape and position of the various endothermic and exothermic peaks in

DTA curve can be used for qualitative identification of the substance. Simultaneous techniques refer to the application of two or more techniques to a sample at the same time. In the present study, DTA-TG simultaneous techniques are used. It is an advantage to use simultaneous techniques because it saves time and sample and it gives an opportunity to set an experiment at the same conditions (Ebeoğlugil, 2011).

3.4.2.2 Particle Size Analysis

The particle size distribution (PSD) is also known as grain size distribution. In this analysis particles granules or powders are dispersed in liquid or air medium and then

using some mathematical function, relative amount of particles present, sorted according to size can be defined. Researchers have used different methods to obtain particle size distribution such as (a) laser diffraction methods, (b) optical counting methods, (c) electrical counting methods, (d) sedimentation techniques, (e) sieve analysis and (f) acoustic spectroscopy (Ebeoğlugil, 2011).

In this study, we used Malvern Zeta Sizer Nano ZS90 (EMUM, DEU). This device works with laser diffraction principle to determine particle size of TiO_2 particles. In this method TiO_2 particles were dispersed in distilled water and small amount of dispersion agent Daxad 11 was added to help TiO_2 to disperse in liquid media. When a laser beam passes through a dispersion of particles in the liquid, diffracted light produced. With this respect the angle of diffraction increases as particle size decreases.

3.4.2.3 X-Ray Diffractometer (XRD)

X-ray diffraction (XRD) is one of the essential and most common used techniques to identify different kinds of materials such as powders and crystals and to determine their crystalline structure (based on Bragg's Law that equation shown below). XRD device provide the X-Ray which penetrate the sample in the device. This X-Ray is diffracted when it meet the sample, scattered and diffracted all direction. The diffraction pattern that results is a map of the reciprocal lattice of the crystal and can be used to determine the structure of the crystal using Bragg's law. Bragg's law provides the condition for a plane wave to be diffracted by a family of lattice planes.

$$n.\,\lambda = 2.\,d.\,(\sin\theta) \tag{3.1}$$

Where d is the lattice spacing, θ the angle between the wave vector of the incident plane wave, ko, and the lattice planes, λ its wave length and n is an integer, the order of the reflection. It is equivalent to the diffraction condition in reciprocal space and to the Laue equations (Figure 3.5) (Callister & Rethwisch, 2007).

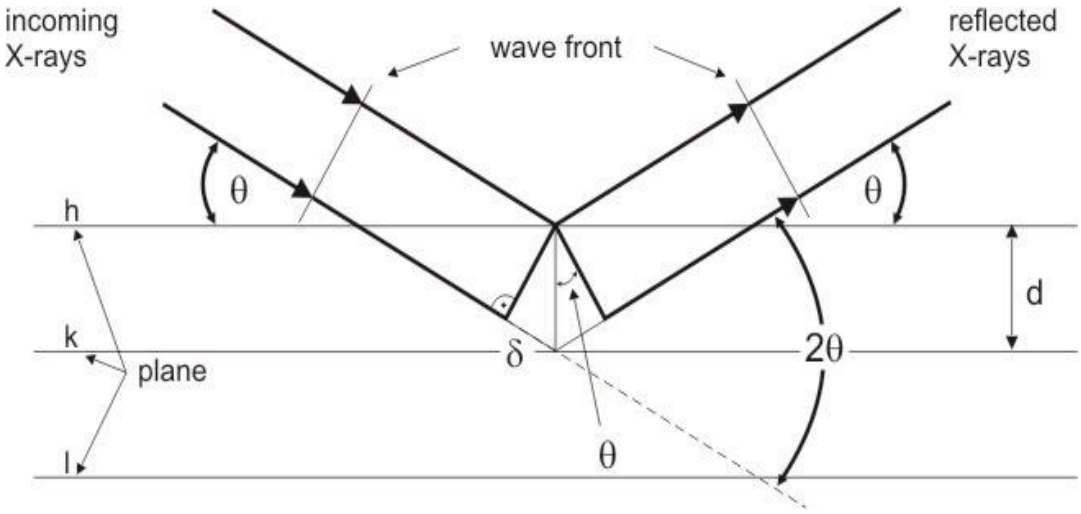

Figure 3.5 X-Ray Diffraction

In this work, Rigaku, D/Max-2200/PC device was employed. X-Ray radiation of CuKα was set at 40 kV and 36 mA with a scanning speed of 2° 2θ/min, from 15° to 80°. Crystalline structure of TiO_2 nanoparticle and Polymeric nanocomposite were determined by using this device.

3.4.2.4 Atomic Force Microscopy (AFM)

Atomic Force Microscopy is one of the strongest methods to determine three dimensional topography and morphology of the surfaces. In our study PVA/TiO_2 and PMMA/TiO_2 nanocomposite thin films surfaces were investigated by using Digital Instruments Nanoscope III. All of the analysis was carried out in tapping mode. With this mode the probe of the devices oscillate at constant frequency during the cantilever scans across the surface. The amplitude of oscillation of the tip varies as it moves nearer to the surface of the film, this change is used as feedback to control the sample-tip distance and deduce the surface height of the film.

3.4.2.5 Scanning Electron Microscopy (SEM)

Scanning electron microscopy (SEM) is most common and practical method to obtain morphology of specimen surfaces which is in solid phase. SEM devices use electron beam poses high energy to scan across the specimen surface. Thank to this

high–energy electron surface topography and elemental composition of the specimen can be determined. There are two types of electron are produced during scanning process; back scatter and secondary electrons. For topography analysis back scatter electron are collected by special detector placed in device. Back scatter electrons are produced by the elastic scattering between specimen atoms and electron in the beam which come from filament wire on the top of the SEM devices. Since heavy elements (high atomic number) backscatter electrons more strongly than light elements (low atomic number), and thus appear brighter in the image. Secondary electrons that are ejected from the k-shell of the specimen atoms by inelastic scattering interactions with beam electrons. BSE are used to detect contrast between areas with different chemical compositions. Due to their low energy, these electrons originate within a few nanometers from the sample surface (Lawes, 1987).

3.4.2.6 Thickness Measurement

In order to measure the thickness of films Surface profilometer instrument is used Tip on the device go through via determined distance. It go forward from clean substrate surface to coated area. Hight difference between two are gives us to thickness of the film. The thickness of the nanocomposite films was determined through Ambios Technology XP-2 Surface Profilometer.

3.4.2.7 Spectrophotometer

The optical properties of the Polymer/TiO_2 nanocomposite and pure polymeric thin films were investigated using UV–Vis Thermo Scientific Evolation 600 device. Reflectance and transmittance spectra of the film between 200 nm and 600 nm were obtained and the bang gap values of each were calculated using these two spectra.

3.4.2.8 Dielectric Measurements

Dielectrical properties of PVA/TiO_2 and PMMA/TiO_2 nanocomposites coatings were investigated using Novocontrol Alpha-N High Resolution Dielectric Analyzer. This device can produce electric field whose frequency can vary between 10^7 and 10^{-2}. In our study we determined that frequency range should be between 10^0 -10^7. Real part of permittivity, imaginary part of permittivity, loss factor (tanδ) AC conductivity and resistivity and were measured as dielectric parameters. The sample material was placed between two external capacitor plates. This technique has the advantage, that the sample preparation is very easy and straightforward.

CHAPTER FOUR
RESULTS AND DISCUSSION

4.1 Solution Characteristics

4.1.1 pH Results

One of the most important parts of preparing solution is pH value. Because pH value of the solution influence the formation of the polymeric three-dimensional structure of the gel during the gelation process. That is reason why it should be controlled. When the solution is acidic ramified structure randomly occurs however separated clusters are formed from the solutions showing basic characters. Ti precursor dissolved in absolute ethanol and GAA added into the solution. The pH values of the solutions decreased as a function of acetic acid content in the solution. The pH values of Titanium (IV) isopropoxide solutions were found as 4.62.

4.1.2 Turbidity Results

Turbidity is an indicator to inspect how well the precursors were dissolved in the solvent. Turbidity values vary between 0 and 1000 ntu. Turbidity can be called as relive cloudiness of fluid. Closer value to 0 is clearer solution was obtained. VELP TB1 turbidimeter was employed to measure turbidity of the solution In our study turbidity values were determined as 6.12, 15.52, 14.24 for Ti precursor solution, PVA solution and PMMA solution respectively.

4.2 Process Optimization

4.2.1 Thermal Analysis

Thermal analysis were carried out in Nitrogen atmosphere from room temperature to 600 °C at heating rate of 10 C/min. Cylindrical Al_2O_3 crucibles of diameter 4 mm and depth 2 mm were used. Thermal characterizations of sol-gel derived TiO_2,

PVA/TiO_2 and PMMA/TiO_2 nanocomposite structure were examined using DTA-TG device. Prior to measurements, TiO_2 xerogel powders were firstly dried at room temperature for 12 hours. Figure 4.1 illustrates DTA-TGA curves of the TiO_2 powder xerogel, As is evident from these figures, At temperature of 100 ^oC to 300 ^oC, a weight loss of 50 % was recorded which could be attributed to the removal of unhydrolyzed isopropoxide ligands bonded in the titanium. Meanwhile from the DTA curves, a sharp exothermic reaction peak appeared at 414 ^oC indicating a phase change of the powder from amorphous to anatase phase (Hafizah & Sopyan, 2009).

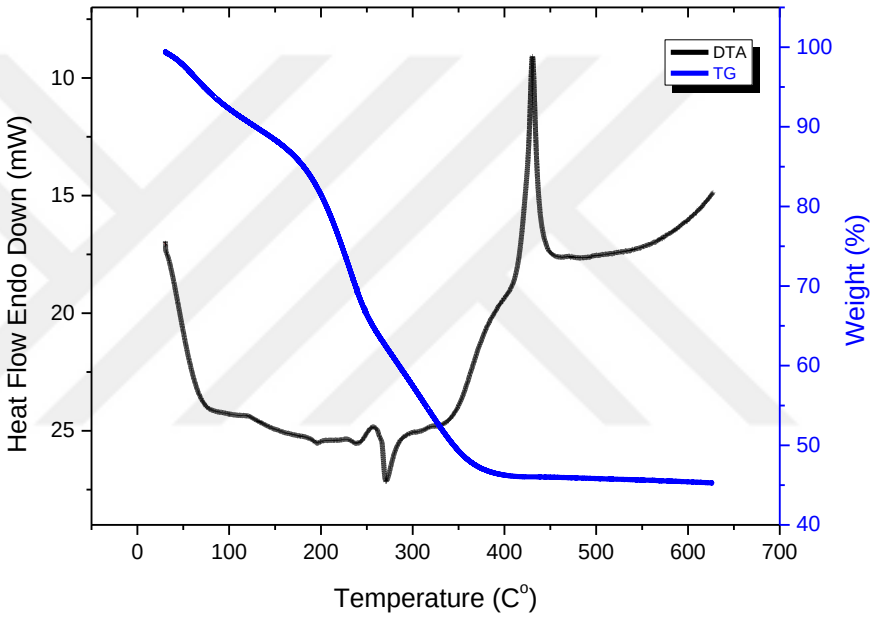

Figure 4.1 DTA-TG curves for TiO_2

Figure 4.2 depicts thermal characteristic of pure PMMA and PMMA/TiO_2 including 20 % TiO_2 nanoparticles by weight of PMMA content. It is obvious that PMMA has two decomposition stages. First decomposition stage occurs at approximately 220 ^oC which represent degradation of vinyl terminated PMMA (PMMA-$CH=CH_2$). The second stage start at 320 ^oC which correspond main chain scission (Hussain & Mohammad, 2004). Moreover it is evident from Figure 4.2, presence of TiO_2 increase the thermal stability of composite structure because of stability of anatase phase up to 600 ^oC.

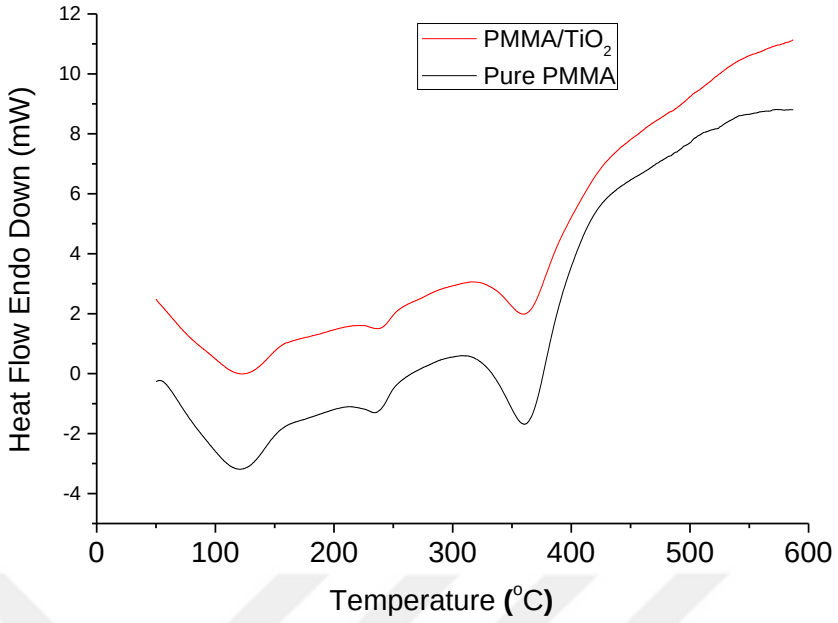

Figure 4.2 DTA curves of pure PMMA and PMMA/TiO_2 nanocomposites

DTA curves of pure PVA and PVA/TiO_2 nanocomposites obtained in Nitrogen atmosphere are depicted in Figure 4.3. The first event occurs in the 50-130 ºC temperature range, is accompanied by a 2% weight loss and is related to the removal of the physically adsorbed water. The peaks at approximately 220–370 ^{o}C are among decomposition of side chain of PVA. Decomposition of main chain of PVA was occurred in the temperature range of 450 and 600 ^{o}C. ΔH of decomposition in pure PVA 595,5 J/g.

Decomposition of side chain of PVA was occurred an 450–600 ^{o}C. The amplitude of decomposition peak of main chain in pure PVA and in PVA/TiO_2 nanocomposite are different. Whilst ΔH of decomposition in pure PVA 595,5 J/g, it is 82,6 J/g in PVA/TiO_2 nanocomposite. This result is an indication that the oxide causes increase the thermal stability of the polymer.

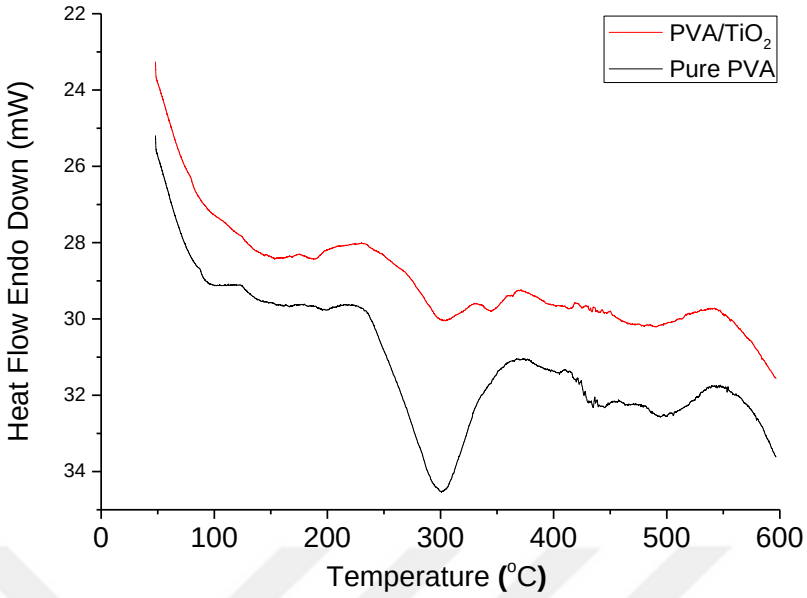

Figure 4.3 DTA curves of pure PVA and PVA/TiO_2 nanocomposites

4.2.2 FTIR Analysis

The purpose of this section is to elucidate what type bonding can occur during heat treatment of TiO_2, to understand the nature of their bonds, and thus to assist to be determined their process optimization. With this respect, FTIR spectrum of solution of TiO_2 precursor, TiO_2 gel and TiO_2 particle samples for various temperatures were recorded with FTIR spectrophotometer for each sample 25 scans were recorded with a resolution of 4 cm^{-1}. The spectra were represented as relative absorbance versus the wave number (cm^{-1}). Figure 4.4 presents the FTIR spectra of the TiO_2 solution heat-treated at different temperatures. The large bands in the region of 3600–3100 cm^{-1} is attributed to stretching vibrations of the metal-attached hydroxyl group (-OH), which indicates the product hydrolyzed (Maira et al., 2001). The peak became weaker with the increasing of heat-treated temperature. The sharp peak at approximately 2971 cm^{-1} is ascribed to the asymmetric C–H stretching mode of $–CH_3$ groups, whereas these peaks at around 2926 cm^{-1} and 2878 cm^{-1} are assigned to the asymmetric and symmetric C-H stretching mode of the $-CH_2$ group that derived from the presence of the ethanol and acetic acid. The intensity of these peaks decreased with the increasing of heat-treated temperature because of the vaporization

and removing of ethanol and acetic acid in the solution. In the case of the high-treated temperature, one can be observed that a peak at around 1626 cm^{-1} which also belongs to hydroxyl (-OH) group appeared. The bands appeared at 1378 cm^{-1} is related to the vibration mode of carboxylic group because of the acetic acid and ethanol (Vojisavljevic, Chevreux, Jouin & Malič, 2014). The characteristic stretching vibrations of C-O of the ethanol are positioned at 1089 cm^{-1} and 1046 cm^{-1}. The presence of the strong bands at 880 cm^{-1} correspond to antisymmetric stretching and antisymmetric in-plane bending of NO_3^- in the nitrate groups (Vojisavljevic et al., 2014). The peaks beneath 810 cm^{-1} are attributed to the stretching vibrations corresponding to the Me-O bonds such as Ti-O or O-Ti-O (Abbas, Bensaha & Taroré, 2015).

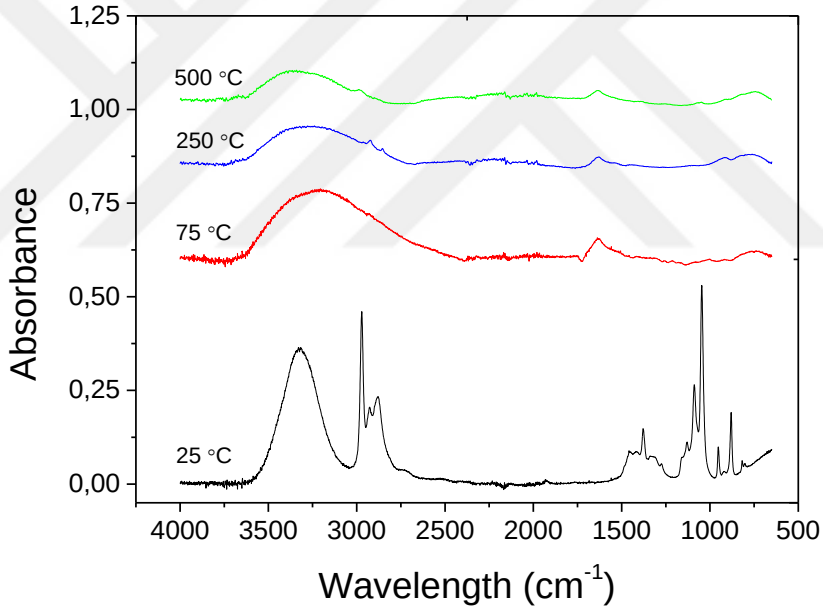

Figure 4.4 The FTIR spectra of the TiO_2 solution and powder at different temperatures

In Figure 4.5, FTIR spectra of PMMA based films were depicted. The broad peak between 3700 and 3200 cm^{-1} represent the stretching vibration of Ti–OH and O–H formed by Ti–OH. The peak at 600 and 830 cm^{-1} correspond to the absorption of Ti–O–Ti and Ti–O–Si would prove that TiO_2 has been embedded into polymer matrix by covalent bond (Jin, Qi, Su, Tong & Zhu, 2013). The several bands between 1270 and 1140 cm^{-1} indicate vibrations of the ester group (ν_{AS}C–O–C + ν_SC–O) (Su,

Wang, Wang, Fu & Weng, 2010). The strong and sharp absorption at 1731 cm^{-1} may correspond to the stretching vibration of the C=O group in PMMA (Jin et al., 2013). 2918 cm^{-1} and 2852 cm^{-1} are because of CH_2 asymmetric and symmetric stretching respectively (Roy, Gupta, Sindhu, Parveen & Ramamurthy, 2013).

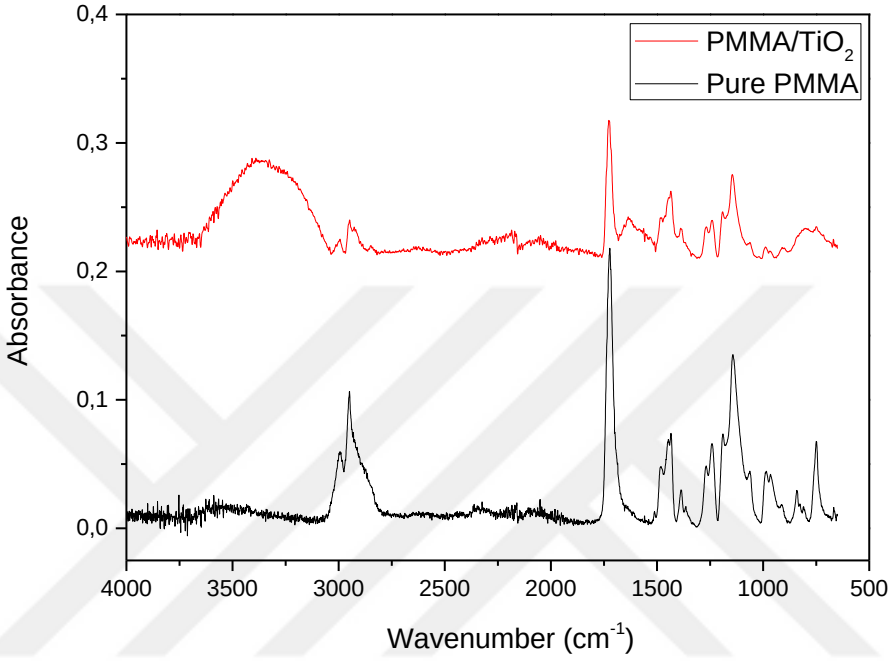

Figure 4.5 The FTIR spectra of the PMMA and PMMA/TiO_2

The FTIR spectra of pure PVA as well as composite are shown in Figure 4.6, in absorbance mode. In the spectra pure PVA and the composites showed a peak around 3300 cm^{-1}, is due to OH group in the polymer backbone, 2918 cm^{-1} and 2852 cm^{-1} are due to CH_2 asymmetric and symmetric stretching respectively. The peak observed around 1413 cm^{-1} is due to C–C stretching (Roy et al., 2013) . Several peaks related to TiO_2 are observed in PVA/TiO_2 samples. The peaks at 1620-1630 cm^{-1} are assigned to vibrations of hydroxyl groups and the overlapped broad peaks appearing at 3100–3600 cm^{-1} are assigned to vibrations of hydroxyl groups. This suggests the presence of TiO_2 in the polymer PVA matrix (Yasumori, Shinoda, Kameshima, Hayashi & Okada, 2001).

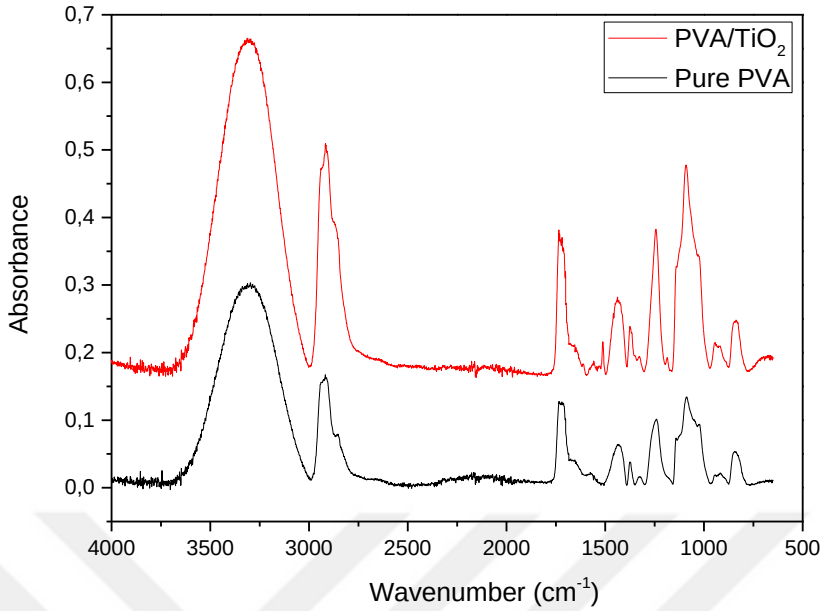

Figure 4.6 FTIR spectra of the PVA and PVA/TiO_2

4.3 Phase Analysis

X-ray diffraction (XRD) patterns of pure TiO_2 nanoparticles, PVA/TiO_2 and PMMA/TiO_2 nanocomposites, pure PVA and PMMA were obtained by means of a Rigaku diffractometer with a Cu K_α irradiation (wavelength, λ=0.15418 nm). Scans were carried out over the range 2θ=10–90° in increments of 2°. Figure 4.7 demonstrate XRD pattern of pure TiO_2 nanoparticles, PVA/TiO_2 nanocomposites and pure PVA. The all main diffraction peaks at 25.38° (101), 37.96° (004), 48.04° (200), 53.94° (105) and 54.20° (211) coincide with the JCPDS values (PDF Card No: 00-021-1272) which correspond to crystal structure of anatase (Kenanakis, Vernardou, Dalamagkas & Katsarakis, 2015). There are also relatively large peaks in XRD patterns of pure PVA and PVA TiO_2 nanocomposite structure. These peaks centered 2θ=19,82^o and 22,9^o which indicate crystalline PVA structure (Fernandes et al., 2011). it is observed that spectra of PVA/TiO_2 nanocomposite demonstrate presence of crystalline TiO_2 particle in PVA matrix. The presence of highly crystalline TiO_2 leads to increase crystallinity of PVA.

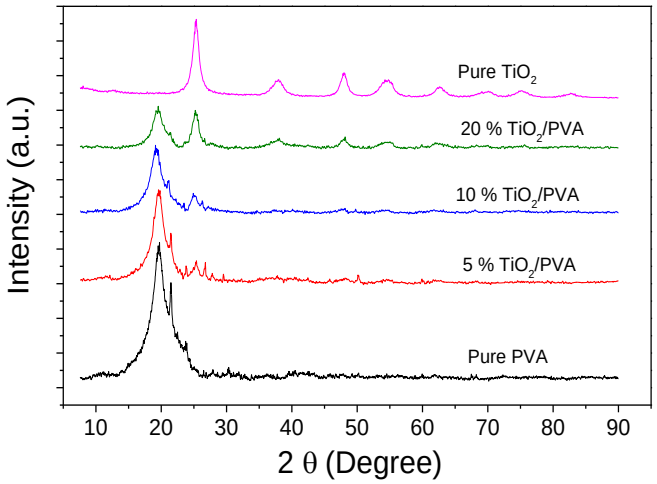

Figure 4.7 XRD pattern of pure TiO_2 nanoparticles, PVA/TiO_2 nanocomposites and pure PVA

X-ray diffraction patterns of PMMA based composite films and pure TiO_2 are presented in Figure 4.8. Broad peaks at around $2\theta = 15.45^o$, 29.93^o and 42.220^o correspond amorphous structure of PMMA (Tomar, Mahendia & Kumar, 2011). Moreover crystalline anatase TiO_2 phase can be seen in PMMA matrix. The intensity of anatase peaks increase with increasing TiO_2 content in PMMA matrix. Furthermore presence of TiO_2 increase the crystallinity of PMMA/TiO_2 nanocomposite

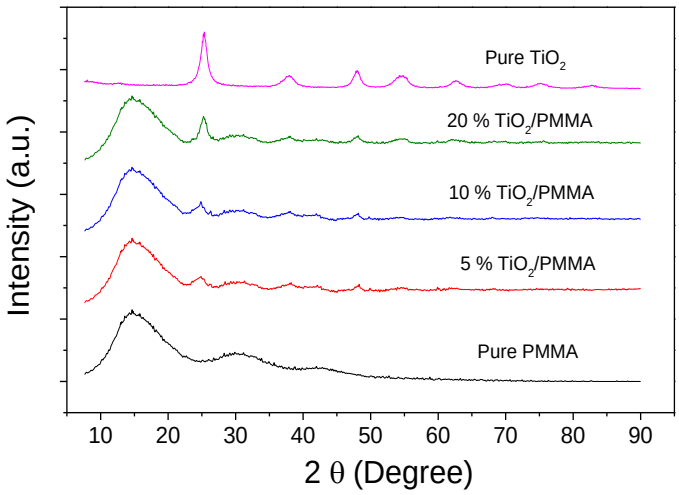

Figure 4.8 XRD pattern of pure TiO_2 nanoparticles, PMMA/TiO_2 nanocomposites and pure PMMA

4.4 Powder Analysis

TiO_2 particle sizes were measured by means of Mastersizer particle size machine. Particle size distribution of TiO_2 nanoparticles dispersed in water is shown in Figure 4.9. It is clearly seen that TiO_2 particles were successfully synthesized in nanoscale and average particle size is calculated 84 nm. Before the measurement TiO_2 particles were pastelled and dispersed in distilled water. Daxad 11 which is surfactant added into suspension to sustain in liquid medium

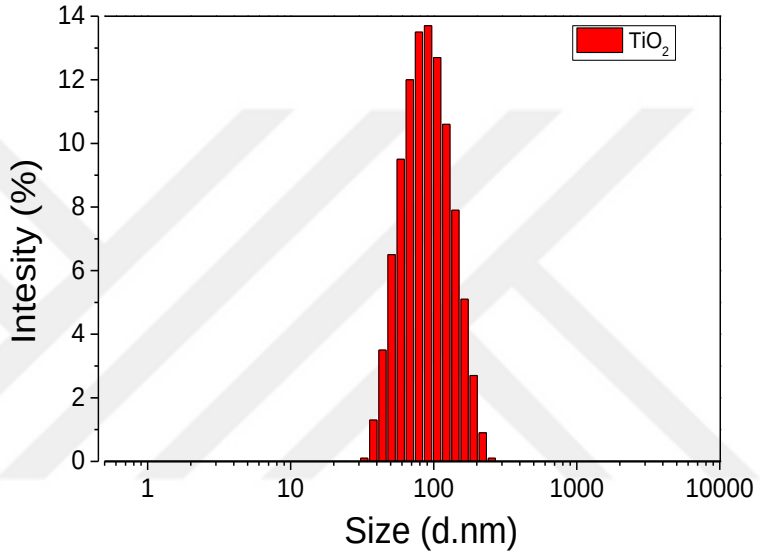

Figure 4.9 Particle size distribution of TiO_2 powder

4.5 Microstructure Analysis

4.5.1 AFM images

One of the effective ways to characterize surface of nano scale thin film is AFM technique. All of the prepared nanocomposite thin films in Table 3.4 spinning parameter for different polymer/TiO_2 dispersion were measured with this technique. There are two type of thin film such as PVA and PMMA based films. First type is PMMA based thin film. These films include 10 % TiO_2 ratio with PMMA content.

AFM scanning area was 100µm^2 and resolution was 256 pixels. Figure 4.10, 4.11, 4.12 illustrate 2D and 3D AFM images of thin film which are produced from 1 % PMMA polymeric solution including 10 % TiO_2 nanoparticles by weight of PMMA content. 3 different spinning parameter 2500, 5000 and 7500 rpm were used to determine best results.

When Figure 4.10 were examined, it is obtained that thin film that produced with 2500 rpm have non homegen structure. Furthermore TiO_2 particle could be seen easily in AFM images. However there are relatively larger particles. This is maybe because of low spin rate. In addition it is possible that TiO_2 particles agglomerate during the spinning time. Surface roughness of this film is 55.5 nm.

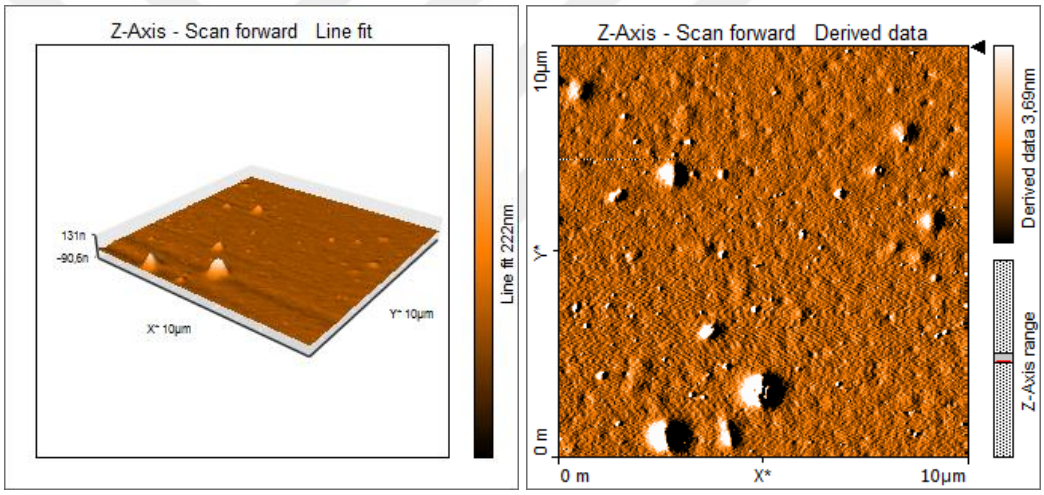

Figure 4.10 2D and 3D AFM images of 1PMMA25 nanocomposite thin film

Figure 4.11 demonstrate thin film which is produced from 1 % PMMA polymeric solution including 10 % TiO_2 nanoparticles by weight of PMMA content. Max spinning speed was adjusted at 5000 rpm. Once Figure 11 was compared with the film produced at 2500 rpm, it can be said that better results were obtained. For example particles are smaller and the film surface is smoother. Nonetheles there could be some pinhole which could be formed due to the high spinning rate. In this case SEM images will supply more accurate evident. Surface roughness of this film is 38.59 nm

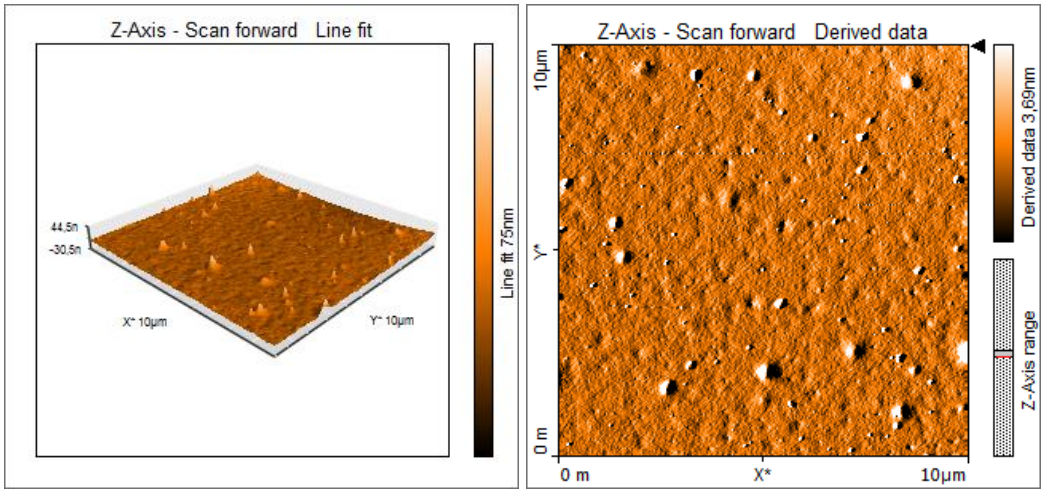

Figure 4.11 2D and 3D AFM images of 1PMMA50 nanocomposite thin film

Figure 4.12 depicts 2D and 3D AFM images of PMMA/TiO_2 nanocomposite thin film which was produced at 7500 rpm spinning speed. As it can be seen easily, surface morphology of this film not smooth and have many huge holes. This result shows 7500 rpm spinning rate is not appropriate for 1 %PMMA solution including 10 % TiO_2 nanoparticles by weight of polymer content. Roughness of this film is relatively high when compared with film coated at 2500 and 5000 rpm. Surface roughness of this film is 497.4 nm.

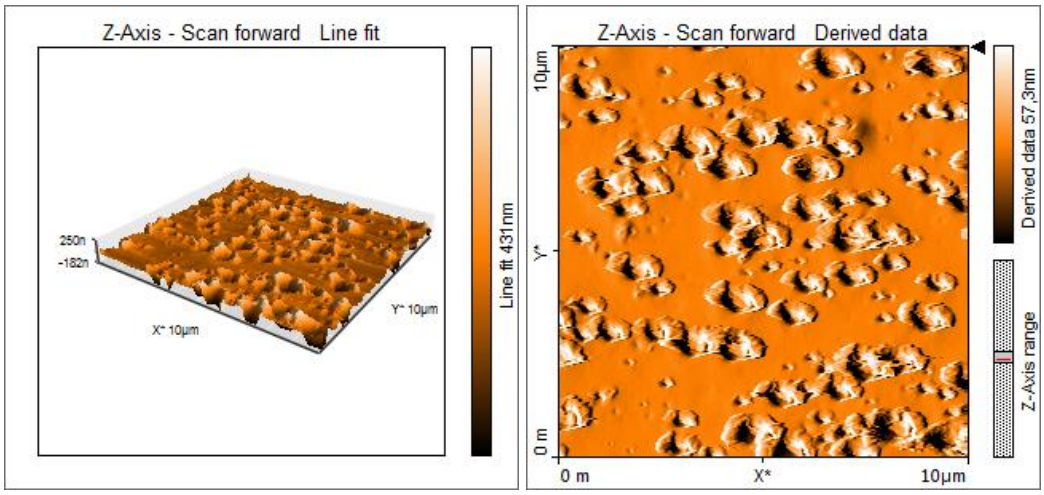

Figure 4.12 2D and 3D AFM images of 1PMMA75 nanocomposite thin film

Figure 4.13 shows AFM images of thin film obtained from 2 % PMMA solution including 10 % TiO_2 as ratio of PMMA concentration at 2500 rpm spinning rate. We have similar surface morphology with previous thin film which produced from 1 % PMMA solution. There are agglomerated particles almost 1 micron. Surface roughness of this film is 65.9 nm

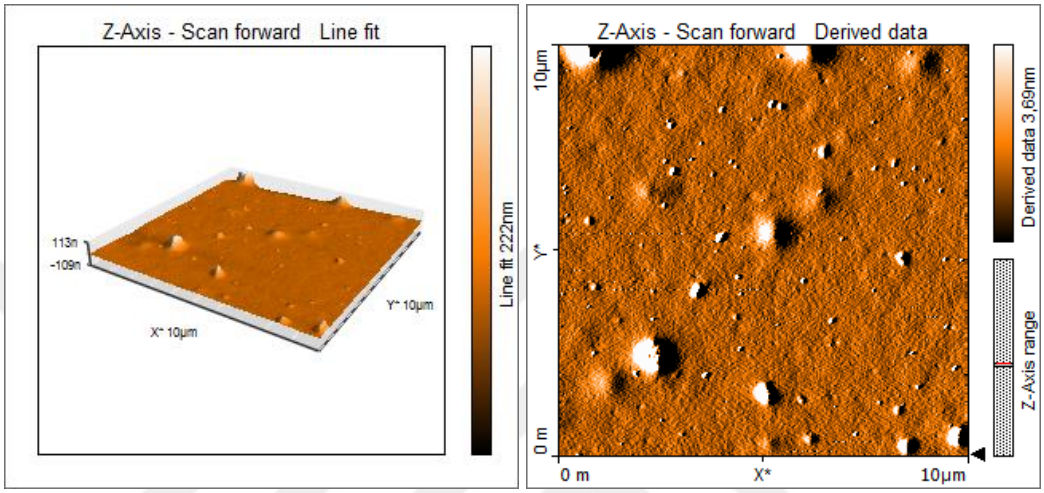

Figure 4.13 2D and 3D AFM images of 2PMMA25 nanocomposite thin film

Figure 4.14 presents AFM images of thin film obtained from 2 % PMMA solution which has 10 % TiO_2 nanoparticle by weight of PMMA content. This film was formed at 5000 rpm spinning speed. There are relatively smaller particles when compared with previous thin film which was produced at 2500 rpm. Surface roughness is 74.15 which is relatively higher than 65.9

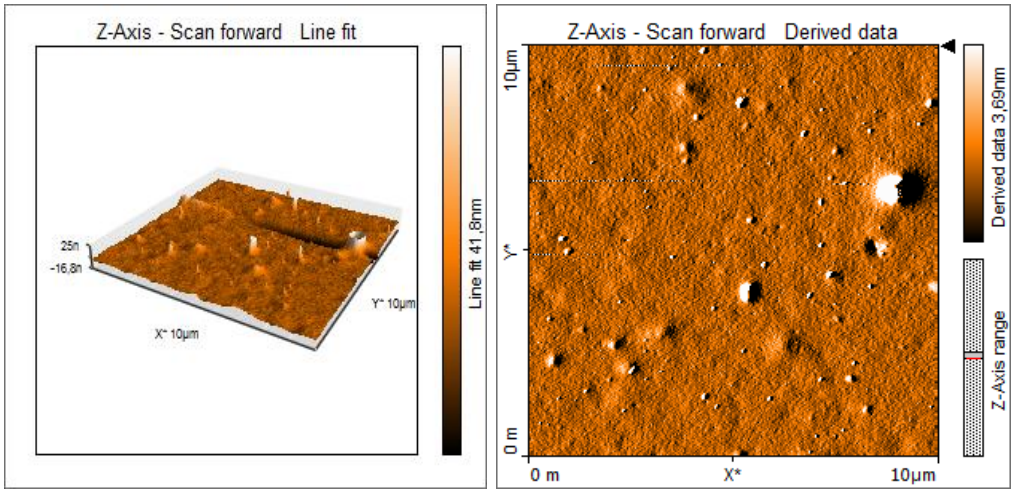

Figure 4.14 2D and 3D AFM images of 2PMMA50 nanocomposite thin film

Figure 4.15 shows AFM images of thin film obtained from 2 % PMMA solution including 10 % TiO_2 as ratio of PMMA concentration at 7500 rpm spinning speed. We have almost same surface morphology with previous thin film which produced from 1 % PMMA solution. There are big hole on the film surface and roughness is dramatically higher other films which were formed lower spinning rate. The surface roughness is 850 nm.

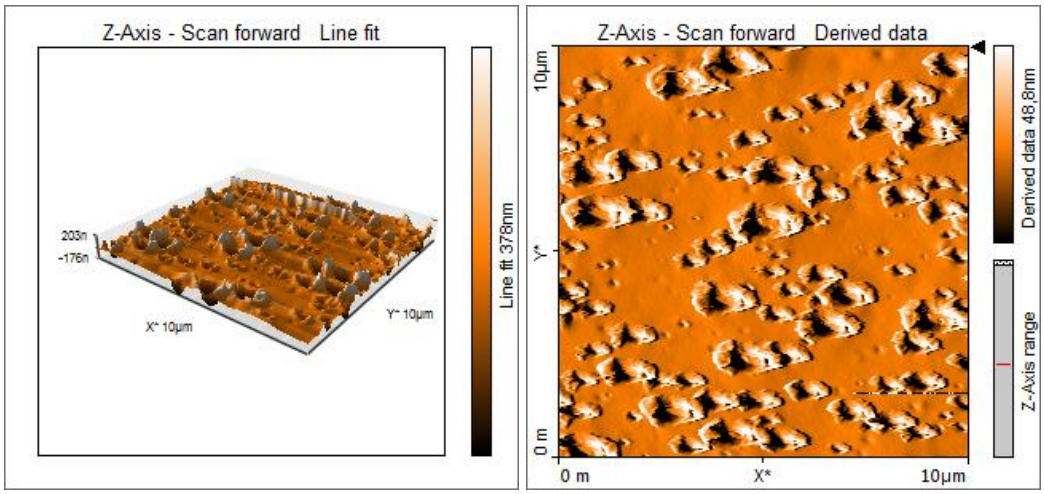

Figure 4.15 2D and 3D AFM images of 2PMMA75 nanocomposite thin film

When we examined AFM images of nanocomposite thin films obtained from 4 % PMMA solution which is illustrated in Figure 4.16-4.17-4.18 It obvious that surfaces of the film have huge holes and ripples. The surface quality of all these three film

which were produced different spinning rate is not better as previous films. This could be because of high concentration of the polymeric solution which is 4 % PMMA. The film which was produced 5000 rpm has some ridge. Furthermore there are much more ridge film produced 7500 rpm. With this respect we concluded that high concentration of the solution which leads to increase viscosity causes the defect on the film surfaces. The other possibility is that solvent of PMMA which is Chloroform relatively more volatile than distilled water. Evidently because of the higher volatility and faster evaporation, of chloroform could cause the non-uniform film surface. These findings are in good agreement with literature (Norrman, Ghanbari-Siahkali & Larsen, 2005; Walsh & Franses, 2003). The Surface roughnesses of the film are dramatically high such as 143.11, 240.9, 524.07 nm for Figure 4.16, 4.17 and 4.18 respectively.

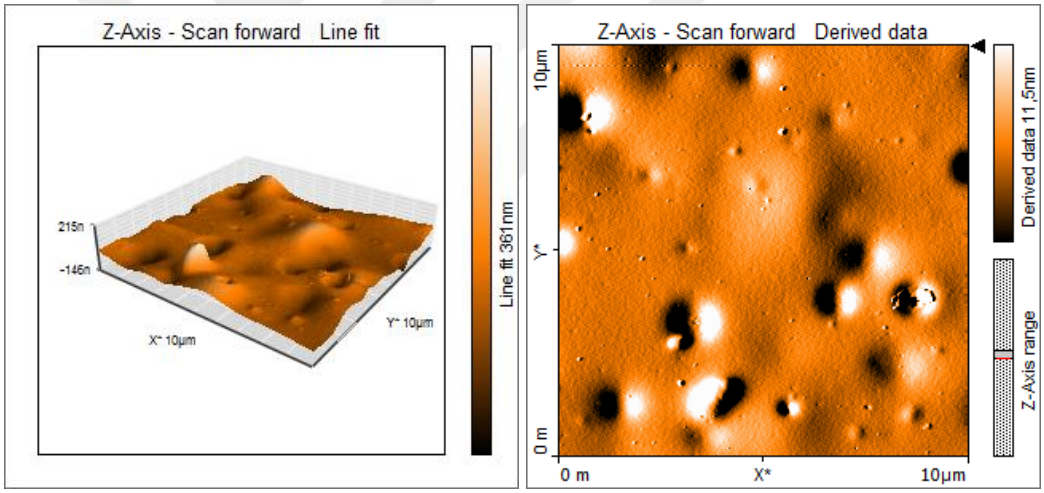

Figure 4.16 2D and 3D AFM images of 4PMMA25 nanocomposite thin film

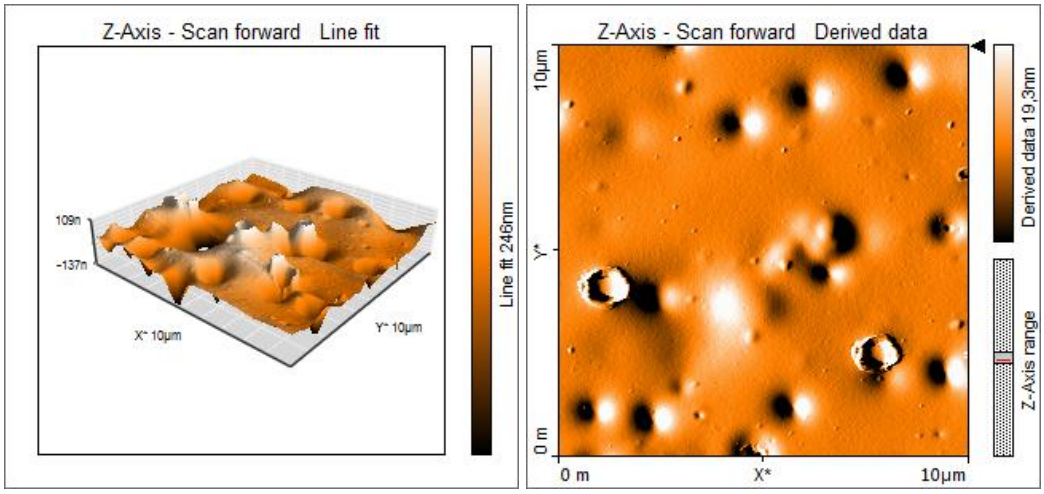

Figure 4.17 2D and 3D AFM images of 4PMMA50 nanocomposite thin film

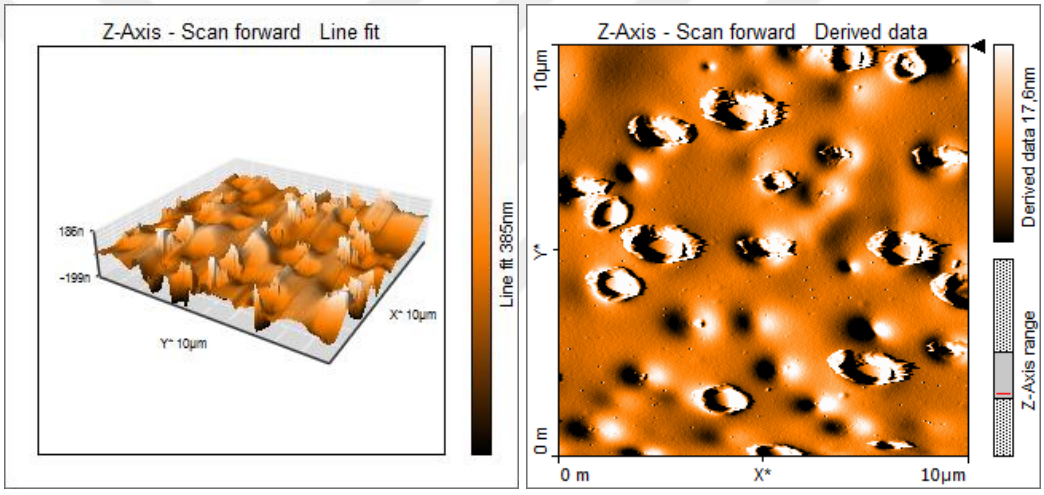

Figure 4.18 2D and 3D AFM images of 4PMMA75 nanocomposite thin film

The second type of polymeric nanocomposite thin film is PVA/TiO_2. AFM measurements of PVA/TiO_2 thin film was carried out using same imaging parameter with PMMA/TiO_2 which is 100 μm^2 as scanning area and 256 pixels as resolution. There different solution was prepared which have three different polymer concentrations such as 1 %, 2 %, 3%. Each individual solution was spin coated using 3 different max spinning speeds such as 2500 rpm, 5000 rpm and 7500 rpm.

Figure 4.19 demonstrate thin film which is produced from 1 % PVA polymeric solution including 10 % TiO_2 nanoparticles by weight of PVA content. Max spinning speed was adjusted at 2500 rpm. When Figure 4.19 is examined, some TiO_2 clustered

could be seen. The reason behind the clusters could be low spinning speed. These findings are in good agreement with literature (Norrman et al., 2005; Walsh & Franses, 2003). The TiO_2 particles are not scattered homogeneously on the substrate surface because of low centrifugal force. However PVA/TiO_2 thin films are smoother than PMMA/TiO_2 thin films. The surface roughness of present film is 15.9 nm.

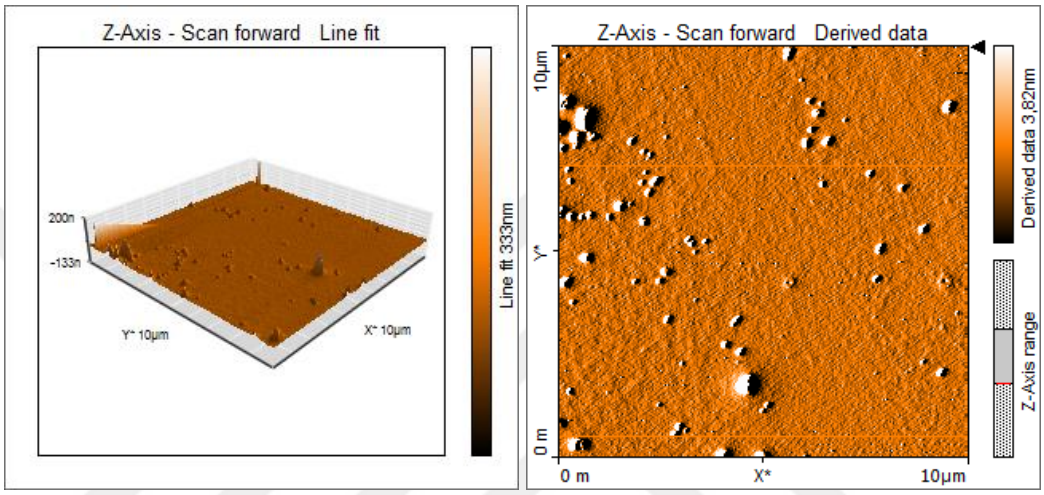

Figure 4.19 2D and 3D AFM images of 1PVA25 nanocomposite thin film

AFM image of thin film which is produced from exact same content with previous solution. This solution was coated at 5000 rpm. It could be seen that in Figure 4.20 TiO_2 particles scattered more homogenously on the surface. This is probably because of relatively high centrifuge force. But still some holes exist on the film surface. The surface roughness of present film is 58.7 nm.

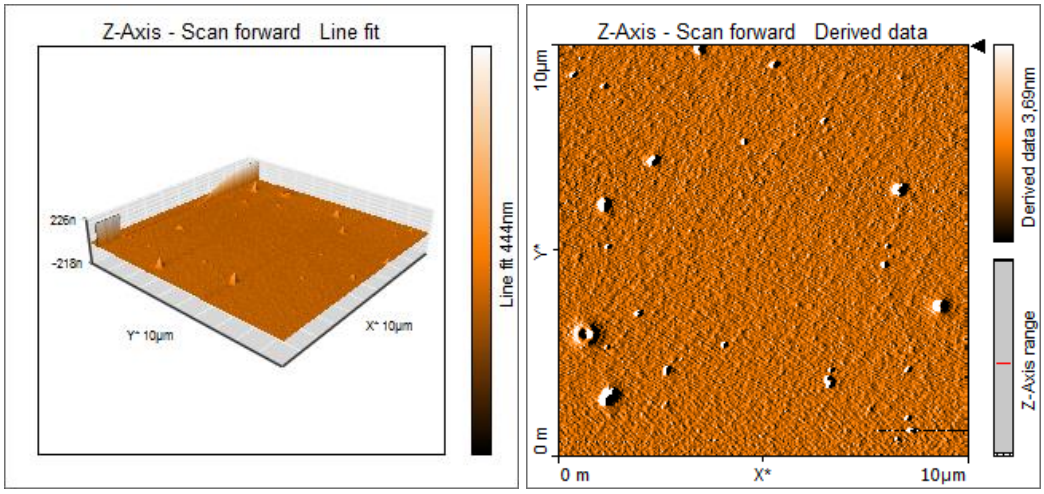

Figure 4.20 2D and 3D AFM images of 1PVA50 nanocomposite thin film

AFM images the film which is illustrated in Figure 4.21 contain some long line on the film surface but no crack exist. Low viscosity and high centrifugal force may be reason behind this situation. Because of these line defects the surface roughness of present film is relatively higher than the film coated at 2500 and 5000 rpm. The surface roughness of present film is 15.9 nm.

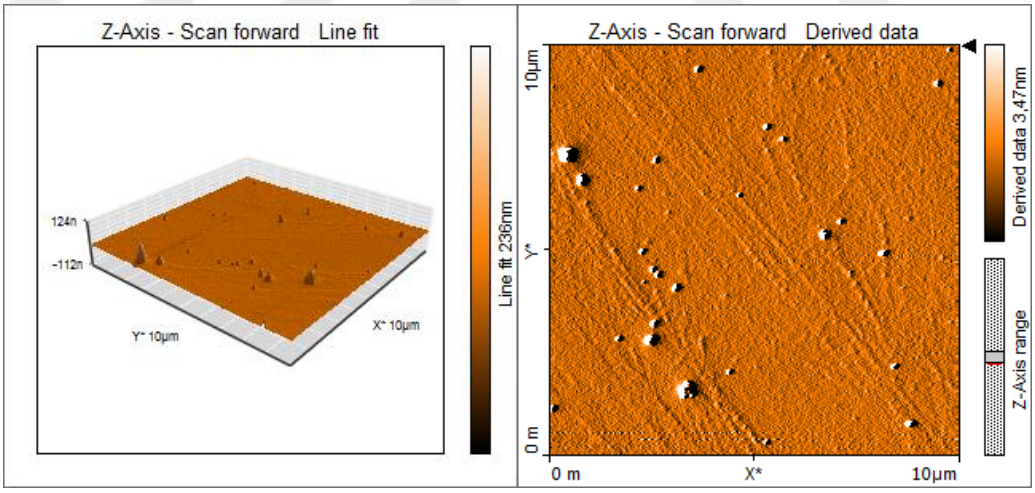

Figure 4.21 2D and 3D AFM images of 1PVA75 nanocomposite thin film

Figure 4.22-4.23-4.24 show AFM images of thin films which were produced from 2 % PVA solution. The surface quality of all these three film which were produced different spinning rate is better than previous films. This could be because of optimum concentration of the polymeric solution which is 2 % PVA. Although the

film formed at 5000 rpm has some hole, According to our experience best results were obtained by using 2 % PVA solution. These results are in agreement with the literature (Lock et al., 2008). Solution viscosity is optimum at this concertation. Non-ionic surfactant Triton X-100 had been mixed with PVA solution to get lower the surface tension. Obviously this surfactant has us obtain good surface morphology and low surface roughness. There are no agglomerated particles or cluster. TiO_2 nanoparticle was homogenously distributed on the surface. The roughness of the surfaces are 25, 18, 15 nm for Figures 4.22,4.23 and 4.24 respectively.

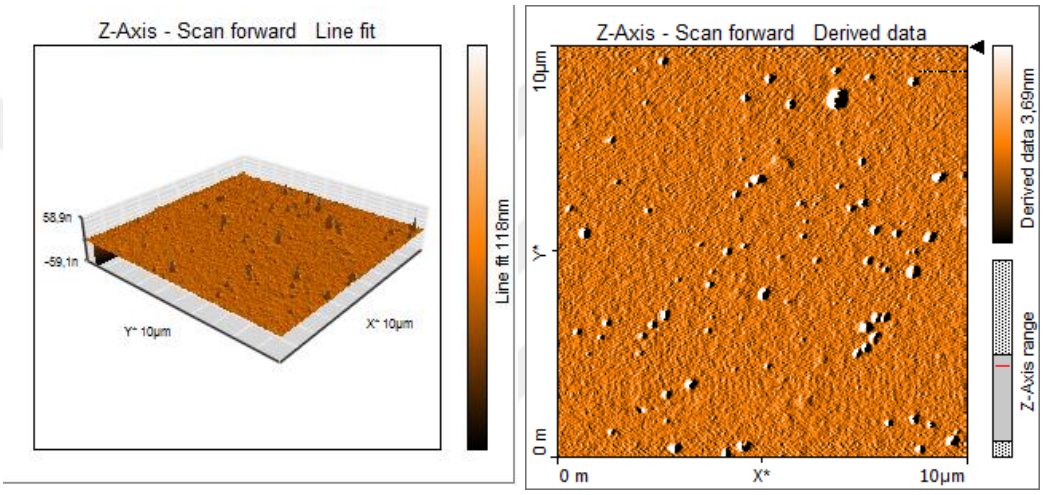

Figure 4.22 2D and 3D AFM images of 2PVA25 nanocomposite thin film

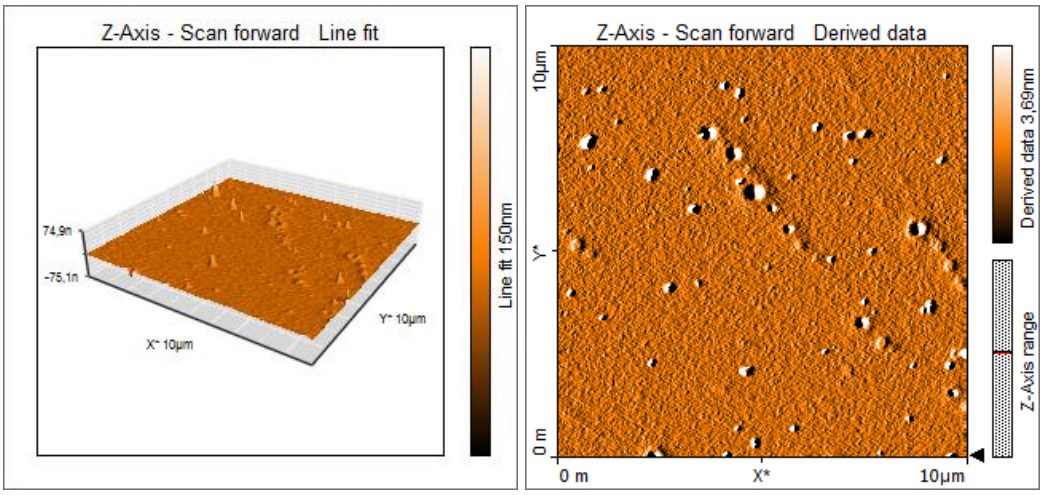

Figure 4.23 2D and 3D AFM images of 2PVA50 nanocomposite thin film

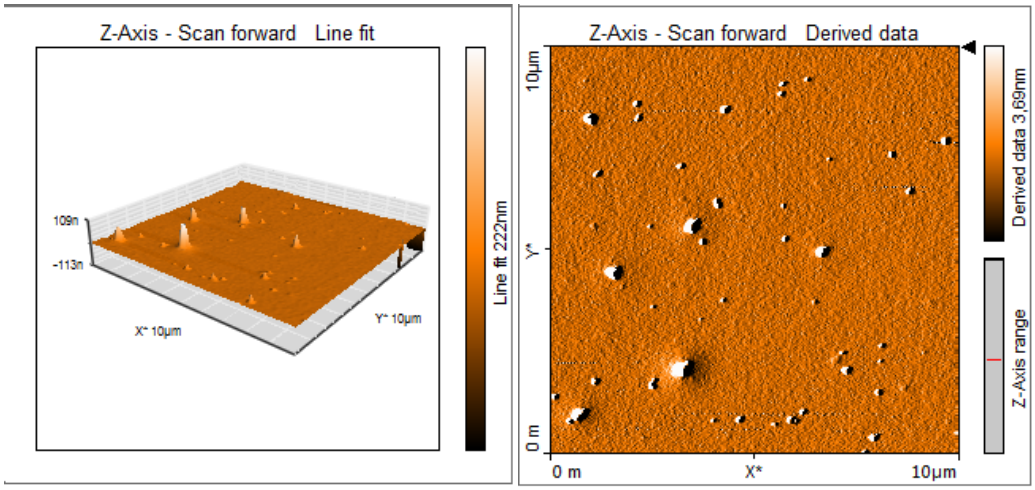

Figure 4.24 2D and 3D AFM images of 2PVA75 nanocomposite thin film

Figures 4.25, 4.26 and 4.27 shows AFM images of thin films which were produced from 4 % PVA solution. When we examined the AFM images it is easy to see relatively larger particles on the film surface. Because of the higher concentration of the polymer solution is highly viscos. With this respect fine particles tent to agglomerate and form bigger particle. Although ultrasonic treatment was done, agglomeration couldn't be prevented. The surface roughness of the film are 97.3, 57.1, 45.8 nm for the film produced at 2500, 5000, 7500 rpm.

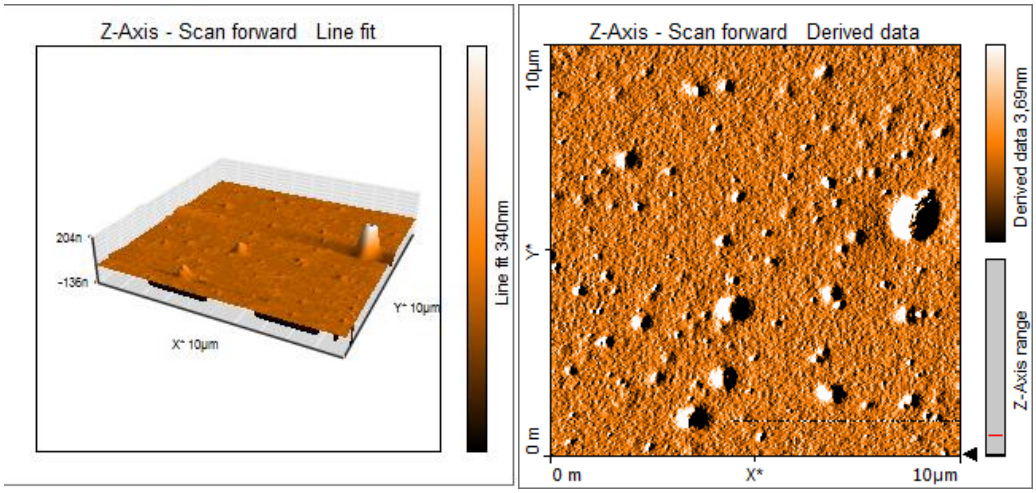

Figure 4.25 2D and 3D AFM images of 4PVA25 nanocomposite thin film

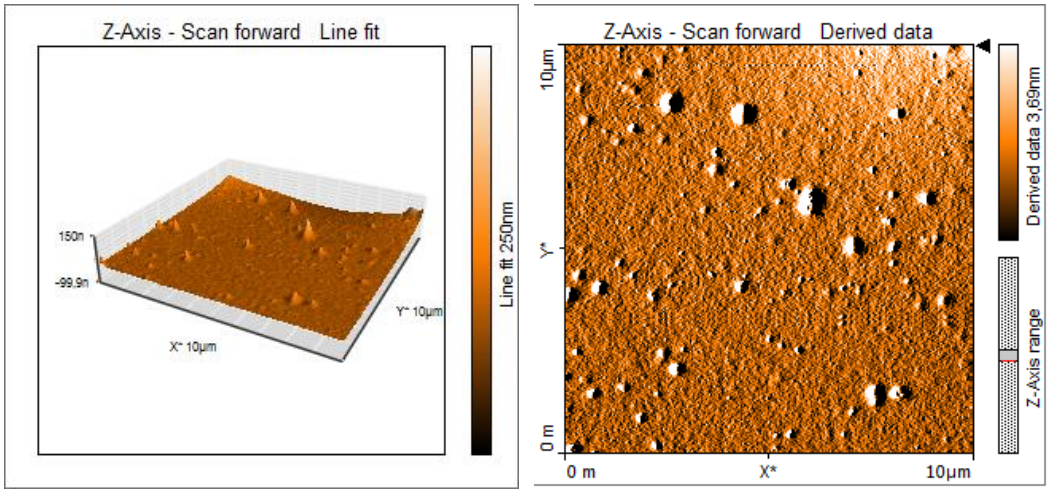

Figure 4.26 2D and 3D AFM images of 4PVA50 nanocomposite thin film

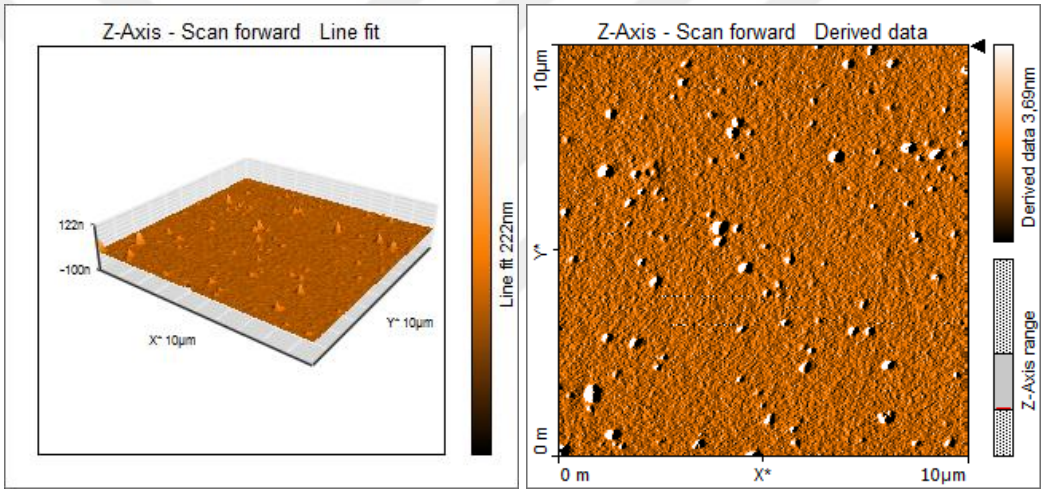

Figure 4.27 2D and 3D AFM images of 4PVA75 nanocomposite thin film

4.5.2 SEM Analysis

The surface topographies and characteristics of films on Si substrates were examined by using SEM. Morphology of the films micro cracks, porosities grain size were examined by SEM. Microstructures of the pure and TiO_2 added polymer films are given in between Figures 4.28 and 4.50 in detail. Polymeric nanocomposite films have different surface structure depending their filler content and matrix polymer. Surface futures of the thin film are highly effective on dielectric properties of the samples. Concerning the microstructure of nanocomposite coatings, SEM observation was performed to obtain an optimum sample. Figure 4.28 and 4.29

depicts SEM micrographs of pure PMMA and PVA films on substrate. Crack-free continuous polymeric thin film was produced from their 2 % solution. SEM micrographs of all of the nanocomposite film were performed except the nanocomposite thin film obtained at 7500 rpm PMMA based nanocomposite films and obtained from 4 % PMMA solution. Because it was concluded from AFM observation that high concentration of PMMA relatively higher spin speed caused non homogenous structure and high surface roughness on the film surface. It was not necessary to performed SEM analysis of this film.

All thin films were coated from solutions after producing TiO_2 powders with different using sol-gel technique. SEM examination of nanocomposite thin films shows a porous and having larger particles microstructure on the surface.

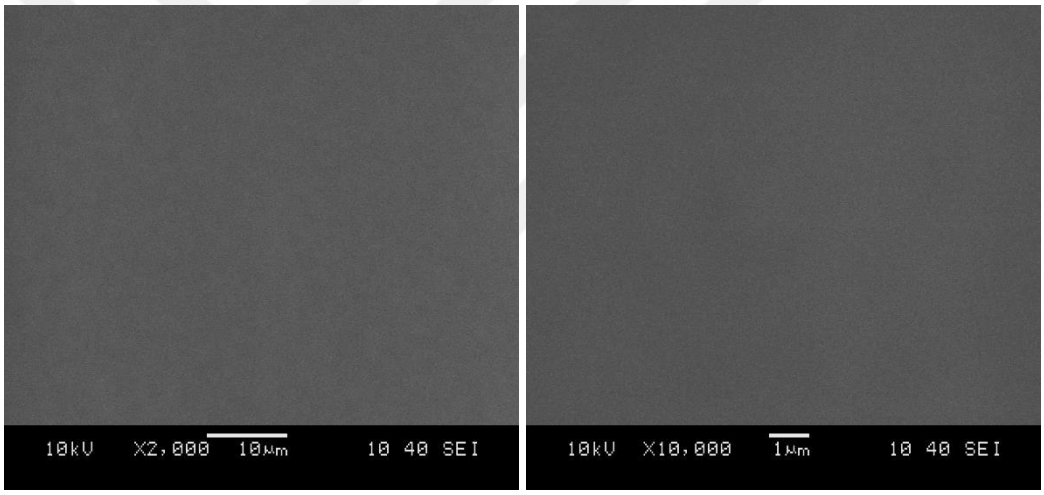

Figure 4.28 SEM images of pure PMMA thin film

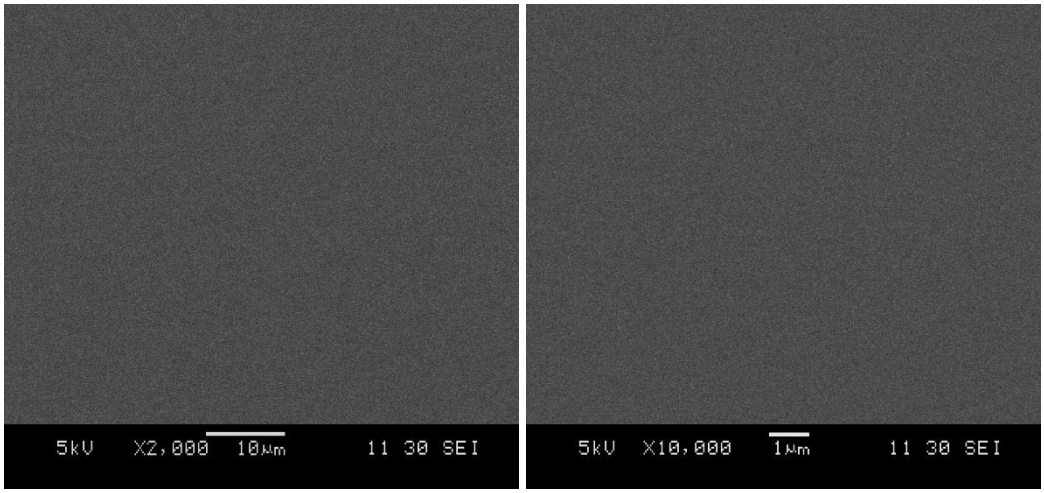

Figure 4.29 SEM images of pure PVA thin film

Figure 4.30-4.31shows SEM micrograph of thin films which were produced from 1 % PMMA solution including 10 % TiO_2 nanoparticles by weight of PMMA content. This film produced 2500 and 5000 rpm spin speed respectively. When we examined the SEM micrograph it is easy to see non homogeneous surface. There are some defects such as holes. These holes are not available on Pure PMMA thin film which has same polymer concentration. Presence of nanoscale TiO_2 particles caused defect on the surface morphology.

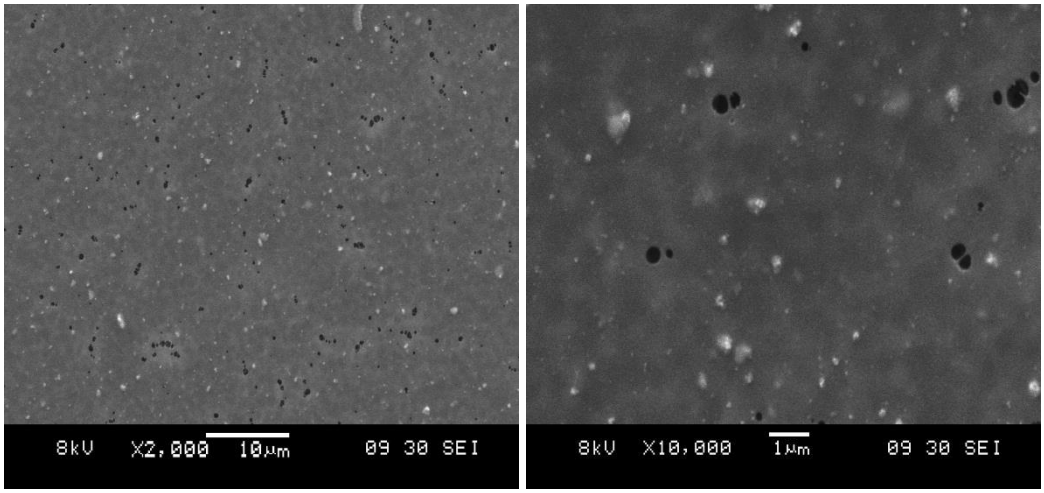

Figure 4.30 SEM images of 1PMMA25 nanocomposite thin film

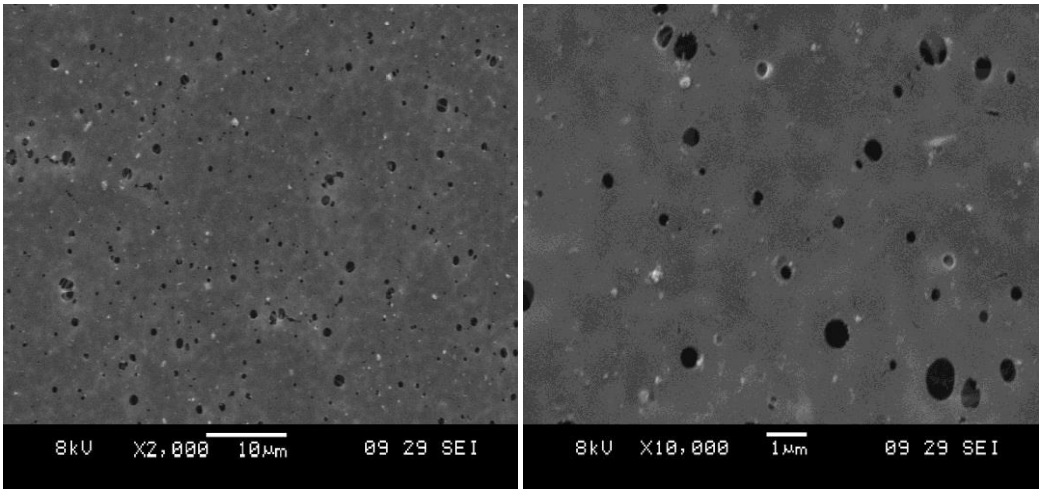

Figure 4.31 SEM images of 1PMM50 nanocomposite thin film

However when we increase the PMMA concentration, holes disappeared. But another surface defect started to be existing. Figure 4.32-4.33 presents SEM micrograph of thin film obtained from 2 % PMMA solution which has 10 % TiO_2 nanoparticle by weight of PMMA content. Because of the high viscosity depending on polymer concentration, bubbles were formed on the film surface. To avoid these two defects which is bubble effect and porous structure, surfactant use could be appropriate solution. This may be carried out another study.

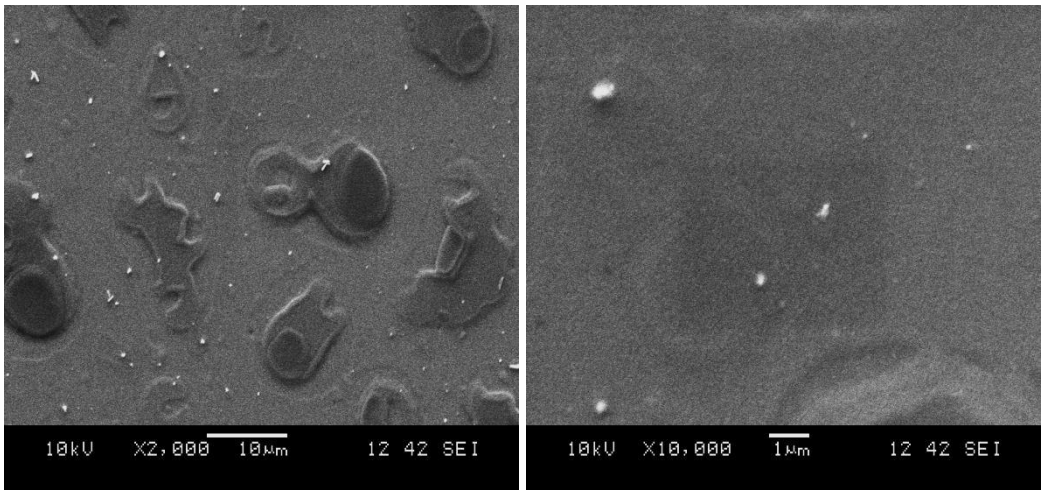

Figure 4.32 SEM images of 2PMMA25 nanocomposite thin film

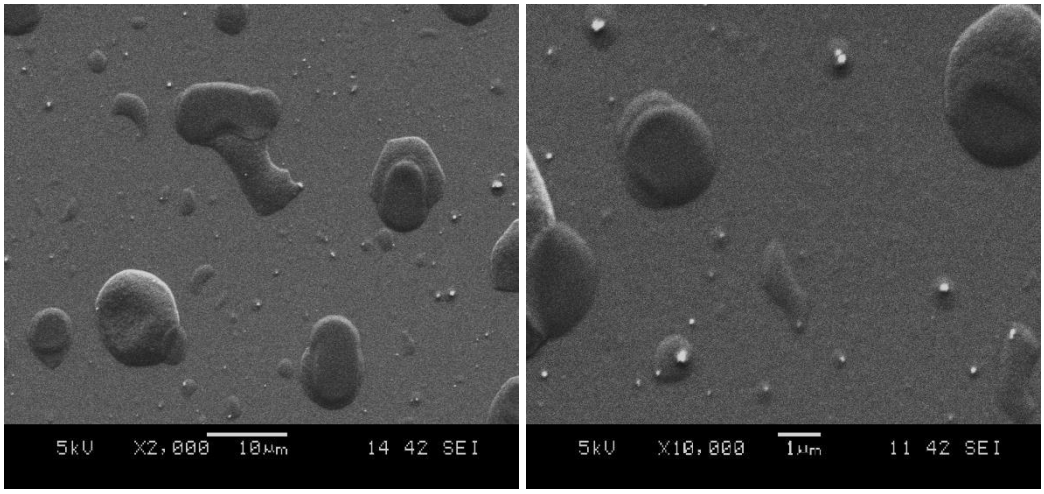

Figure 4.33 SEM images of 2PMMA50 nanocomposite thin film

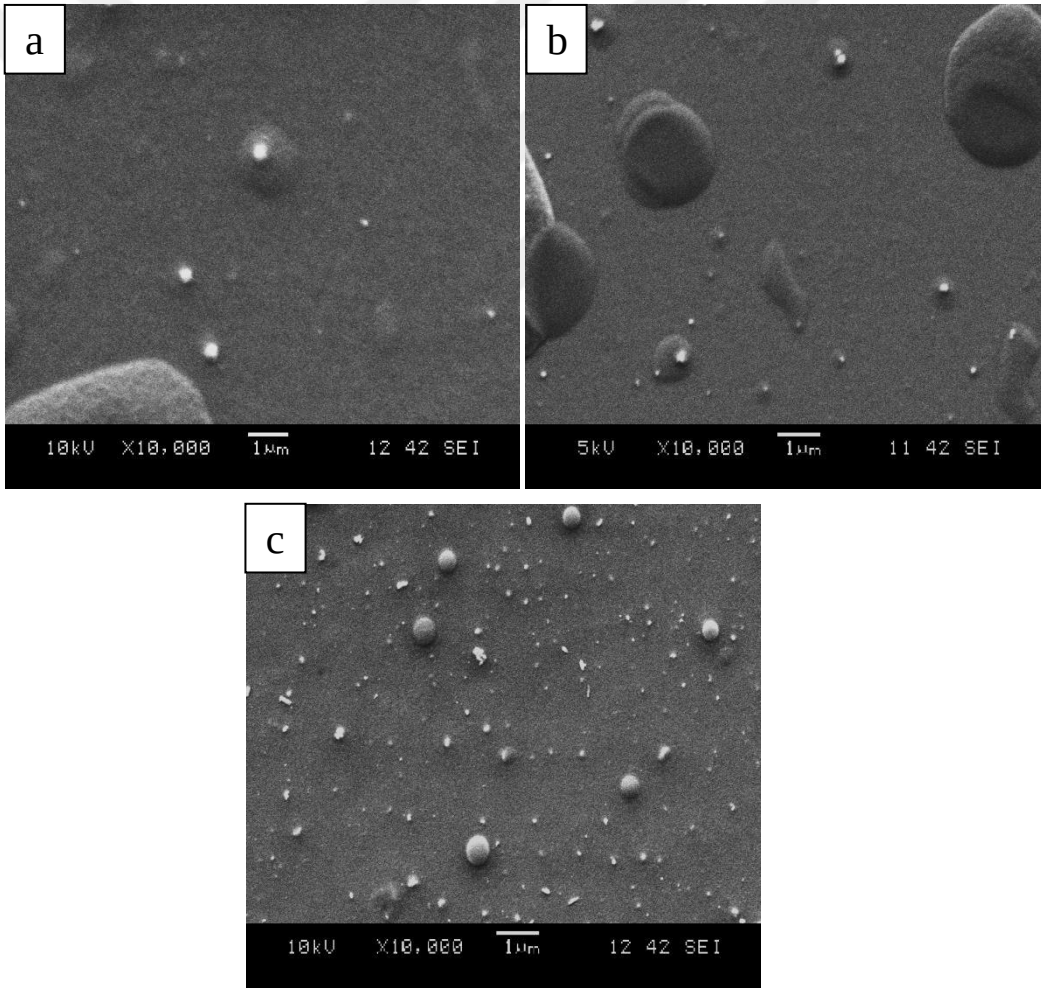

Figure 4.34 SEM images of PMMA/TiO_2 thin film including (a) 5 % wt TiO_2, (b) 10% wt TiO_2 (c) 20 % wt TiO_2

Figure 4.34 shows SEM micrograph of PMMA/TiO_2 thin film including 5 % wt, 10 % wt and 20 %wt TiO_2. Increasing TiO_2 could be easily seen TiO_2 nanoparticles causes the bubbles on surface. This is because of the interaction between ceramic nanoparticles and polymer matrix. This shows us PMMA and TiO_2 is suitable to mix each other or some surfactant should be used to avoid bubbles.

PVA based nanocomposite thin film were illustrated between Figures 4.35 and 4.44. We used different PVA solution with three different concentrations and three different spinning speeds. All of the solution has 10 % TiO_2 nanoparticle by weight of PVA content. Each individual PVA solution coated at 2500, 5000, 7500 separately. After observation AFM and SEM images, optimum parameters and best films were determined. There different solution which has three different TiO_2 content was then prepared and thin films coated with this solution.

Figures 4.35, 4.36 and 4.37 shows nanocomposite thin film coated at 2500, 5000, 7500 rpm spinning speed respectively. These films were produced using 1 % PVA solution including 10 % TiO_2 nanoparticle by weight of PVA content. As it can be that there is no hole or any structural defect on the film surface. Continuous thin film was coated successfully.

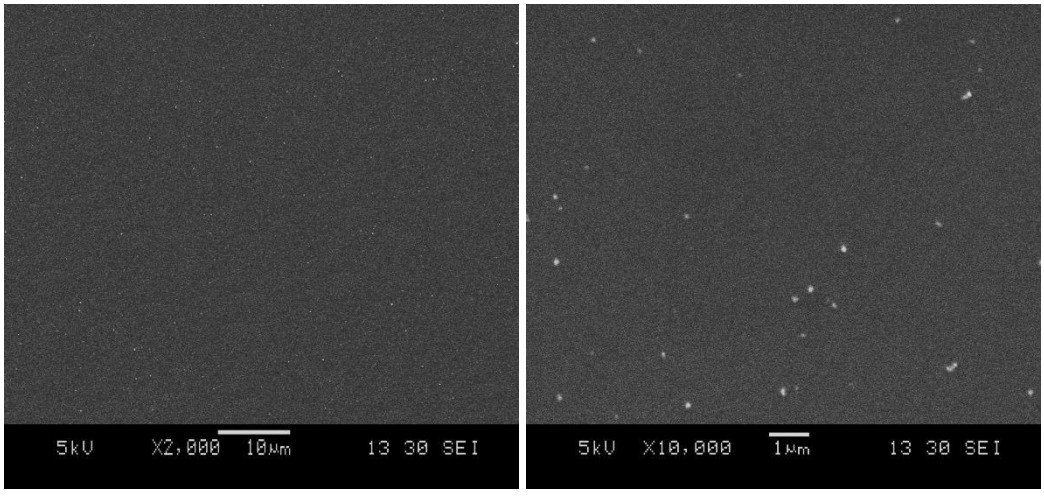

Figure 4.35 SEM images of 1PVA25 nanocomposite thin film

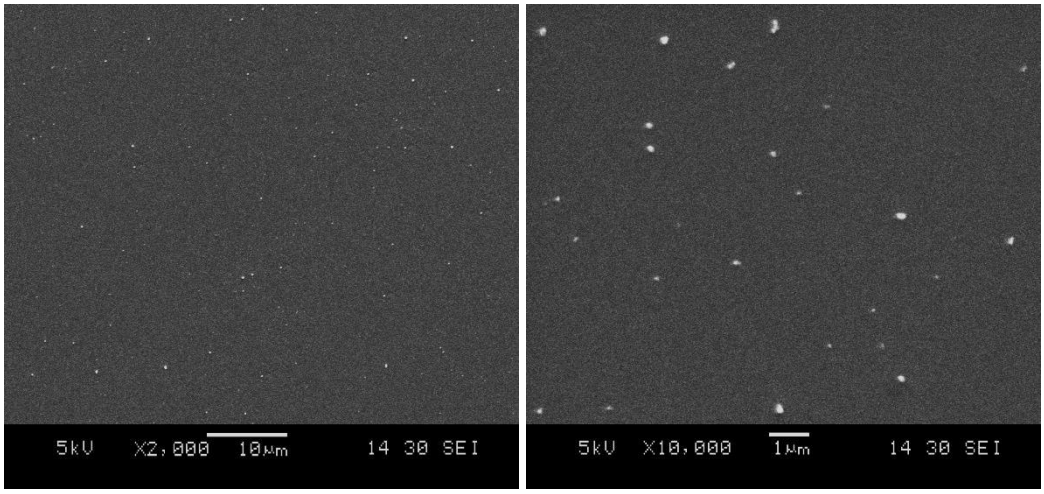

Figure 4.36 SEM images of 1PVA50 nanocomposite thin film

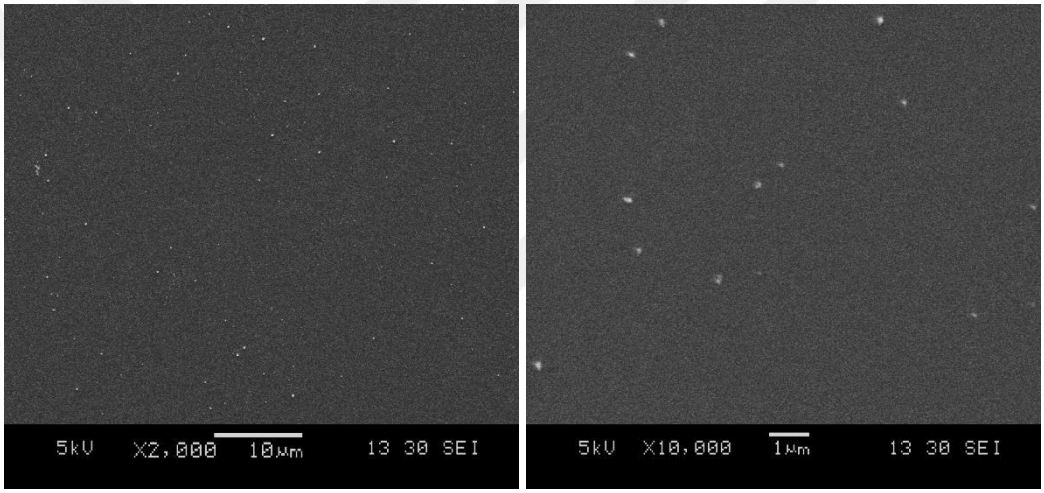

Figure 4.37 SEM images of 1PVA75 nanocomposite thin film

Microstructures of nanocomposite thin film produced using 2 % PVA solution including 10 % TiO_2 nanoparticle by weight of PVA content were given in Figure 4.38, 4.39 and 4.40. These figures show that it is possible to obtain nanocomposite thin films having continuous and homogeneous microstructure by spin coating method. When we compared the SEM images, It can be seen that Figure 4.38 has larger particles. This could be because of low spin speed and high concentration and viscosity. When viscosity increased, TiO_2 particles tend to agglomerate and form bigger particles. However none of the films include crack, hole or non-continuous structure. All of thin film having continuous and homogeneous microstructure.

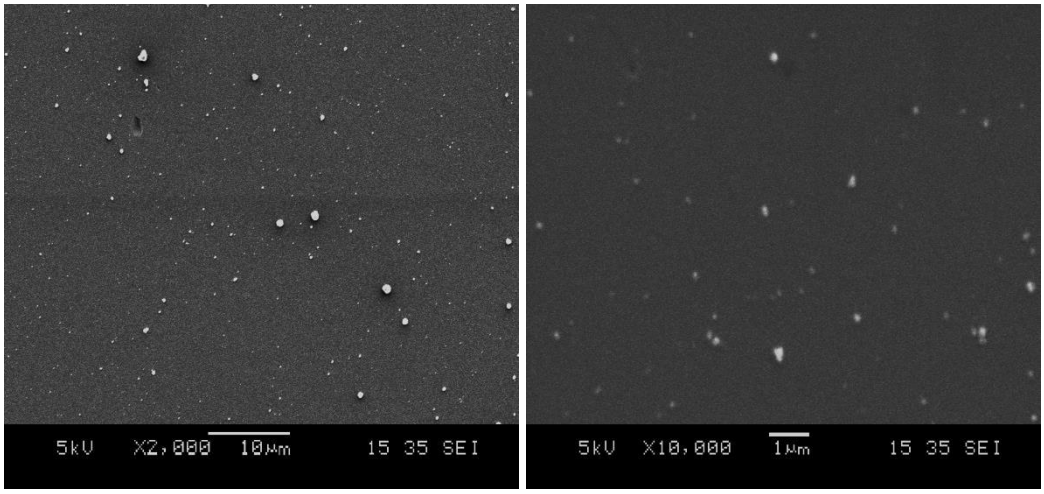

Figure 4.38 SEM images of 2PVA25 nanocomposite thin film

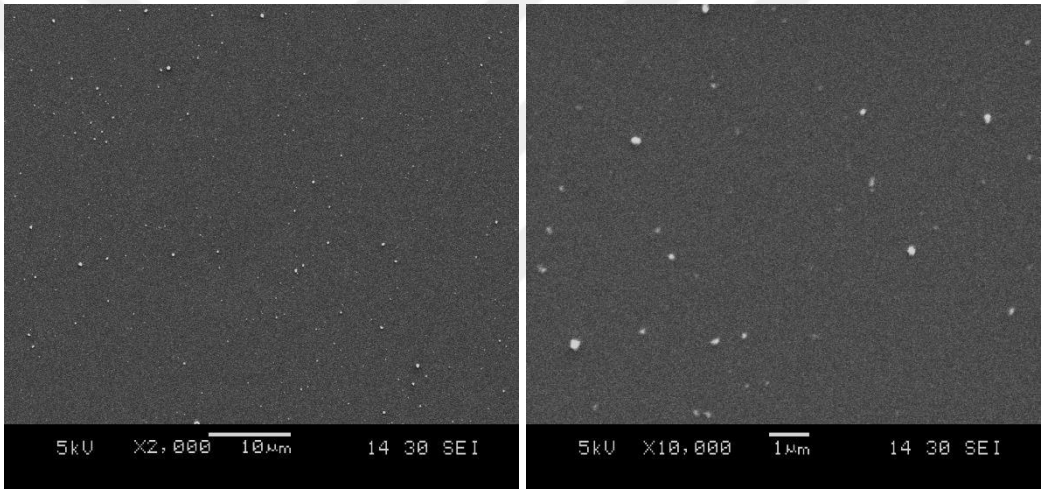

Figure 4.39 SEM images of 2PVA50 nanocomposite thin film

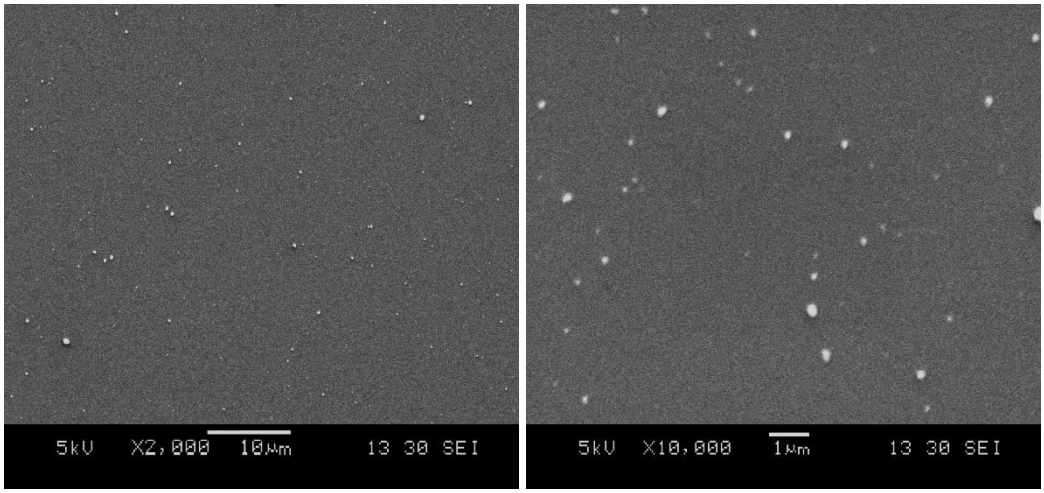

Figure 4.40 SEM images of 2PVA75 nanocomposite thin film

The surface morphology of film produced using 4 % PVA solution including 10 % TiO_2 nanoparticle by weight of PVA content were given in Figure 4.41, 4.42 and 4.43. These SEM micrographs revealed that 4 % PVA solution is not proper solution to produce thin film by using spin coating method. Because of the high PVA concentration, viscosity is high. Higher viscosity caused high cohesion force between PVA molecules. During the spin coating process solution could not spread on the Si substrate because of the high cohesion force. With this respect some structural defect such as big holes occur. These holes are approximately 1μm. This is not acceptable to use integrated circuit.

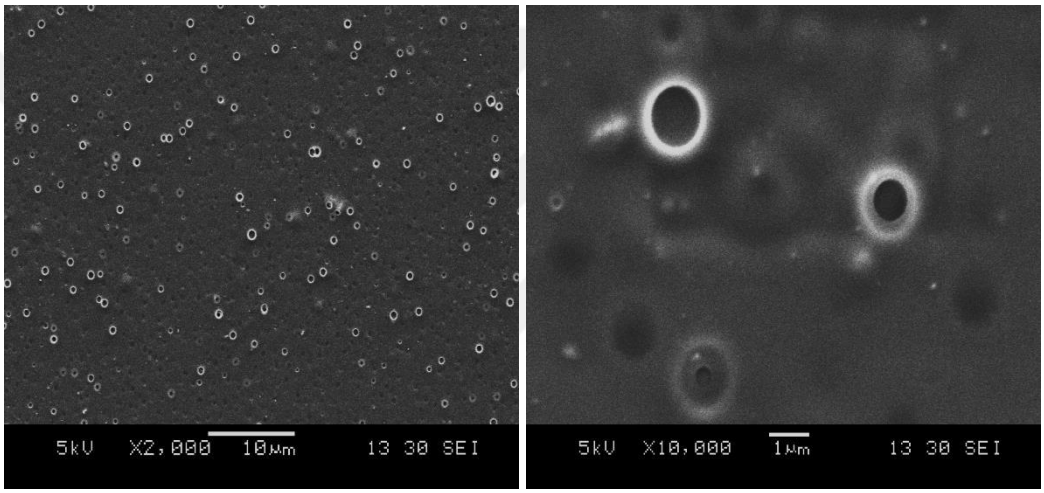

Figure 4.41 SEM images of 4PVA25 nanocomposite thin film

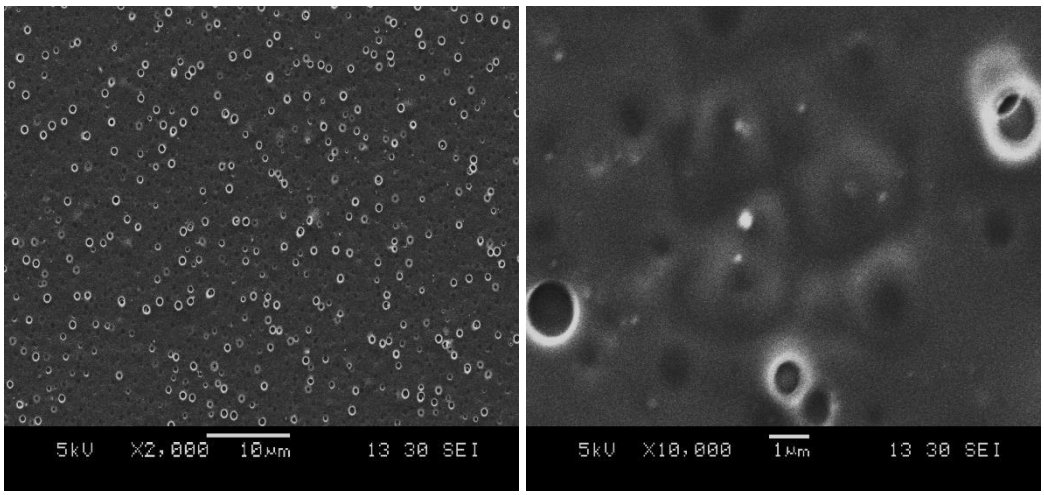

Figure 4.42 SEM images of 4PVA50 nanocomposite thin film

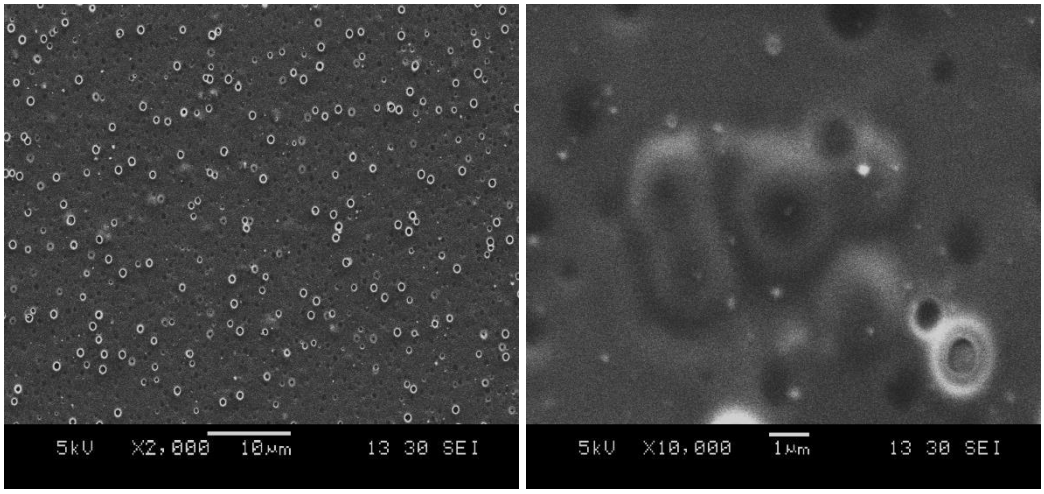

Figure 4.43 SEM images of 4PVA75 nanocomposite thin film

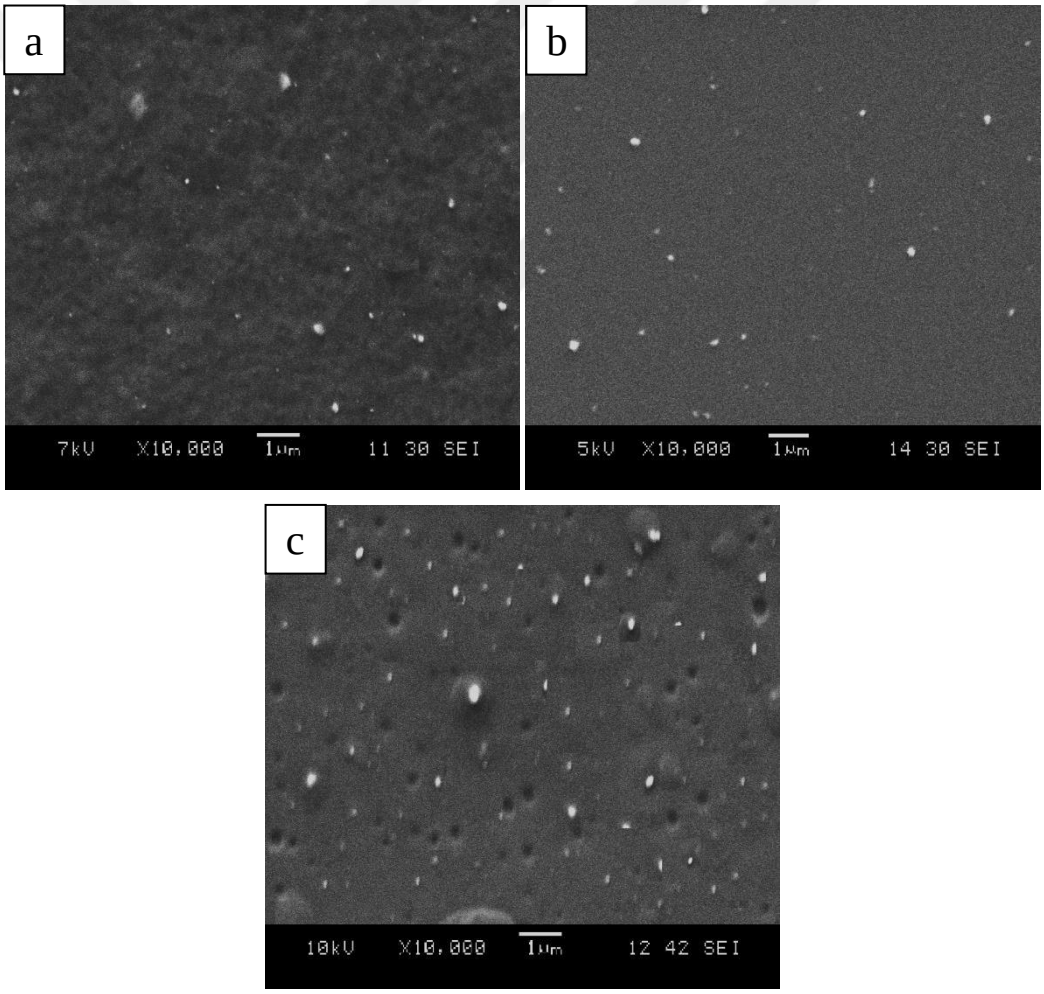

Figure 4.44 SEM images of PVA/TiO_2 thin film including (a) 5 % wt TiO_2, (b) 10% wt TiO_2 (c) 20 % wt TiO_2

Figure 4.44 shows SEM micrograph of PVA/TiO_2 thin film including 5 % wt, 10 % wt and 20 %wt TiO_2. Increasing TiO_2 could be easily seen While thin film including 5 % wt and 10 % wt TiO_2 nanoparticles do not have any crack, pin-hole or non-homogenous structure thin film including 20 % wt $TiO_{2\ have}$ many holes. This is because of the too much TiO_2 adding.

4.6 Film Thickness

The thickness of the PMMA nanocomposite thin films is depicted in Figure 4.45. The film thickness depends on the viscosity which is result of the solution concentration. The more concentrated solution, the thicker film is obtained. Because of relatively higher viscosity 4 % wt PMMA solution leads the thickest film. the average film thickness of 4PMMA50, 2PMMA50 and 1PMMA50 are 458, 243 and 128 nm. Same phenomenon is valid for PVA based nanocomposite thin film. The thickness of the PVA nanocomposite thin films is depicted in Figure 4.46. The thickness of film increases with increasing solution concentration. The average film thicknesses are 410, 323 and 173 for 4PVA50, 2PVA50 and 1PVA50 respectively. However increasing film thickness leads increasing roughness of the surface. The balance between these two parameters is important factor for thin film especially in electronic devices. According to corporation with SEM and AFM result 1PMMA50 samples is suitable for using in electronic ınstrument.

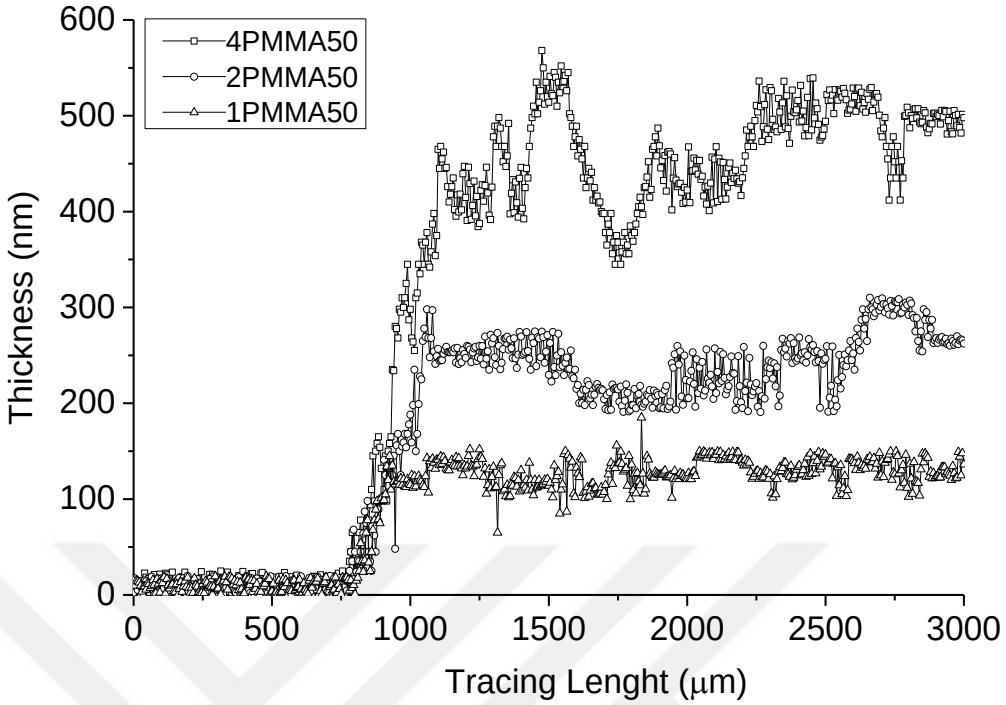

Figure 4.45 Thickness of PMMA based nanocomposite films

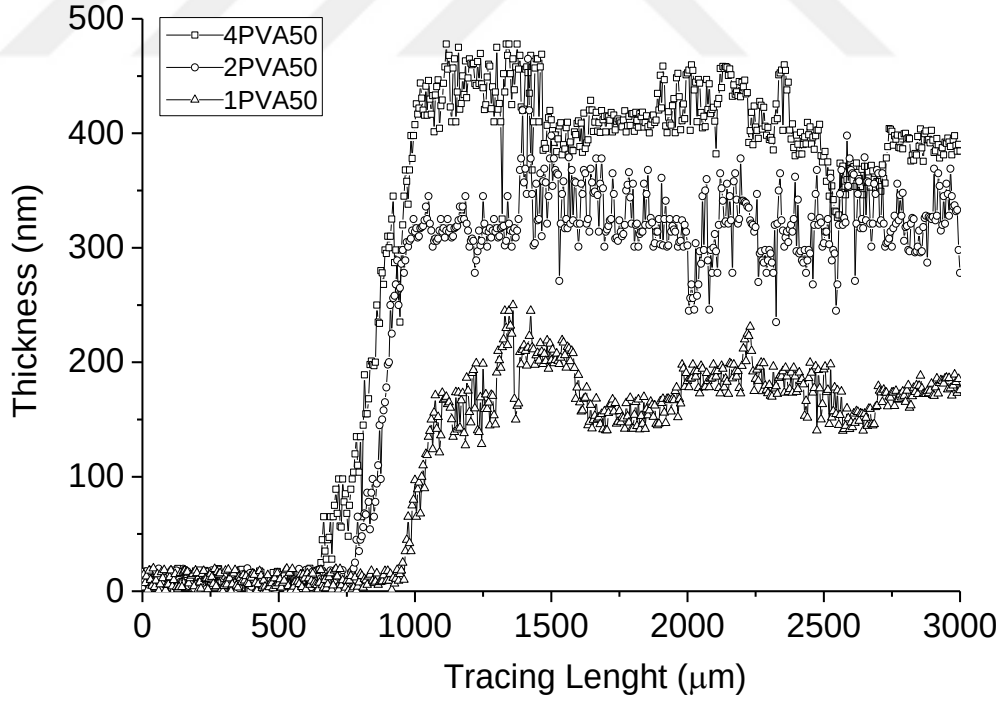

Figure 4.46 Thickness of PVA based nanocomposite films

4.7 Optical Properties

Figures 4.47 and 4.48 show the transmittance spectrums of PMMA/TiO_2 and PVA /TiO_2 nanocomposites respectively films measured in wavelengths between 200nm and 600, respectively. It was found that transmittance of films increase as with wavelength for both PMMA/TiO_2 and PVA/TiO_2 films. Higher transmittance than about 90% was obtained for pure PMMA and PVA above 250 nm wavelength. However transmittance of PMMA/TiO_2 and PVA/TiO_2 is lower than 10 % at UV region. That is because TiO_2 particle substantially absorb UV light. The observed increase of transmittance with wavelength is due to the increase in crystalline size associated with higher densification of the films (Agbo & Nnabuchi, 2011).

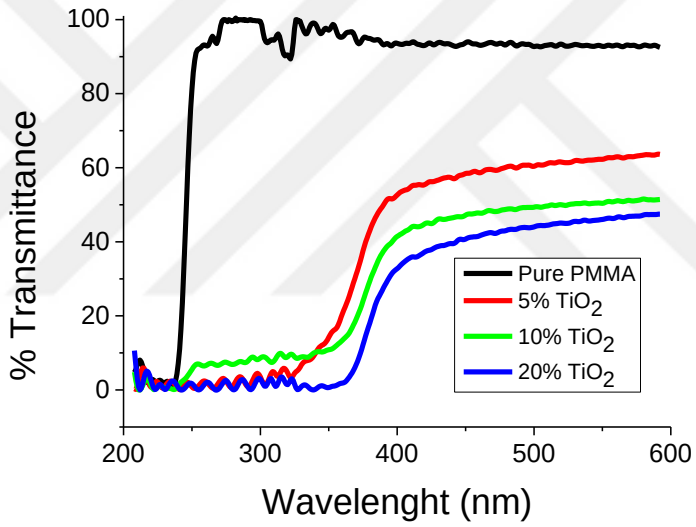

Figure 4.47 Transmittance Spectra of Pure PMMA and PMMA/TiO_2 nanocomposite thin film with different TiO_2 content

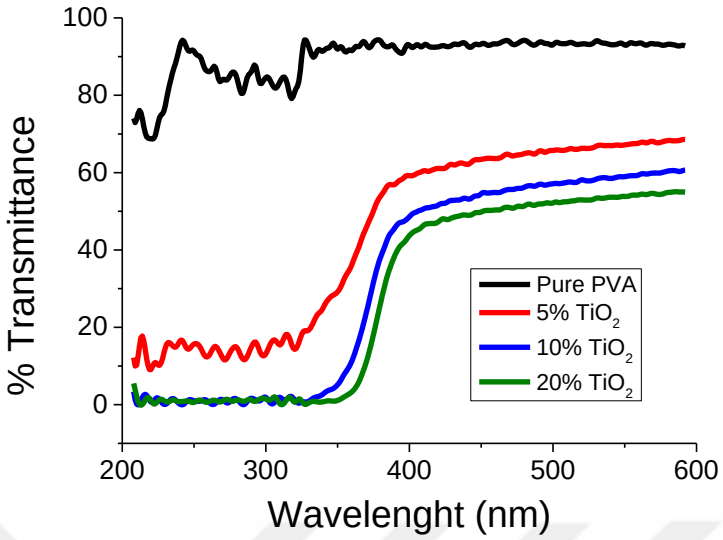

Figure 4.48 Transmittance Spectra of Pure PVA and PVA/TiO_2 nanocomposite thin film with different TiO_2 content

Figures 4.49 and 4.50 depict reflectance spectra of PMMA/TiO_2 and PVA/TiO_2 nanocomposite films. Average reflectance increases with increasing TiO_2 content. This increase in the reflectance spectrum can be attributed to the internal and surface scattering effects of the samples. At lower wavelengths, the reflectance spectrums of both films have sharp decreasing and give an absorption edge. This decreasing can be attributed to the electronic transition between valance and conduction bands which is related to the optical bandgap of the samples (Hendi, Alorainy & Yakuphanoglu, 2014).

Reflectance spectra of PMMA/TiO_2 and PVA/TiO_2 films show a sharp ultraviolet cut-off at approximately 350 nm owing to the optical reflectance of the TiO_2. Optical quality of transparent films could be determined by calculate value of %R+ %T. In our study value of %R+ %T is approximately 100 in visible region indicates that the PMMA/TiO_2 and PVA/TiO_2 films are non-absorbing and the light scattering is negligible.

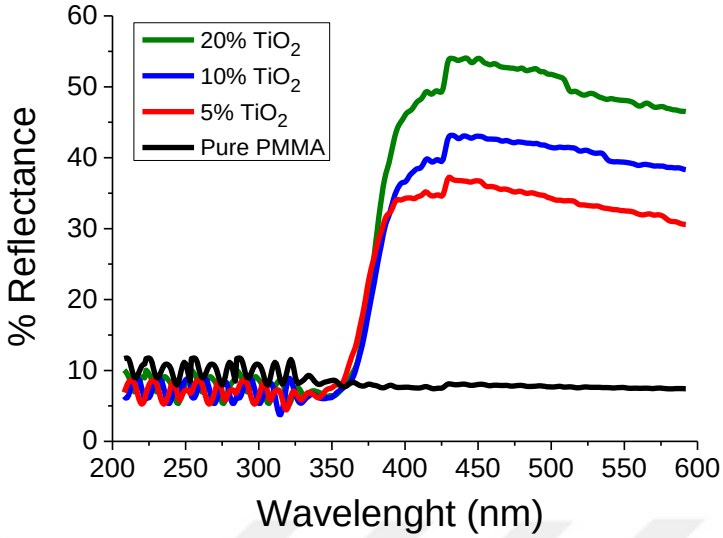

Figure 4.49 Reflectance Spectra of pure PMMA and PMMA/TiO_2 nanocomposite thin film with different TiO_2 content

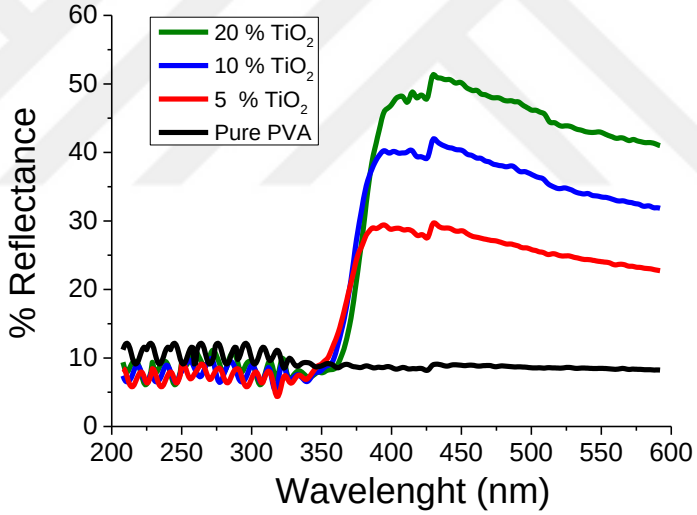

Figure 4.50 Reflectance Spectra of Pure PVA and PVA/TiO_2 nanocomposite thin film with different TiO_2 content

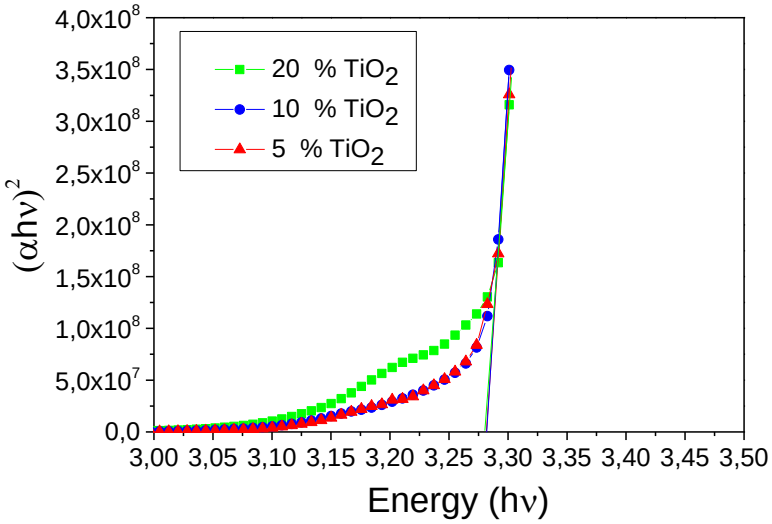

Figure 4.51 $(\alpha h\upsilon)^2$ vs $(h\upsilon)$ of PMMA/TiO_2 nanocomposite films

Band gap plot of the PMMA/TiO_2 and PVA/TiO_2 nanocomposites films were illustrated in Figure 4.51 and 4.52 respectively. The optical band gaps of the samples are determined by the following relation. (Hendi et al., 2014; Mermer & Sozbilen, 2014)

$$(\alpha h\nu)=A(h\nu-E_g)^{1/2} \qquad (4.1)$$

where A is a constant, is α the absorption coefficient, hν is the photon energy and Eg is the optical band gap. The optical band gap values of these films were determined from the intercept of $(\alpha h\upsilon)^2$ vs. hυ curves and are given in Table 4.1. As seen in Table 4.1, the effect of TiO_2 into PVA and PMMA does not let a major change but it enhances the optical gap a little.

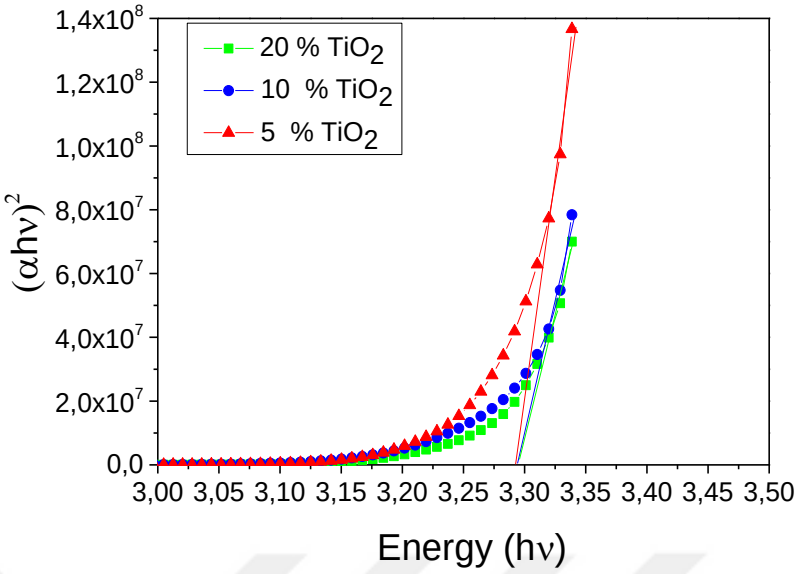

Figure 4.52 $(\alpha h\upsilon)^2$ vs $(h\upsilon)$ of PVA/TiO_2 nanocomposite films

Table 4.1 Optical properties of pure and polymeric nanocomposite thin film

Matrix	TiO_2 Content	T_{ave} (%)	R_{ave} (%)	E_g (eV)
PVA	0 % (Pure PVA)		7.920	-
	5 %	60.805	18.552	3.274
	10 %	58.371	24.514	3.288
	20 %	42.267	29.323	3.286
PMMA	0 % Pure (PMMA)	85.331	8.564	-
	5 %	35.920	22.395	3.288
	10 %	29.83	25.495	3.292
	20 %	23.86	30.929	3.278

4.8 Dielectric Properties

The variations of dielectric properties of pure polymer and their nanocomposite with respect to frequency with TiO_2 nano-fillers and at different filler concentrations are shown in following section. The measurements were carried out at constant temperature to avoid influence of the temperature differences. Dielectric properties of nanocomposite were determined by relaxation mechanism and dielectric polarization. In present case dielectric polarization and relaxion mechanism associated with polymer matrix and TiO_2 fillers and interfacial polarizations at the

polymer-particle interfaces. Especially in nanocomposite structures volume fraction of interfaces is relatively higher. So interfacial polarization interfacial polarizations are most likely to take place (Singha & Thomas, 2008).

4.8.1 Real Part of Permittivity

Figure 4.53a and 4.53b presents the real part of complex permittivity (ε′) as a function of frequency of pure PMMA, PVA and their composites. The real part of complex permittivity of all samples decreases with increasing frequency and have plateau at higher frequency. This behavior can be due to the frequency dependence of the polarization mechanisms. Concerning to this mechanism, it can suggested that polarization at interface is effective mechanism at low frequency regime while electronic and ionic polarization effects are dominant at higher frequencies. Furthermore, the dependence of dielectric constant on frequency also points out the material-electrode interface polarization processes which occur at low frequency regime. On the other hand difference between pure PVA and PVA/TiO_2 is dramatic. While real part of permittivity of PVA/TiO_2 including 20 % TiO_2 nanoparticle by weight of PVA content is 14.92 at 1 Hz, it is 3.58 for pure PVA. Because of the presence of TiO_2, dielectric constants of the composite structure are higher than that of pure PVA.

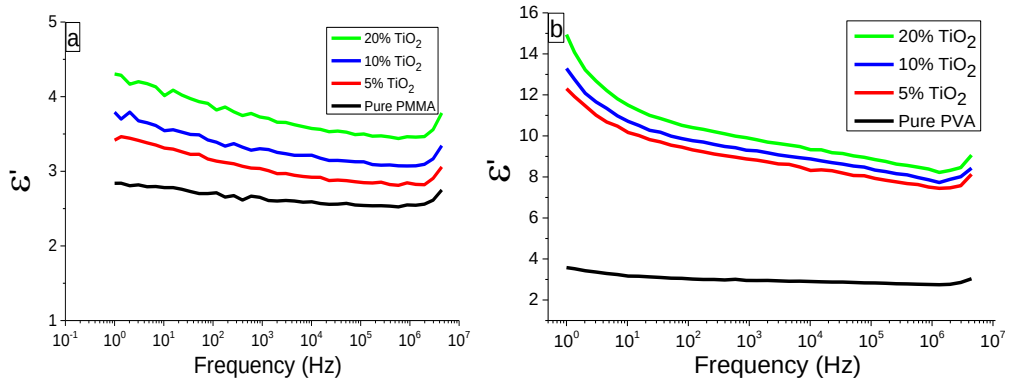

Figure 4.53 Real part of permittivity of PMMA based films (a), and PVA based films (b) function of frequency

When the real permittivity measurement result of PMMA based nanocomposite structures were examined, it could be seen the difference of ε′ value between pure PMMA and PMMA/TiO_2 is not as high as value between pure PVA and PVA/TiO_2. Non homegen structures could be seen in SEM micrograph in PMMA based nanocomposite structures. There are some bubbles and holes in these films. These kinds of defects can affect dielectric properties negatively. There also could be another possibility which is because of the presence of nanoscale TiO_2 particles. These possibilities are discussed in detail following section.

4.8.1.1 Frequency Dependence

The polymer component of permittivity is governed by the number of orientable dipoles present in the system and their ability to orient under an applied electric field (Eloundou, 2002; Livi, Levita & Rolla, 1993). Usually, the molecular groups which are attached perpendicular to the longitudinal polymer chain contribute to the dielectric relaxation mechanisms. All free dipolar groups in long polymer chain is able to orient in at relatively low frequencies leading higher permittivity. However when applied electrical field frequency is increased, dipolar groups in polymer find it difficult to follow the altering field. So the contributions of these dipolar groups to the permittivity goes on reducing resulting in a continuously decreasing permittivity of the polymer system at higher frequencies. Same dielectrical rules are valid for TiO_2 particles. Increasing applied electric field frequency results decreasing in permittivity of the particles.

Similarly, the inherent permittivity in TiO_2 particles also decrease with increasing frequencies of the applied field (Levinson & Philipp, 1976; Zhang, Zhang, Wang, Mo & Zhang, 1996). With this respect the permittivity of nanocomposite decrease as electric field frequency increase because of combined decreasing effect of the permittivity for both polymer and the filler particles.

Strong ionic polarization occurs in TiO_2 molecules because of Ti^{4+} and O^{2-} ions. Therefore, TiO_2 should have significant effect on total permittivity of structure that it

placed in (Zhang et al., 1996). Zhang and his colleagues showed that between 10^5-10^3 Hz, the permittivity of both nano-sized TiO_2 bulk is almost constant and between 10^3-10^2 Hz, the permittivity slope with respect to frequency begins to increase. In our study we observed similar trend as it seen in Figure 4.53a and 4.53b

A similar trend is observed in the permittivity variations of polymer/TiO_2 composite system in Figure 4.53a and 4.53b. The effect of the filler on the permittivity variations depending on altering frequency can be considered to be very minimal. Because, the slope is very similar with pure PMMA. However in PVA based composite there is considerable change. The slope of the permittivity between 10^5-10^3 Hz is much closed as that seen for pure PVA. This is due to the presence of TiO_2. This observation is in agreement with Zhang and his colleagues work (Zhang et al., 1996). It also possible that interfacial polarization between TiO_2 and polymer matrix contribute to slope in the real part of permittivity in PVA/TiO_2 (Zhang et al., 1996).

PMMA/TiO_2, which unlike in the case of PVA/TiO_2 nanocomposite system, is not bound to the filler surface. This shows us the filler in polymer do not show same interfacial polarization. Interfacial polarization may be mitigated in nanocomposite structure with inorganic fillers (Nelson & Fothergill, 2004). Probably, the presence of a large volume fraction of interfaces in PMMA/TiO_2 impedes ion migration and drifting causing a reduction in the accumulation of heterocharges. In another aspect, the strong bonding and interaction between the nanoparticle and the first polymer nanolayer may lead to a stable interface with lesser numbers of free ions and defects to contribute to interfacial polarization in the bulk of the nanocomposite.

4.8.1.2 Occurrence of Lower Permittivity

Relatively low permittivity value of PMMA/TiO_2 as compared with PVA/TiO_2 may be because of the restriction of the bulk polarization mechanism. This means that there is a hindrance to the mobility of polar groups in PMMA. This mobility contributes to permittivity value in PMMA/TiO_2 nanocomposite structure.

Laboratory experiment showed that when nanoparticles are embedded in polymer matrix the mobility of polymer chains may be hindered (Mansencal, Haidar, Vidal, Delmotte & Chezeau, 2001; Papakonstantopoulos, Doxastakis, Nealey, Barrat & de Pablo, 2007; Picu & Ozmusul, 2003; Tsagaropoulos & Eisenberg, 1995) As discussed in section 3.1 above, the interactions between polymer (PMMA) chains and nanoparticle lead to the formation of a highly immobile polymer nanolayers close to the nanoparticle surface due to strong bonding of the charged particle surface and the polymer chains (Tsagaropoulos & Eisenberg, 1995). With considering that immobile nanolayers exist for all nanoparticles in PMMA matrix, This restriction in the mobility could be possible. Another aspect is that entanglement in polymer chain because of the presence of TiO_2 can reduce chain mobility (Picu & Rakshit, 2007; Sternstein & Zhu, 2002). The immobility and entanglement dynamics of the polymer chains are a function of the filler concentration and only those polymer chains which come in contact with the nanoparticles will become immobile or entangled. These theories can be extended for PMMA nanocomposites in the present study and it can be suggested that the occurrence of lower permittivity values than expected with TiO_2 nano-fillers are due to the immobility of PMMA chains.

4.8.1.3 Effect of Filler Concentration

It can be seen from Figures 4.53a and 4.53b that pure polymer has lowest permittivity value and with increasing nano filler concentrations in both PVA and PMMA, the nanocomposite permittivity increases. Because permittivity value of TiO_2 the is higher than that of pure polymer, TiO_2 nanoparticles will influence the final permittivity of Polymer/TiO_2 system. But the effect of TiO_2 in PMMA permittivity is less than its effect in PVA. This observation is due to the differences in the interface interaction of PVA-TiO_2 and PMMA-TiO_2 In order to understand the influence of filler permittivity, an example of an PMMA nanocomposite is considered for which at 0.1 % wt filler loading. Permittivity differences with this composite system and pristine PMMA is lower than PVA/TiO_2 composite which includes same amount of TiO_2 particles. Furthermore, at low nano-filler loadings, the thin immobile nanolayers around the nanoparticles allow the nanoparticles to have a

far stronger interaction with the second layer of loosely bound polymer (Tsagaropoulos & Eisenberg, 1995). As it was mentioned before, chain mobility restriction influences effect of individual permittivity of TiO_2 content. Especially in PMMA, this phenomenon occurs more effectively. This is probably the reason why the relatively lower nanocomposite permittivity is observed in PMMA/TiO_2. As the nano filler concentration increases in PMMA, the effect of filler permittivity slowly comes into play due to an increase in the number of nanoparticles in the PMMA matrix. The extent of polymer chain immobility in nanocomposites is a function of the filler concentration. The more the number of nanoparticles causes the increase of the immobility leading lower resultant permittivity value. So indirectly, the effective permittivity should reduce with increasing nano filler concentration. But again, the nanocomposite permittivity is also a function of the number of nanoparticles in the matrix and with increasing filler concentration; the permittivity will tend to go up due to the influence of filler permittivity. The interaction dynamics between these two processes which happen simultaneously in the nanocomposite is difficult to understand at this point and needs further study. But, it can be assumed that the rate of chain immobilization and the rate of permittivity enhancement with respect to filler loading will determine the variations in the nanocomposite permittivity (Singha & Thomas, 2008).

4.8.2 Imaginary Part of Permittivity

Imaginary part of permittivity (ε'') of PMMA/TiO_2 and PVA/TiO_2 are depicted in Figure 4.54a and 4.54b. Value of ε'' are compatible with ε' values. As ıt could be seen in the Figure 4.54, ε'' values of PMMA/TiO_2 are higher than PVA/TiO_2. This observation is agreed with ε'. Similar trend was obtained. Imaginary part of PMMA/TiO_2 system is lower than PVA/TiO_2 system.

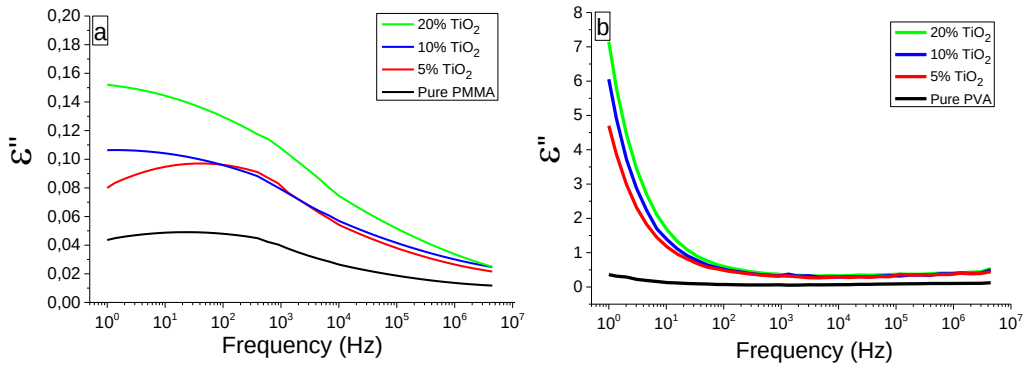

Figure 4.54 Imaginary part of permittivity of PMMA based films (a), and PVA based films (b) function of frequency

4.8.3 Dielectric Loss (Tan δ)

Dielectric loss values of PMMA and PVA based nanocomposites with TiO_2 fillers are presented in Figures 4.55a and 4.55b respectively. Dielectric loss depends on the several parameters such as electrical conductivity in the polymer number of charge carriers in the bulk of the material, the relaxation time of the charge carriers and the frequency of the applied electric field. The dielectric loss marginally decreases with increasing frequency. In Polymer/TiO_2 nanocomposite system, matrix material which is polymer dominates the variation of tan delta. However, with increasing TiO_2 content, dielectric loss value increases too. This observation probably is due to the presence of a significant number of nanoparticles in the system which influences the electrical conductivity mechanism in the nanocomposite. For the tan delta variations in the case of TiO_2 filled PMMA and PVA nanocomposites, the value of Tan δis higher than pure PMMA and pure PVA. But because of the low dielectric value of PMMA/TiO_2 nanocomposite system, tan delta is not as higher as that of PVA/TiO_2.

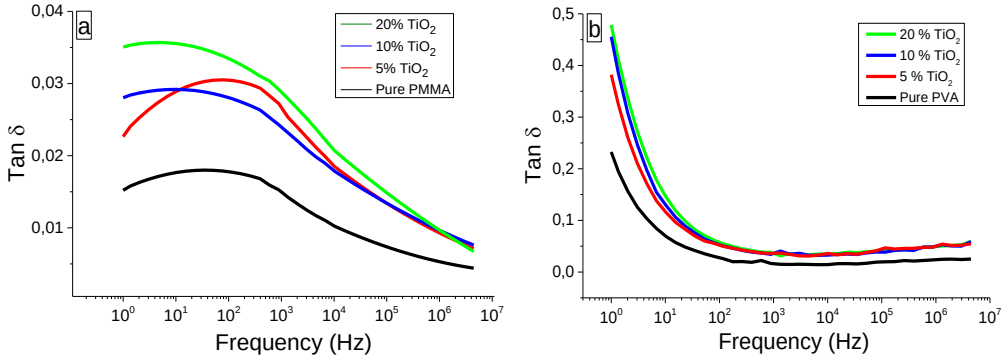

Figure 4.55 Dielectric loss of PMMA based film (a), and PMMA based films (b) as function of frequency

4.8.4 AC Conductivity

The A.C. conductivity of PMMA/TiO_2 and PVA/TiO_2 nanocomposites was measured between 1 and 3MHz frequency range using impedance spectroscopy technique. Figure 4.56a and 4.56b shows the frequency dependent A.C. conductivity plots of the samples. PMMA matrix samples have very similar trends with PVA. The conductivity of nanocomposite PMMA was slightly higher than that of pure PMMA for all frequency values. A.C. conductivities of PMMA/TiO_2 nanocomposites at 1 Hz are found to be 1.34 x 10^{-12}, 1.55 x 10^{-12} and 1.83 x 10^{-12} $S.cm^{-1}$ for 5wt%, 10wt% and 20wt% TiO_2 doping, respectively while ac conductivity of pure PMMA was 1.023 x 10^{-12} $S.cm^{-1}$ at 1 Hz.

The conductivity of nanocomposite PVA was slightly higher than that of pure PVA for all frequency values. A.C. conductivities of PVA/TiO_2 nanocomposites at 1 Hz are found to be 6.80 x 10^{-12}, 7.62 x 10^{-12} and 8.71 x 10^{-12} $S.cm^{-1}$ for 5wt%, 10wt% and 20wt% TiO_2 doping, respectively while ac conductivity of pure PVA was 4.78 x 10^{-12} $S.cm^{-1}$ at 1 Hz. This increase is due to the change in nano-microscopic parameters such as crystalline size and morphology of polymer after adding TiO_2 nanoparticles. These results are in agreement with the literature (Reddy, Lee & Gopalan, 2007).

Concerning the frequency dependency of A.C. conductivity PVA/TiO_2 nanocomposites presented almost the same behavior. A.C. conductivity of pure PVA changed with frequency above 1 kHz while PVA/TiO_2 nanocomposites had frequency dependent properties beyond 10 kHz. A.C. conductivity over the certain frequency obeyed the following formula (Karaoğlu et al., 2011; Mott & Davis, 2012).

$$\sigma \text{a.c.}\ (w) = Awn \tag{4.2}$$

where w is the angular frequency, n is the frequency exponent and A is a temperature independent constant.

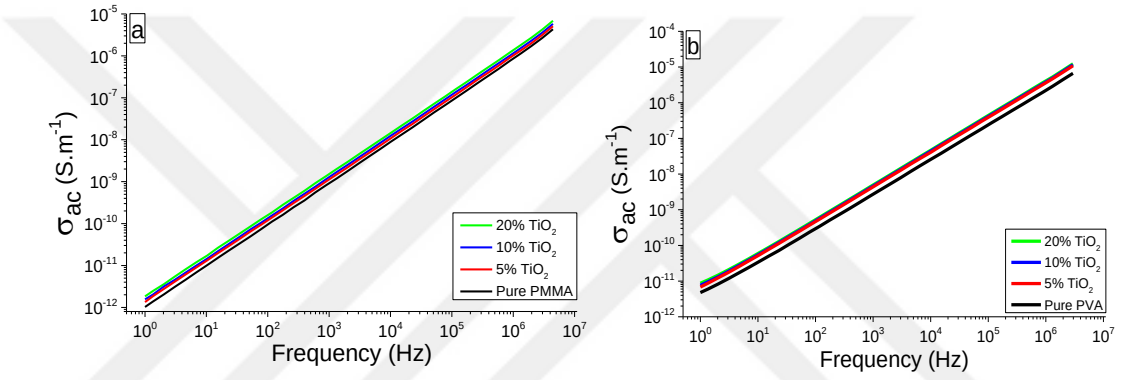

Figure 4.56 A.C. conductivity plots of pure and nanocomposite PMAA and PVA based samples as a function of frequency

CHAPTER FIVE
CONCLUSION

5.1 General Results

In the context of this thesis, PMMA and PVA based nanocomposite thin films including variable amount of sol-gel derived TiO_2 nanoparticles were produced by cost effective spin coating technique. The summarized results can be outlined as follows

1. Turbidity value of PMMA, PVA and Ti precursor which is Titanium (IV) isopropoxide solutions were measured as 14.24, 15.22, 6.12. These values suggest that polymer granules and precursor of Ti were dissolved completely in their proper solution.

2. The pH measurement of Ti precursor solution shows that the solution was acidic because of the addition of GAA. pH value was found to be 4.62

3. According to particles size distribution result, the average size of the ceramic particle was found to be 84 nm. This observation shows that the TiO_2 particles were successfully synthesize in nanoscale

4. The thermal analysis of xerogel obtained from Ti precursor solution indicates three thermal phenomena. The first endothermic peaks represent this solvent removal. The combustion process of organic groups occurred at ~250^oC as a second thermal phenomenon. At temperature of 100 ^oC to 300 ^oC, a weight loss of 50 % was recorded which could be attributed to the removal of unhydrolyzed isopropoxide Meanwhile from the DTA curves, a sharp exothermic reaction peak appeared at 414 ^oC indicating a phase change of the powder from amorphous to anatase phase. Additionally PMMA and PVA have two decomposition stages between 25-600 ^oC Moreover it is evident from thermal analysis of PMMA/TiO_2 and PVA/TiO_2, presence of TiO_2

increase the thermal stability of composite structure because of stability of anatase phase up to 600 ^{o}C.

5. In order to optimize the production of TiO_2 nanoparticle production FTIR analyses were performed to determine the removal of organic components in the structure. The intensities and noise of the vibrations decreased with increasing temperature and the spectrum becomes smoother for all spectrums while the oxide content increasing. The large bands in the region of 3600–3100 cm^{-1} is attributed to stretching vibrations of the metal-attached hydroxyl group (-OH), which indicates the product hydrolyzed. Furthermore to show presence of TiO_2 nanoparticle in the polymer matrix, FTIR spectra of PMMA/TiO_2 and PVA/TiO_2 were obtained. According to result vibrations of the metal-attached hydroxyl group (-OH) which is not exist in FTIR spectrum of pure PMMA and PVA.

6. XRD measurements were carried out to determine crystalline structure of the product. As result of the measurements highly crystalline anatase phase of TiO_2 could be synthesized successfully. In addition TiO_2 increase the crystallinity of amorphous PMMA and PVA matrix

7. The roughness of the thin films, 2D and 3D pictures were obtained by AFM device. According to result the roughnesses of the films increase as the concentration of solution and TiO_2 content increases. Furthermore spin speed influence surface quality. Higher spin speed than 5000 rpm effect negatively the surface quality. Best results were obtained 2 % polymeric solution with 2500 and 5000 rpm spin speed.

8. SEM micrograph revealed that TiO_2 nanoparticles were homogenously distributed through film. However PMMA based film have some defect on the surface such as pin holes and bubbles. On the other hand 1 % wt and 2 % wt PVA film including TiO_2 films have smooth and homogenous surface with no

crack. This may be due to the ester bound on PVA structure. But increasing solution concentration causes holes.

9. Film thickness measurements were carried out by profilometer. The results indicate that the more concentrated solution, the thicker film we have. While the average film thickness of 4PMMA50, 2PMMA50 and 1PMMA50 are 458, 243 and 128 nm., the average film thicknesses are 410, 323 and 173 nm for 4PVA50, 2PVA50 and 1PVA50 respectively

10. Optical analysis expose that Reflectance spectra of PMMA/TiO_2 and PVA/TiO_2 films show a sharp ultraviolet cut-off at approximately 350 nm owing to the optical reflectance of the TiO_2. It was found that transmittance of films increase as with wavelength for both PMMA/TiO_2 and PVA/TiO_2 films. Higher transmittance than about 90% was obtained for pure PMMA and PVA above 250 nm wavelength. However transmittance of PMMA/TiO_2 and PVA/TiO_2 is lower than 10 % at UV region. That is because TiO_2 particle substantially absorb UV light. In our study value of %R+ %T is approximately 100 in visible region indicates that the PMMA/TiO_2 and PVA/TiO_2 films are non-absorbing and the light scattering is negligible. Additionally bad-gap values of the all samples were calculated using Tauc equation, it was concluded that the effect of TiO_2 into PVA polymer does not let a major change but it enhances the optical gap a little.

11. Dielectric measurement exhibit that presence TiO_2 nanoparticle highly influences the dielectric properties of the film .Both real and imaginary part of permittivity value for all samples increase as TiO_2 content increase. Furthermore it was observed that dielectric loss values (Tan δ) and A.C. conductivity were affected by TiO_2 nanoparticle. Increasing particle content cause to increase dielectric loss and A.C. conductivity. However it is important to specify effect of TiO_2 nanoparticles in PMMA and PVA matrixes is not same. Reason behind this phenomenon could be reducing chain mobility of PMMA because existence of the TiO_2 nanoparticles other aspect is that it

maybe because of the non-homogenous structure of PMMA/TiO2 nanocomposite structure. Bubbles and hole in that structure can affect dielectric properties negatively. On the other hand addition of TiO_2 into the PVA matrix was performed successfully without any structural defect therefore the dielectric properties were improved. It was concluded that PVA/TiO_2 nanocomposite thin films have big potential to be employed in various dielectric application.

5.2 Future Plans

It is recommended that further studies should be carried out to achieve more homogeneous, crack-free, pin-hole-free especially for PMMA based nanocomposite films. To do this TiO_2 surface can be modified via creating core-shell region on the surface using different surfactant or different solvent can be used to dissolve PMMA granules. Spinning parameter should be improved by chancing acceleration time and speed. Also mechanical properties of PVA/TiO_2 and PMMA/TiO_2 can be examined. In addition dielectric characteristic of these types of structures led them to be used in thin film transistors (TFT) and thin film transistor based sensor applications. With this respect, a further study focused on producing TFT containing these types of nanocomposite dielectric structures can be carried out.

REFERENCES

Abargues, R., Rodriguez-Canto, P. J., Albert, S., Suarez, I. & Martínez-Pastor, J. P. (2014). Plasmonic optical sensors printed from Ag–PVA nanoinks. *Journal of Materials Chemistry C, 2* (5), 908-915.

Abbas, F., Bensaha, R. & Taroré, H. (2015). Hg-doped TiO_2 nanostructures thin film prepared by sol–gel method for gas sensing applications: Correlation between the structural and electrical properties. *Optik-International Journal for Light and Electron Optics, 126* (6), 671-675.

Abdel-Fattah, A. A. & El-Kelany, M. (1998). Radiation-sensitive indicator based on radiation-chemical formation of acids in polyvinyl butyral films containing chloral hydrate. *Radiation Physics and Chemistry, 51* (3), 317-325.

Adhikari, B. & Majumdar, S. (2004). Polymers in sensor applications. *Progress in Polymer Science, 29* (7), 699-766.

Agbo, P. & Nnabuchi, M. (2011). Core-shell TiO_2/ZnO thin film: Preparation, characterization and effect of temperature on some selected properties. *Chalcogen. Lett, 8*, 273-282.

Ahmad, Z. (2012). Polymeric dielectric materials. In *Dielectric Material*, 3-26.

Ajayan, P. M., Schadler, L. S. & Braun, P. V. (2006). *Nanocomposite science and technology* Weinheim: John Wiley & Sons.

Al Zahrany, A. A., Rabaeh, K. A. & Basfar, A. A. (2011). Radiation-induced color bleaching of methyl red in polyvinyl butyral film dosimeter. *Radiation Physics and Chemistry, 80* (11), 1263-1267.

Aleksic, J., Zielke, P. & Szymczyk, J. A. (2002). Temperature and flow visualization in a simulation of the czochralski process using temperature-sensitive liquid crystals. *Annals of the New York Academy of Sciences, 972* (1), 158-163.

Ali, U., Karim, K. J. B. A. & Buang, N. A. (2015). A review of the properties and applications of poly (methyl methacrylate)(PMMA). *Polymer Reviews, 55* (4), 678-705.

Amin, E. M., Karmakar, N. C. & Winther-Jensen, B. (2013). Polyvinyl-alcohol (PVA)-based rf humidity sensor in microwave frequency. *Progress In Electromagnetics Research B, 54*, 149-166.

Andrady, A. L., Merkel, T. C. & Toy, L. G. (2004). Effect of particle size on gas permeability of filled superglassy polymers. *Macromolecules, 37* (11), 4329-4331.

Augustyniak, I., Knapkiewicz, P., Sareło, K., Dziuban, J., Debourg, E., Pons, P. & Olszacki, M. (2015). Micromechanical high-doses radiation sensor with bossed membrane and interferometry optical detection. *Sensors and Actuators A: Physical, 232*, 353-358.

Baker, M. I., Walsh, S. P., Schwartz, Z. & Boyan, B. D. (2012). A review of polyvinyl alcohol and its uses in cartilage and orthopedic applications. *Journal of Biomedical Materials Research Part B: Applied Biomaterials, 100* (5), 1451-1457.

Balazs, A. C., Emrick, T. & Russell, T. P. (2006). Nanoparticle polymer composites: Where two small worlds meet. *Science, 314* (5802), 1107-1110.

Barber, P., Balasubramanian, S., Anguchamy, Y., Gong, S., Wibowo, A., Gao, H., Ploehn, H. J. & Zur Loye, H.-C. (2009). Polymer composite and nanocomposite dielectric materials for pulse power energy storage. *Materials, 2* (4), 1697-1733.

Barnes, C. P., Sell, S. A., Boland, E. D., Simpson, D. G. & Bowlin, G. L. (2007). Nanofiber technology: Designing the next generation of tissue engineering scaffolds. *Advanced Drug Delivery Reviews, 59* (14), 1413-1433.

Basfar, A. A., Moftah, B., Rabaeh, K. A. & Almousa, A. A. (2015). Novel composition of polymer gel dosimeters based on n-(hydroxymethyl)acrylamide for radiation therapy. *Radiation Physics and Chemistry, 112,* 117-120.

Bhargav, P. B., Mohan, V. M., Sharma, A. & Rao, V. N. (2009). Investigations on electrical properties of (PVA:Naf) polymer electrolytes for electrochemical cell applications. *Current Applied Physics, 9* (1), 165-171.

Bhat, N., Nate, M., Bhat, R. & Bhatt, B. (2007). Effect of gamma-irradiation on polyvinyl alcohol films doped with some dyes and their use in dosimetric studies. *Indian Journal of Pure and Applied Physics, 45* (6), 545-548.

Bin, Y., Mine, M., Koganemaru, A., Jiang, X. & Matsuo, M. (2006). Morphology and mechanical and electrical properties of oriented PVA–VGCF and PVA–MWNT composites. *Polymer, 47* (4), 1308-1317.

Bohnke, O., Frand, G., Rezrazi, M., Rousselot, C. & Truche, C. (1993). Fast ion transport in new lithium electrolytes gelled with PMMA. 2. Influence of lithium salt concentration. *Solid State Ionics, 66* (1), 105-112.

Bouropoulos, N., Psarras, G., Moustakas, N., Chrissanthopoulos, A. & Baskoutas, S. (2008). Optical and dielectric properties of ZnO - PVA nanocomposites. *Physica Status Solidi (a), 205* (8), 2033-2037.

Callister, W. D. & Rethwisch, D. G. (2007). *Materials science and engineering: An introduction.* New York: Wiley.

Celik, E., Keskin, I., Kayatekin, I., Ak Azem, F. & Özkan, E. (2007). Al_2O_3–TiO_2 thin films on glass substrate by sol–gel technique. *Materials Characterization, 58* (4), 349-357.

Chakraborty, S., Bera, M., Bhattacharya, S. & Maiti, C. (2005). Current conduction mechanism in TiO_2 gate dielectrics. *Microelectronic Engineering, 81* (2), 188-193.

Chandar Shekar, B., Sathish, S. & Sathyamoorthy, R. (2011). Morphology, structure and conduction properties of PVA nano scale thin films for field effect organic thin film transistors applications. *International Journal of Nanotechnology and Applications, 5*, 297-308.

Chen, G., Weng, W., Wu, D. & Wu, C. (2003). PMMA/Graphite nanosheets composite and its conducting properties. *European Polymer Journal, 39* (12), 2329-2335.

Chen, X., Wei, S., Yadav, A., Patil, R., Zhu, J., Ximenes, R., Sun, L. & Guo, Z. (2011). Poly (propylene)/carbon nanofiber nanocomposites: Ex situ solvent-assisted preparation and analysis of electrical and electronic properties. *Macromolecular Materials and Engineering, 296* (5), 434-443.

Croce, F., Curini, R., Martinelli, A., Persi, L., Ronci, F., Scrosati, B. & Caminiti, R. (1999). Physical and chemical properties of nanocomposite polymer electrolytes. *The Journal of Physical Chemistry B, 103* (48), 10632-10638.

Devallance, D. B. & Nan, N. (2014). Bio-based carbon/polyvinyl alcohol piezoresistive sensor material *57th SWST International Convention 7th Wood Structure and Properties Conference 6th European Hardwood* (467).

Drazkowski, D. B., Lee, A. & Haddad, T. S. (2007). Morphology and phase transitions in styrene-butadiene-styrene triblock copolymer grafted with isobutyl-substituted polyhedral oligomeric silsesquioxanes. *Macromolecules, 40* (8), 2798-2805.

Dupare, D., Shirsat, M. & Aswar, A. (2009). Inorganic acids doped PANI-PVA composites films as a gas sensor. *The Pacific Journal of Science and Technology, 10* (1), 417-422.

Ebeoğlugil, M. F. (2011). *Processing, characterization and development of rare earth doped lead magnesium niobate ferroelectric ceramic capacitors by sol-gel technique.* Phd Thesis, Dokuz Eylül University, Izmir.

El-Toony, M. (2011). Synthesis of GMA/ PVA cast membrane reinforced with alumina for fuel cell applications. *Nature and Science, 9*, 160-172.

Eloundou, J. P. (2002). Dipolar relaxations in an epoxy–amine system. *European Polymer Journal, 38* (3), 431-438.

Erol, M., Sancakoglu, O., Yurddaskal, M., Yildirim, S. & Çelik, E. (2013). A comparison on physical, structural, and photocatalytical properties of TiO_2 nanopowders produced using sol-gel and flame spray pyrolysis. *International Journal of Applied Ceramic Technology, 10* (6), 931-938.

Fernandes, D., Hechenleitner, A. W., Lima, S., Andrade, L., Caires, A. & Pineda, E. G. (2011). Preparation, characterization, and photoluminescence study of PVA/ZnO nanocomposite films. *Materials Chemistry and Physics, 128* (3), 371-376.

Fromageau, J., Brusseau, E., Vray, D., Gimenez, G. & Delachartre, P. (2003). Characterization of PVA cryogel for intravascular ultrasound elasticity imaging. *Ultrasonics, Ferroelectrics, and Frequency Control, IEEE Transactions on, 50* (10), 1318-1324.

Fu, S.-Y., Feng, X.-Q., Lauke, B. & Mai, Y.-W. (2008). Effects of particle size, particle/matrix interface adhesion and particle loading on mechanical properties of particulate–polymer composites. *Composites Part B: Engineering, 39* (6), 933-961.

Fu, Y.-S., Du, X.-W., Kulinich, S. A., Qiu, J.-S., Qin, W.-J., Li, R., Sun, J. & Liu, J. (2007). Stable aqueous dispersion of ZnO quantum dots with strong blue emission via simple solution route. *Journal of the American Chemical Society, 129* (51), 16029-16033.

Gaaz, T. S., Sulong, A. B., Akhtar, M. N., Kadhum, A. A. H., Mohamad, A. B. & Al-Amiery, A. A. (2015). Properties and applications of polyvinyl alcohol, halloysite nanotubes and their nanocomposites. *Molecules, 20* (12), 22833-22847.

Goseki, R. & Ishizone, T. (2015). Poly (methyl methacrylate)(PMMA). In *Encyclopedia of Polymeric Nanomaterials* (1702-1710): Springer.

Hafizah, N. & Sopyan, I. (2009). Nanosized TiO_2 photocatalyst powder via sol-gel method: Effect of hydrolysis degree on powder properties. *International Journal of Photoenergy, 2009*.

Hall, D. B., Underhill, P. & Torkelson, J. M. (1998). Spin coating of thin and ultrathin polymer films. *Polymer Engineering & Science, 38* (12), 2039-2045.

Hench, L. L. & West, J. K. (1990). The sol-gel process. *Chemical Reviews, 90* (1), 33-72.

Hendi, A., Alorainy, R. & Yakuphanoglu, F. (2014). Humidity sensing characteristics of Sn doped Zinc oxide based quartz crystal microbalance sensors. *Journal of Sol-Gel Science and Technology, 72* (3), 559-564.

Hiroki, A., Yamashita, S., Kimura, A., Nagasawa, N. & Taguchi, M. (2015). Effect of heavy ion irradiation on optical property of radiation-crosslinked hydroxypropyl cellulose gel containing methacrylate monomers. *Nuclear Instruments and Methods in Physics Research Section B: Beam Interactions with Materials and Atoms, 365, Part B*, 583-586.

Hussain, R. & Mohammad, D. (2004). X-ray diffraction study of the changes induced during the thermal degradation of poly (methyl methacrylate) and poly (methacryloyl chloride). *Turkish Journal of Chemistry, 28* (6), 725-730.

Irimia-Vladu, M. & Fergus, J. W. (2006). Suitability of emeraldine base polyaniline-PVA composite film for carbon dioxide sensing. *Synthetic Metals, 156* (21), 1401-1407.

Jaroenworaluck, A., Regonini, D., Bowen, C. R., Stevens, R. & Allsopp, D. (2007). Macro, micro and nanostructure of TiO_2 anodised films prepared in a fluorine-containing electrolyte. *Journal of Materials Science, 42* (16), 6729-6734.

Jiang, K., Fei, T., Jiang, F., Wang, G. & Zhang, T. (2014). A dew sensor based on modified carbon black and polyvinyl alcohol composites. *Sensors and Actuators B: Chemical, 192*, 658-663.

Jin, J., Qi, R., Su, Y., Tong, M. & Zhu, J. (2013). Preparation of high-refractive-index PMMA / TiO_2 nanocomposites by one-step in situ solvothermal method. *Iranian Polymer Journal, 22* (10), 767-774.

Kalaitzidou, K., Fukushima, H. & Drzal, L. T. (2007). Multifunctional polypropylene composites produced by incorporation of exfoliated graphite nanoplatelets. *Carbon, 45* (7), 1446-1452.

Kao, K. C. (2004a). 1 - introduction. In *Dielectric phenomena in solids* (1-39). San Diego: Academic Press.

Kao, K. C. (2004b). 2 - electric polarization and relaxation. In *Dielectric phenomena in solids* (41-114). San Diego: Academic Press.

Karaoğlu, E., Baykal, A., Deligöz, H., Şenel, M., Sözeri, H. & Toprak, M. S. (2011). Synthesis and characteristics of poly (3-pyrrol-1-ylpropanoic acid)(PPyAA)–fe 3 o 4 nanocomposite. *Journal of Alloys and Compounds, 509* (33), 8460-8468.

Kenanakis, G., Vernardou, D., Dalamagkas, A. & Katsarakis, N. (2015). Photocatalytic and electrooxidation properties of TiO_2 thin films deposited by sol–gel. *Catalysis Today, 240*, 146-152.

Kern, W. (1970). Cleaning solutions based on hydrogen peroxide for use in silicon semiconductor technology. *RCA Review, 31*, 187-206.

Kern, W. (1990). The evolution of silicon wafer cleaning technology. *Journal of The Electrochemical Society, 137* (6), 1887-1892.

Kim, G. H., Yoon, S.-M., Am Kim, C. & Suh, K. S. (2005). Electrical and chemical properties of photo-cross-linked polymeric insulating materials. *Japanese Journal of Applied Physics, 44* (3L), L416.

Kumar, D., Jat, S. K., Khanna, P. K., Vijayan, N. & Banerjee, S. (2012). Synthesis, characterization, and studies of PVA/co-doped ZnO nanocomposite films. *International Journal of Green Nanotechnology, 4* (3), 408-416.

Lamastra, F., Bianco, A., Meriggi, A., Montesperelli, G., Nanni, F. & Gusmano, G. (2008). Nanohybrid PVA/ZrO_2 and PVA/Al_2O_3 electrospun mats. *Chemical Engineering Journal, 145* (1), 169-175.

Lee, J., Bhattacharyya, D., Easteal, A. & Metson, J. (2008). Properties of nano- ZnO /poly (vinyl alcohol)/poly (ethylene oxide) composite thin films. *Current Applied Physics, 8* (1), 42-47.

Levinson, L. M. & Philipp, H. (1976). Ac properties of metal-oxide varistors. *Journal of Applied Physics, 47* (3), 1117-1122.

Livi, A., Levita, G. & Rolla, P. (1993). Dielectric behavior at microwave frequencies of an epoxy resin during crosslinking. *Journal of applied polymer science, 50* (9), 1583-1590.

Maira, A., Coronado, J., Augugliaro, V., Yeung, K. L., Conesa, J. & Soria, J. (2001). Fourier transform infrared study of the performance of nanostructured TiO_2 particles for the photocatalytic oxidation of gaseous toluene. *Journal of Catalysis, 202* (2), 413-420.

Majewski, L. A., Schroeder, R. & Grell, M. (2005). Low-voltage, high-performance organic field-effect transistors with an ultra-thin TiO_2 layer as gate insulator. *Advanced Functional Materials, 15* (6), 1017-1022.

Mane, A., Navale, S., Mane, R., Naushad, M. & Patil, V. (2015). Synthesis and structural, morphological, compositional, optical and electrical properties of dbsa-doped ppy–wo 3 nanocomposites. *Progress in Organic Coatings, 87*, 88-94.

Mansencal, R., Haidar, B., Vidal, A., Delmotte, L. & Chezeau, J. M. (2001). High-resolution solid-state nmr investigation of the filler–rubber interaction: 2. High-

speed [1h] magic-angle spinning nmr spectroscopy in carbon-black-filled polybutadiene. *Polymer International, 50* (4), 387-394.

Mermer, O. & Sozbilen, H. (2014). Optical and microstructural properties of pure and ru doped sno2 semiconducting thin films. *Journal of Optoelectronics and Advanced Materials, 16* (11-12), 1306-1310.

Meyerhofer, D. (1978). Characteristics of resist films produced by spinning. *Journal of Applied Physics, 49* (7), 3993-3997.

Mott, N. F. & Davis, E. A. (2012). *Electronic processes in non-crystalline materials.* Oxford: Oxford University Press.

Moulson, A. J. & Herbert, J. M. (2003). *Electroceramics: Materials, properties, applications*. Chichester: John Wiley & Sons.

Nelson, J. K. & Fothergill, J. C. (2004). Internal charge behaviour of nanocomposites. *Nanotechnology, 15* (5), 586.

Norrman, K., Ghanbari-Siahkali, A. & Larsen, N. (2005). 6 studies of spin-coated polymer films. *Annual Reports Section" C"(Physical Chemistry), 101*, 174-201.

Olson, D. C., Piris, J., Collins, R. T., Shaheen, S. E. & Ginley, D. S. (2006). Hybrid photovoltaic devices of polymer and ZnO nanofiber composites. *Thin Solid Films, 496* (1), 26-29.

Ortiz, R. o. P., Facchetti, A. & Marks, T. J. (2009). High-k organic, inorganic, and hybrid dielectrics for low-voltage organic field-effect transistors. *Chemical Reviews, 110* (1), 205-239.

Papakonstantopoulos, G. J., Doxastakis, M., Nealey, P. F., Barrat, J.-L. & de Pablo, J. J. (2007). Calculation of local mechanical properties of filled polymers. *Physical Review E, 75* (3), 031803.

Petersson, L., Kvien, I. & Oksman, K. (2007). Structure and thermal properties of poly (lactic acid)/cellulose whiskers nanocomposite materials. *Composites Science and Technology, 67* (11), 2535-2544.

Picu, R. & Ozmusul, M. (2003). Structure of linear polymeric chains confined between impenetrable spherical walls. *The Journal of Chemical Physics, 118* (24), 11239-11248.

Picu, R. & Rakshit, A. (2007). Dynamics of free chains in polymer nanocomposites. *The Journal of Chemical Physics, 126* (14), 144909.

Pierre, A. C. (2013). *Introduction to sol-gel processing.* Newyork: Springer Science & Business Media.

Ramos, J., Mejia, I., Murphy, J., Quevedo, M., Garcia, P. & Martinez, C. (2014). Synthesis of titanium oxide nanoparticles using DNA-complex as template for solution-processable hybrid dielectric composites. *Journal of Alloys and Compounds*.

Reddy, K. R., Lee, K. P. & Gopalan, A. I. (2007). Novel electrically conductive and ferromagnetic composites of poly (aniline-co-aminonaphthalenesulfonic acid) with iron oxide nanoparticles: Synthesis and characterization. *Journal of Applied Polymer Science, 106* (2), 1181-1191.

Roy, A. S., Gupta, S., Sindhu, S., Parveen, A. & Ramamurthy, P. C. (2013). Dielectric properties of novel PVA/ZnO hybrid nanocomposite films. *Composites Part B: Engineering, 47*, 314-319.

Sagadevan, S. & Sundaramb, A. S. (2014). A brief review of the relevant dielectric theories of solids. *Latin-American Journal of Physics Education, 8* (3), 397.

Saikia, D., Saikia, P., Gogoi, P. & Saikia, P. (2011). Synthesis, characterization and photovoltaic application of silver doped Cds/ PVA nanocomposite thin films. *Dig J Nanomater Bios, 6*, 589-597.

Sanchez, C., Lebeau, B., Chaput, F. & Boilot, J. P. (2003). Optical properties of functional hybrid organic–inorganic nanocomposites. *Advanced Materials, 15* (23), 1969-1994.

Shenhar, R., Norsten, T. B. & Rotello, V. M. (2005). Polymer-mediated nanoparticle assembly: Structural control and applications. *Advanced Materials, 17* (6), 657-669.

Singh, N., Agarwal, A., Sanghi, S. & Khasa, S. (2012). Dielectric loss, conductivity relaxation process and magnetic properties of Mg substituted Ni–Cu ferrites. *Journal of Magnetism and Magnetic Materials, 324* (16), 2506-2511.

Singha, S. & Thomas, M. J. (2008). Dielectric properties of epoxy nanocomposites. *Dielectrics and Electrical Insulation, IEEE Transactions on, 15* (1), 12-23.

Sinirlioğlu, D. (2010). *Synthesis and characterization of inorganic-rganicnanocomposite polymeric materials via controlledpolymerization methods and ‘‘click” reactions.* M.Sc. Thesis, Fatih University, İstanbul.

Smyth, C. P. (1966). Dielectric polarization and relaxation. *Annual Review of Physical Chemistry, 17* (1), 433-456.

Sternstein, S. & Zhu, A.-J. (2002). Reinforcement mechanism of nanofilled polymer melts as elucidated by nonlinear viscoelastic behavior. *Macromolecules, 35* (19), 7262-7273.

Su, W., Wang, S., Wang, X., Fu, X. & Weng, J. (2010). Plasma pre-treatment and TiO_2 coating of PMMA for the improvement of antibacterial properties. *Surface and Coatings Technology, 205* (2), 465-469.

Sugumaran, S. & Bellan, C. (2014). Transparent nano composite PVA–TiO_2 and PMMA–TiO_2 thin films: Optical and dielectric properties. *Optik-International Journal for Light and Electron Optics, 125* (18), 5128-5133.

Thostenson, E. T., Ren, Z. & Chou, T.-W. (2001). Advances in the science and technology of carbon nanotubes and their composites: A review. *Composites Science and Technology, 61* (13), 1899-1912.

Tintu, R., Saurav, K., Sulakshna, K., Nampoori, V., Radhakrishnan, P. & Thomas, S. (2010). $Ge_{28}Se_{60}Sb_{12}$/ PVA composite films for photonic applications. *Journal of Non-Oxide Glasses, 2* (4), 167-174.

Tjong, S. (2006). Structural and mechanical properties of polymer nanocomposites. *Materials Science and Engineering: R: Reports, 53* (3), 73-197.

Tomar, A., Mahendia, S. & Kumar, S. (2011). Structural characterization of PMMA blended with chemically synthesized pani. *Advances in Applied Science Research, 2* (3), 327-333.

Tsagaropoulos, G. & Eisenberg, A. (1995). Dynamic mechanical study of the factors affecting the two glass transition behavior of filled polymers. Similarities and differences with random ionomers. *Macromolecules, 28* (18), 6067-6077.

Vaia, R. A. & Maguire, J. F. (2007). Polymer nanocomposites with prescribed morphology: Going beyond nanoparticle-filled polymers. *Chemistry of Materials, 19* (11), 2736-2751.

Vojisavljevic, K. M., Chevreux, P., Jouin, J. & Malič, B. (2014). Characterization of the alkoxide-based sol-gel derived $La_{9.33}Si_6O_{26}$ powder and ceramic. *Acta Chimica Slovenica, 61* (3), 530-541.

Vollenberg, P. & Heikens, D. (1989). Particle size dependence of the young's modulus of filled polymers: 1. Preliminary experiments. *Polymer, 30* (9), 1656-1662.

Walsh, C. B. & Franses, E. I. (2003). Ultrathin PMMA films spin-coated from toluene solutions. *Thin Solid Films, 429* (1–2), 71-76.

Wang, G., Moses, D., Heeger, A. J., Zhang, H.-M., Narasimhan, M. & Demaray, R. (2004). Poly (3-hexylthiophene) field-effect transistors with high dielectric constant gate insulator. *Journal of Applied Physics, 95*, 316-322.

Wang, H., Li, Y., Ba, X., Huang, L. & Yu, Y. (2015). TiO_2 thin films with rutile phase prepared by dc magnetron co-sputtering at room temperature: Effect of cu incorporation. *Applied Surface Science, 345*, 49-56.

Wang, Q., Xia, H. & Zhang, C. (2001). Preparation of polymer/inorganic nanoparticles composites through ultrasonic irradiation. *Journal of Applied Polymer Science, 80* (9), 1478-1488.

Yahya, N., Akhtar, M., Masun, A. & Kashif, M. (2011). Synthesis and characterization of ZnO-CNTs filled PVA composite as em detector. *Journal of Applied Sciences*, 11, 1303-1308.

Yasumori, A., Shinoda, H., Kameshima, Y., Hayashi, S. & Okada, K. (2001). Photocatalytic and photoelectrochemical properties of TiO-based multiple layer thin film prepared by sol-gel and reactive-sputtering methods. *Journal of Materials Chemistry, 11* (4), 1253-1257.

Zhang, L., Zhang, H., Wang, G., Mo, C. & Zhang, Y. (1996). Dielectric behaviour of nano- TiO_2 bulks. *Physica Status Solidi (a), 157* (2), 483-491.

Zheng, W. & Wong, S.-C. (2003). Electrical conductivity and dielectric properties of PMMA /expanded graphite composites. *Composites Science and Technology, 63* (2), 225-235.